

WASSERSTEIN LEAST SQUARES: A CANONICAL REGRESSION METHOD FOR PROBABILITY DISTRIBUTIONS

URIEL MARTÍNEZ LEÓN AND JONATHAN NILES-WEED

ABSTRACT. We perform a mathematical and statistical analysis of the Wasserstein least squares problem, a regression method for vector-valued covariates and distribution-valued responses. Our proposal contrasts with other distributional regression methods by having a direct interpretation in terms of random variables, as a nonparametric analogue of the classic random-effects model. On the mathematical side, we use a strategy of [Lavenant \(2024\)](#) to show that Wasserstein least squares is the *canonical* extension of Euclidean least squares to the space of probability distributions from the perspective of convex analysis; this viewpoint gives rise to multimarginal and dual formulations of the Wasserstein least squares problem, extending a similar theory for Wasserstein barycenters. We perform a statistical analysis of the Wasserstein least squares problem under the template deformation model, showing, surprisingly, that estimation is possible at the $n^{-1/2}$ rate. As a special case, we obtain improved rates of estimation for Wasserstein barycenters, which are an exponential improvement over those established by [Ahidar-Coutrix et al. \(2020\)](#). Finally, we propose a heuristic particle method for Wasserstein least squares and use it to conduct a novel analysis of large-scale demographic data from the RAND Health and Retirement Study.

1. INTRODUCTION

Legendre’s 1805 publication of the method of least squares is a turning point in the history of mathematical statistics. In contrast to later justifications of the subject—particularly that of Gauss, which appeared in 1809—Legendre motivates his method not by a probabilistic model but by practical considerations. (See [Stigler, 1986](#), for a historical review of the development and popularization of the least squares method.) For Legendre, the usefulness of least squares was justified by several interrelated facts:

- (1) The naturalness and interpretability of linear relationships between covariates and responses;
- (2) The simplicity of the first-order optimality conditions for the minimization problem (the *normal equations*); and
- (3) The consistency of the least squares method with the method of averaging: in the case of repeated measurements of the same object, least-squares minimization reduces to computation of the arithmetic mean.

Later, Gauss’s probabilistic developments connected the least-squares objective to statistical estimation in the presence of random errors whose law bears his name.

2020 *Mathematics Subject Classification.* 62J05, 49Q22, 60A10.

Key words and phrases. Wasserstein distance, optimal transport, distributional regression, random coefficient model, Fréchet regression.

The power and ubiquity of linear least squares has led to the growth of a large literature that seeks to extend its reach beyond the Euclidean setting in which it was initially proposed, for instance, by allowing the independent variables (*covariates*) and dependent variables (*responses*) to take values in infinite-dimensional Hilbert spaces, on manifolds, or in general metric spaces (Hsing and Eubank, 2015; Petersen and Müller, 2019; Ramsay and Silverman, 2005). From a statistical perspective, generalizing beyond the Euclidean setting requires specifying both a method (analogous to Legendre’s least squares proposal) and a statistical model (analogous to Gauss’s theory of random errors) under which the method returns sensible results.

The goal of this work is to propose and study a version of the least squares method, with vector-valued covariates but responses which take values in the space of probability distributions. We are far from the first to propose such a method (see Section 1.2 for an in-depth summary), but we take a different approach to most existing statistical work on the problem. Our philosophy can be summarized by saying that rather than view probability distributions as elements of an arbitrary metric space, we *lift* standard linear least squares to the space of probability distributions by allowing our regression coefficients to be random variables. (This is analogous to the construction of the Wasserstein space by lifting a given base metric to the space of random variables, Savaré and Sodini, 2022).

Given covariates $\mathbf{x} \in \mathbb{R}^p$ and a response $y \in \mathbb{R}$, Legendre’s proposal begins with the structural assumption that

$$(1) \quad y \approx \boldsymbol{\beta}^\top \mathbf{x},$$

for an unknown vector of parameters $\boldsymbol{\beta} \in \mathbb{R}^p$. More generally, for responses in \mathbb{R}^d , (1) takes the form

$$(2) \quad \mathbf{y} \approx \mathbf{B}^\top \mathbf{x}$$

for an unknown $\mathbf{B} \in \mathbb{R}^{p \times d}$.

In its simplest form, our proposal is based on the following analogous structural assumption: given covariates $\mathbf{x} \in \mathbb{R}^p$ and a *distribution-valued response* $\nu \in \mathcal{P}(\mathbb{R}^d)$, we suppose

$$(3) \quad \nu \approx \text{Law}(\mathbf{B}^\top \mathbf{x}),$$

where \mathbf{B} is a random variable.¹

From the perspective of applications, (3) is a natural model in a number of domains. In econometrics, in the context of repeated cross-sectional data, an analyst observes covariate–response pairs for individuals stratified into groups (for example, survey waves, age bands, regions), but the individuals sampled vary across groups, so that within-individual variation cannot be tracked. Following Deaton (1985), the standard econometric approach is to aggregate respondents into cohorts and to fit a linear regression to the resulting cohort-level *averages*, yielding the so-called pseudo-panel estimator (see, e.g., Verbeek, 2017). In (3), we enrich this approach by modeling the full conditional distribution ν rather than only its first moment.

In computational biology for single-cell data, Bunne et al. (2023) propose an optimal-transport method for examining the impact of treatment interventions and

¹Our statistical analysis adopts the fixed design assumption under which \mathbf{x} is deterministic, but our results also give valid conditional guarantees under random design as well if we suppose that \mathbf{B} is independent of \mathbf{x} . In this context, (3) should be interpreted as $\nu \approx \text{Law}(\mathbf{B}^\top \mathbf{x} \mid \mathbf{x})$.

genetic perturbations on cell populations. They model the baseline state of a population of cells by a probability measure $\mu \in \mathcal{P}(\mathbb{R}^d)$, and consider the perturbed states $\nu_1, \dots, \nu_n \in \mathcal{P}(\mathbb{R}^d)$ for a population of cells that obtains after applying n different perturbations of the cells’ environment (for example, introducing a drug or using CRISPR to perform a genetic “knockout”). [Bunne et al. \(2023\)](#) posit the existence of a parametrized family of optimal transport maps $\{T_c\}_{c \in C}$ indexed by “contexts” C corresponding to the medical or genetic interventions in question, which satisfy $\nu_i = (T_{c_i})_{\#}\mu$. Supposing that context c_i is identified with a vector \mathbf{x}_i in \mathbb{R}^p and that $T_{c_i} = \sum_{j=1}^p x_{ij} T_j$ for a dictionary T_1, \dots, T_p of potential transport maps, we obtain our model by setting $\text{Law}(\mathbf{B}) = (T_1, \dots, T_p)_{\#}\mu$.

Finally, in demography, the relation between observed cohort distributions of outcomes such as mortality, morbidity, or fertility, and the unobserved heterogeneity of the underlying population is a long-standing concern. In their seminal paper, [Vaupel et al. \(1979\)](#) introduced the *frailty model*, in which each individual is endowed with an unobserved random scalar z that multiplicatively scales their mortality hazard, so that the cohort-level survival distribution arises by mixing over the population-level distribution of z . They argued that ignoring this heterogeneity systematically biases standard estimates of life expectancy and of rates of individual aging. Writing $\mathbf{x} \in \mathbb{R}^p$ for cohort-level covariates (year of birth, sex, country, education, and the like) and $\boldsymbol{\beta}$ for a random vector of individual-level traits, the principle that cohort distributions reflect a population-level distribution over individual parameters takes its simplest linear form in model (3), with $\nu = \text{Law}(\boldsymbol{\beta}^\top \mathbf{x})$.

More generally, the relation (3) may be viewed as a random-effects model ([Laird and Ware, 1982](#)). Such models are typically written in the form

$$(4) \quad \mathbf{y}_{ij} = \boldsymbol{\beta}^\top \mathbf{w}_{ij} + \mathbf{b}_i^\top \mathbf{z}_{ij} + \varepsilon_{ij},$$

where $\boldsymbol{\beta}$ are fixed (deterministic) effects, $\mathbf{b}_i \sim \mathcal{N}(0, \Sigma)$ are random effects, and $\varepsilon_{ij} \sim \mathcal{N}(0, \sigma^2)$ is independent noise. We observe that (4) is a particular case of (3), when \mathbf{B} has a (possibly non-centered) Gaussian distribution and the approximation symbol in (3) reflects the presence of additive noise.

However, our model (3) goes beyond (4) in several ways. First, we make *no* parametric assumptions on \mathbf{B} . Our model is therefore closer to the fully nonparametric random coefficient model whose study was initiated by [Beran and Hall \(1992\)](#) and developed in the multivariate setting by [Hoderlein et al. \(2010\)](#). Second, our precise statistical setting (see Section 1.1.4) adopts the “template-deformation model” ([Boissard et al., 2015](#)), in which the approximation symbol in (3) reflects possibly nonlinear distortions of $\mathbf{B}^\top \mathbf{x}$. We recover classical additive noise as a very special case, but our statistical theory is more general.

Paralleling Legendre’s least squares method for (2), we propose to fit covariate–response data $(\mathbf{x}_1, \nu_1), \dots, (\mathbf{x}_n, \nu_n)$ under (3) by solving

$$(5) \quad \min_{\mathbf{B}} \sum_{i=1}^n W_2^2(\nu_i, \text{Law}(\mathbf{B}^\top \mathbf{x}_i))$$

Here, the minimization is taken over all $\mathbb{R}^{p \times d}$ -valued random variables \mathbf{B} . This procedure extends an approach studied by [Karimi et al. \(2021\)](#) and [Karimi and Georgiou \(2021\)](#) for one-dimensional covariates. Following [Fan et al. \(2022\)](#), who studied algorithmic aspects of that approach, we call (5) *Wasserstein least squares*.

From the perspective of practical usefulness, Wasserstein least squares captures the important benefits of its Euclidean analogue:

- (1) Via (3), the solution to (5) has a natural interpretation *at the level of random variables*. This distinguishes our proposal from many other variants of distributional regression and is crucial to applications.
- (2) Convex duality implies that the optimal solution to (5) satisfies a simple first-order optimality condition directly parallel to the normal equations of Euclidean least squares. As in the Euclidean case, these normal equations show that \mathbf{B} can be interpreted as a projection of the data onto the span of the design matrix.
- (3) In the case of repeated measurements (i.e., when the covariates are duplicated), Wasserstein least squares reduces to the well-studied Wasserstein barycenter problem.

Our first main contribution is to give a new mathematical argument that Wasserstein least squares is a principled formulation of regression for probability distributions. While (5) may seem like little more than a formal analogue of the Euclidean least squares problem, we show that this is far from the case: we give an axiomatic justification for (5), establishing it as the canonical *lifting* of ordinary least squares to the space of probability measures, in the sense of Lavenant (2024), by showing it to be the unique functional of the marginal measures ν_1, \dots, ν_n satisfying certain desirable properties. In addition to providing evidence that (5) is a fundamental question, this perspective allows us to develop a convex duality theory for (5); this theory gives us both algorithmic and statistical insights into properties of optimizers of (5).

To perform a statistical analysis of (5), we formalize a model for (3) with two sources of noise. First, to capture the assumption that ν only approximately matches the law of $\mathbf{B}^\top \mathbf{x}$, we adopt the template-deformation model proposed by Boissard et al. (2015). The template-deformation model has emerged as a standard probabilistic framework for distribution-valued regression and the Wasserstein barycenter problem. In this model, the measure corresponding to the law of $\mathbf{B}^\top \mathbf{x}_i$ is corrupted by the application of a random nonlinear warping of \mathbb{R}^d ; formally, we have $\nu_i = (T_i)_\# \text{Law}(\mathbf{B}^\top \mathbf{x}_i)$ for an unobserved random cyclically monotone function T_i . Second, to capture the assumption that ν is only partially observed, we assume that the statistician only has access to i.i.d. samples from ν , and therefore that the responses ν_1, \dots, ν_n in (5) are replaced with nonparametric estimators $\hat{\nu}_1, \dots, \hat{\nu}_n$ constructed on the basis of samples.

Our full statistical model incorporates both template-deformation noise and sampling noise. We obtain finite-sample estimation guarantees for Wasserstein least squares under this model. In fact, since the Wasserstein barycenter problem is a special case of our model, our bounds imply new rates of estimation for Wasserstein barycenters as well. These results complement the rates obtained by Le Gouic et al. (2023), which hold only under very restrictive conditions on the deformations, and provide an exponential improvement on the best available general results for the template deformation model (Ahidar-Coutrix et al., 2020).

We give extensive empirical evidence for the utility of our method. We validate our approach on a number of simulated examples and conduct a new, in-depth analysis of a large public health dataset obtained from the RAND Health and Retirement Study (RAND Center for the Study of Aging, 2025). Our method

extracts insights from this study that other methods for distribution regression do not.

1.1. Our results and approach.

1.1.1. *A canonical regression method for probability distributions.* Given covariate-response pairs $(\mathbf{x}_1, \nu_1), \dots, (\mathbf{x}_n, \nu_n)$, most other approaches to regression adopt the following roadmap: 1. Identify ν_1, \dots, ν_n with elements of a metric space \mathcal{M} . 2. Develop an analogue of the least-squares problem $\min_{\mathbf{B}} \|\mathbf{y}_i - \mathbf{B}^\top \mathbf{x}_i\|^2$ by a) replacing the Euclidean distance with the metric on \mathcal{M} and b) replacing the linear function $\mathbf{x} \mapsto \mathbf{B}^\top \mathbf{x}$ with a suitable generalization to \mathcal{M} . We review these approaches in more detail in Section 1.2.

The statistical properties and implications of this model depend to a great extent on the design choices in the above description. (See Petersen et al., 2022; Song et al., 2026 for two recent review articles.) Moreover, some approaches (such as those based on mean embeddings in reproducing kernel Hilbert spaces) require choosing additional tuning parameters. While this flexibility can be appealing in some applications, it raises the question of whether there exists a regression method for this setting that does not involve any additional choices.

We take a different approach, inspired by Lavenant (2024), which identifies a canonical method through an axiomatic argument. The standard Euclidean least squares problem is based on evaluating the function

$$E(\mathbf{y}_1, \dots, \mathbf{y}_n) = \min_{\mathbf{B} \in \mathbb{R}^{p \times d}} \frac{1}{n} \sum_{i=1}^n \|\mathbf{y}_i - \mathbf{B}^\top \mathbf{x}_i\|^2.$$

We propose to define a new functional $\mathcal{E}(\nu_1, \dots, \nu_n)$ which is uniquely characterized as the *convex extension* (Hiriart-Urruty and Lemaréchal, 1993; Rockafellar, 1970) of E to the space of probability measures. The construction, also called the convex envelope or convex hull, is the analyst’s standard tool for extending convex functions to larger spaces. Though this definition is not explicit, we show that in fact $\mathcal{E}(\nu_1, \dots, \nu_n)$ is *exactly* equal to (5). This provides a new, canonical construction of linear regression on Wasserstein space, and reveals Wasserstein least squares to be, from the viewpoint of convex analysis, the correct analogue of Euclidean least squares for distribution-valued responses.

Our axiomatic justification of Wasserstein least squares extends beyond the linear regression case and applies to general nonparametric regression problems involving distributions, see Section 2.

1.1.2. *Multimarginal formulations and convex duality.* A benefit of the formulation of Wasserstein least squares that we have adopted is its close connection to convex analysis and the theory of optimal transportation. We obtain several results generalizing the theory of Wasserstein barycenters developed by Agueh and Carlier (2011). First, we show that (5) possesses an equivalent “multimarginal” formulation as an optimization problem over the space of couplings of the n measures ν_1, \dots, ν_n . This parallels the analogous multimarginal formulation of the Wasserstein barycenter problem, and also clarifies the interpretation of our procedure: as we show in Proposition 1, Wasserstein least squares finds a coupling between the response measures that maximizes the explained variance of the resulting linear model.

Like the optimal transportation problem itself, we show that the Wasserstein least squares problem also possesses a dual formulation (Theorem 2). This duality theory provides a criterion under which (5) has a unique solution and a natural first-order optimality condition for (5): writing $\nabla\varphi_i$ for the Brenier map from $\text{Law}(\mathbf{B}^\top \mathbf{x}_i)$ to ν_i , Theorem 6 shows that the optimal \mathbf{B} satisfies

$$(6) \quad \sum_{i=1}^n \mathbf{x}_i (\nabla\varphi_i(\mathbf{B}^\top \mathbf{x}_i))^\top = \sum_{i=1}^n \mathbf{x}_i \mathbf{x}_i^\top \mathbf{B} \quad \text{a.s.}$$

Note that $\nabla\varphi_i(\mathbf{B}^\top \mathbf{x}_i) \sim \nu_i$. This equation is the exact Wasserstein analogue of the celebrated normal equations for linear regression:

$$\mathbf{X}^\top \mathbf{Y} = \mathbf{X}^\top \mathbf{X} \mathbf{B}.$$

As in the case of Euclidean least squares, the normal equations offer a powerful geometric interpretation of Wasserstein least squares: the optimal \mathbf{B} is the projection of the random variables $(\nabla\varphi_i(\mathbf{B}^\top \mathbf{x}_i))_{i=1}^n$ onto the column space of \mathbf{X} .

1.1.3. *Algorithms.* Like many optimization problems involving measures, the Wasserstein least squares problem is computationally challenging. We propose a gradient flow algorithm whose stationary points are precisely solutions to (6). This algorithm has a concrete interpretation via (6): at each step, it updates the law of the random variable \mathbf{B} to bring it closer to the projection of $(\nabla\varphi_i(\mathbf{B}^\top \mathbf{x}_i))_{i=1}^n$. As with many optimization problems in Wasserstein space (Altschuler et al., 2021; Chewi et al., 2020, 2025), the objective function in (5) is not geodesically convex, and we cannot rule out the possibility of local minima; nevertheless, our approach is successful in practice. We view obtaining rigorous convergence guarantees for our algorithm as an important open problem.

This algorithm is particularly tractable in two special cases: when each response ν_i is a Gaussian distribution (with arbitrary mean and covariance), or when each response is a univariate distribution. In the former case, we show that the optimal \mathbf{B} may be chosen to be Gaussian as well. That fact implies that the optimization problem may be formulated on the finite-dimensional Bures–Wasserstein manifold. The benefit of this formulation is that the gradient updates may be computed in closed form. In the latter case, when each ν_i is univariate, the special structure of $\mathcal{P}(\mathbb{R})$ makes the Brenier maps in (6) easy to compute. As a result, the resulting gradient descent steps are easy to implement via particle methods, at a cost of $O(nM \log M)$ per iteration, where M is the number of particles.

1.1.4. *Rates of estimation under the template deformation model.* Having developed the Wasserstein least squares approach, we analyze its performance under the template deformation model (Boissard et al., 2015; Panaretos and Zemel, 2020; Zemel and Panaretos, 2019). We suppose that for $i = 1, \dots, n$ and $j = 1, \dots, m$, we observe samples

$$(7) \quad Y_{i,j} = \nabla\phi_i(\mathbf{B}_{i,j}^\top \mathbf{x}_i),$$

where $\mathbf{B}_{i,j}$ are independent copies of an unobserved random variable \mathbf{B} , and $\nabla\phi_i$ are independent copies of the gradient of an unobserved random convex function, satisfying $\mathbb{E}[\nabla\phi_i(\mathbf{y})] = \mathbf{y}$ for all $\mathbf{y} \in \mathbb{R}^d$. When $\nabla\phi_i$ is the function $\mathbf{y} \mapsto \mathbf{y} + \varepsilon_i$ for mean-zero ε_i , (7) is a standard random-coefficient linear model Longford (1993). In general, however, (7) allows for noise in the form of nonlinear “warpings” of \mathbb{R}^d .

Under the assumption that ϕ_i is almost surely smooth and strongly convex, we show that the Wasserstein least squares solution $\widehat{\mathbf{B}}$ satisfies

$$(8) \quad \mathbb{E} \left[\frac{1}{n} \sum_{i=1}^n W_2^2(\text{Law}(\mathbf{B}^\top \mathbf{x}_i), \text{Law}(\widehat{\mathbf{B}}^\top \mathbf{x}_i)) \right] \lesssim n^{-1/2} + m^{-2/d},$$

for $d > 4$, where the implicit constant depends on p , d , and the smoothness and strong convexity bounds for the random deformations. The error bound in (8) reflects the two sources of noise in the model: the first term reflects the problem of estimating the law of \mathbf{B} in the presence of the noise arising from the template deformations $\nabla\phi$, and the second reflects the sampling noise inherent in (7). When $m \rightarrow \infty$ (which corresponds to the case where $\nu_i = (\nabla\phi_i)_\# \text{Law}(\mathbf{B}^\top \mathbf{x}_i)$ is fully observed), (8) shows that the error decays at the $n^{-1/2}$ rate.

As a special case, taking $p = 1$ and $\mathbf{x}_1 = \dots = \mathbf{x}_n$, (8) yields new rates for the problem of estimating Wasserstein barycenters in the template deformation model. Under our assumptions, the best general results for estimation of Wasserstein barycenters, due to [Ahidar-Coutrix et al. \(2020\)](#), prove a rate of convergence at the rate $n^{-1/d}$, exhibiting a steep curse of dimensionality. In the very special case that each ϕ_i is α -strongly convex and β -smooth where $\beta - \alpha < 1$, [Le Gouic et al. \(2023\)](#) prove the remarkable fact that the error decreases at the rate n^{-1} , with no dependence on the dimension. However, their bounds become vacuous when $\beta - \alpha \geq 1$. Our bound is an exponential improvement over the general state of the art; though we fail to recover the sharp bound of [Le Gouic et al. \(2023\)](#) when $\beta - \alpha < 1$, our $n^{-1/2}$ rate applies to strongly convex and smooth deformations for any $\alpha, \beta \in (0, \infty)$.

1.1.5. Empirical results. We apply this framework to Body Mass Index data from the RAND Health and Retirement Study ([RAND Center for the Study of Aging, 2025](#)), a nationally representative longitudinal survey of approximately 45,000 U.S. adults observed across 16 biennial waves (1992–2022) ([Gutin, 2018](#); [Ward et al., 2019](#); [Yang et al., 2021](#)). Treating each demographic cell (birth cohort \times survey wave \times gender) as a distributional observation yields $n = 164$ BMI distributions, which we model with the quadratic design $\mathbf{x}_i = (1, \tilde{a}_i, \tilde{a}_i^2, \tilde{c}_i, \tilde{g}_i)^\top$ encoding normalized age, birth cohort, and gender. The template deformation noise model (**WLR**) makes no distributional assumption on the individual-level heterogeneity beyond the regularity conditions C1–C3, so the analysis is free of the Gaussian random-effect assumption that underpins classical mixed-effects analyses of these data ([Laird and Ware, 1982](#); [Yang et al., 2021](#)).

We estimate Q^* using Algorithm 2 with $M = 20,000$ particles. The estimator returns the full joint distribution over the coefficient vector

$$\boldsymbol{\beta} = (\beta_0, \beta_{\text{age}}, \beta_{\text{age}^2}, \beta_{\text{cohort}}, \beta_{\text{gender}})^\top,$$

recovering the coupling structure of the random effects without parametric assumptions. This joint distribution enables a form of conditional inference that is unavailable in prior-distributional regression methods. Since each particle $\boldsymbol{\beta}_m \sim \widehat{Q}$ represents a plausible individual trajectory under the fitted model, conditioning on an observed BMI value amounts to asking which trajectories in the estimated population are consistent with that observation; the retained subset then predicts the future distribution of BMI for that subpopulation. This conditional forecast is meaningful precisely because \widehat{Q} captures the true population heterogeneity, a claim

that we assess directly by comparing predicted trajectory bands against the actual observed HRS cohort paths in Section 5. We compare our approach to Global Fréchet regression (Petersen and Müller, 2019) and show that Wasserstein least squares substantially outperforms it in coverage under sequential conditioning, and is the only method capable of representing all clinically relevant outcome scenarios; see Section 5 for the full analysis.

We further validate Wasserstein least squares on two synthetic settings (Section B) in which the Wasserstein least squares model class strictly contains the Fréchet family as a special case, demonstrating that the empirical advantage is a structural consequence of the broader scope of our model.

1.2. Related work. There is a significant literature on designing regression methods for distribution-valued data. One initial challenge is a lack of linear structure on the space of probability measures, which necessitates either mapping distributions into a linear space (as is typical in functional data analysis, Hsing and Eubank, 2015), or simply treating them as “random objects” in a metric space (Müller, 2016). There are challenges with either approach. In the former, transformation-based, approach, the mapping is rarely invertible, which makes interpreting the output of estimation procedures in the linear space challenging; in the latter, metric space, approach, the loss of linear structure can cause difficulties for computation and theoretical analysis.

As Petersen et al. (2022) make clear, regression methods under either approach may be unified using the *global Fréchet regression* framework of Petersen and Müller (2019): given a metric d defined between probability measures and data $(\mathbf{x}_1, \nu_1), \dots, (\mathbf{x}_n, \nu_n)$, the predicted output for a new covariate \mathbf{x} is given by

$$(9) \quad \underset{\nu}{\operatorname{argmin}} \frac{1}{n} \sum_{i=1}^n w_i(\mathbf{x}) d^2(\nu_i, \nu),$$

where w_i are (possibly negative) weights designed so that, if ν_i and ν are replaced by vectors and d is the Euclidean metric, the solution to (9) coincides with the solution to standard Euclidean least squares. Different choices of the metric d give rise to different generalizations of this approach.

When d is the Wasserstein metric on the space of univariate measures, we obtain the Wasserstein regression method studied by Petersen and Müller (2019) and Petersen et al. (2021). These works propose a statistical model under which they can study estimation and testing problems on the Wasserstein space; the focus on one dimensional measures plays an essential role in Petersen et al. (2021) in particular, since on \mathbb{R} the Wasserstein metric agrees with an L^2 metric on quantile functions.

When the covariates are also distributions, one obtains a distribution-to-distribution regression problem. Such problems have been studied in detail by Ghodrati and Panaretos (2022) and Chen et al. (2023). Once again, a key challenge lies in defining a suitable class of maps between covariates and responses. Chen et al. (2023) do so by employing the linear structure of the tangent space to a measure in the Wasserstein geometry, whereas Ghodrati and Panaretos (2022) study a “shape constraint” in the form of a monotonicity assumption. A detailed comparison between these two models is provided in Section 3.3 of Ghodrati and Panaretos (2022).

What these methods have in common is their focus on *probability measures* as the key objects of interest, either as covariates or responses. As explained above,

our approach is philosophically different: the primary interpretation of our methods is in terms of *random variables*. One benefit of our perspective is that it leverages a unique feature of the Wasserstein distance as opposed to other metrics, namely, that couplings between random variables play a central role. As we show in Section 5, it is possible to interpret the approach of Petersen and Müller (2019) in terms of random variables in special cases, but their model corresponds to a very rigid constraint on these variables’ joint distribution. For example, in the univariate Gaussian case with a single covariate, global Fréchet regression corresponds to the model $Q_x = \mathcal{N}(\mu_0 + \beta x, (\sigma_0 + \gamma x)^2)$ (Petersen and Müller, 2019, §6.2), whereas our model corresponds to $Q_x = \mathcal{N}(\mu_0 + \beta x, \sigma_0^2 + \gamma^2 x^2 + 2\rho x)$ for any $|\rho| \leq \sigma_0 \gamma$, which is strictly more flexible. This additional freedom has important benefits in applications.

An important precedent for our work is the proposals of Karimi et al. (2021) and Karimi and Georgiou (2021). Their focus was on “utilizing general curves in a Euclidean setting and lifting them to corresponding measure-valued curves in Wasserstein space”; accordingly, they viewed their method as a way to generalize the “straight-line geometry” of simple linear regression. When $p = 1$ (i.e., when there is only a single covariate), our model reduces to theirs. Their theoretical results include deriving a multimarginal formulation (akin to our Proposition 1) and matrix formulation in the Gaussian case (akin to our Lemma 9). Our full axiomatic justification, duality theory, and statistical analysis are new.

Our model also extends statistical work on the Wasserstein barycenter problem under the template deformation model (Ahidar-Coutrix et al., 2020; Le Gouic et al., 2023; Zemel and Panaretos, 2019). Outside of special cases (for example, one-dimensional measures), the best general rates are due to Ahidar-Coutrix et al. (2020), who show that, under our condition C3, barycenters on $\mathcal{P}_2(\mathbb{R}^d)$ can be estimated at the rate $n^{-1/d'}$ for any $d' > d$. A striking improvement of this result is due to Le Gouic et al. (2023): under condition C3 with $\beta - \alpha < 1$, barycenters can be estimated at the parametric rate $1/n$, with no dependence on the ambient dimension. Our results are in some sense intermediate between these regimes: we show that estimation at the rate $\sqrt{d/n}$ is possible for any positive α and β . While we fail to recover the sharp rate obtained by Le Gouic et al. (2023) when β and α are very close, our result applies in far greater generality and is an exponential improvement over the general bounds of Ahidar-Coutrix et al. (2020).

2. WASSERSTEIN LEAST SQUARES AS A LIFTING OF EUCLIDEAN LEAST SQUARES

2.1. Lifting via convex extension. The goal of this section is to describe the canonical lifting procedure that allows us to extend the least squares problem to probability measures, following a strategy developed by Lavenant (2024). As described in the introduction, we first view the method of least squares as a purely deterministic optimization problem, an analogue of which we will develop for the Wasserstein space. We then describe and analyze a statistical model under which our lifted least squares objective serves as a natural estimation procedure.

Consider a generic nonparametric regression problem with fixed nonzero covariates $\{\mathbf{x}_i\}_{i=1}^n \subseteq \mathbb{R}^p$. Given a candidate class \mathcal{F} of regression functions from \mathbb{R}^p to \mathbb{R}^d and responses $\mathbf{y}_1, \dots, \mathbf{y}_n$, the method of least squares amounts to evaluating

$E : (\mathbb{R}^d)^n \rightarrow \mathbb{R}$ given by

$$(10) \quad E(\mathbf{y}_1, \dots, \mathbf{y}_n) = \min_{f \in \mathcal{F}} \frac{1}{n} \sum_{i=1}^n \|\mathbf{y}_i - f(\mathbf{x}_i)\|_2^2.$$

Throughout, we will adopt one of two main assumptions on \mathcal{F} .

Assumption 1. \mathcal{F} is a non-empty, convex, compact subset of $C(\mathbb{R}^p; \mathbb{R}^d)$.

Assumption 2. \mathcal{F} is the set of all linear functions from \mathbb{R}^p to \mathbb{R}^d .

Under either Assumption 1 or Assumption 2, minimizers for the least squares problem exist in \mathcal{F} , which justifies the use of \min in (10). We call E the *Euclidean least squares functional*, to indicate that it is defined on the Euclidean space $(\mathbb{R}^d)^{\otimes n}$.

Our goal is to define a new Wasserstein least squares functional $\mathcal{E} : \mathcal{P}_2(\mathbb{R}^d)^n \rightarrow \mathbb{R}$, which is an analogue of (10) defined on the Wasserstein space. Inspired by the properties of E , we shall require that \mathcal{E} satisfy two requirements:

- (R1) $\mathcal{E}(\delta_{\mathbf{y}_1}, \dots, \delta_{\mathbf{y}_n}) = E(\mathbf{y}_1, \dots, \mathbf{y}_n)$. That is, in the special case where each of the measures ν_i is a Dirac at a single point \mathbf{y}_i , the lifted functional should reduce to its Euclidean counterpart (10).
- (R2) $\mathcal{E}(\nu_1, \dots, \nu_n)$ is a convex, lower-semicontinuous function of (ν_1, \dots, ν_n) .²

These two requirements are natural in light of our statistical goals. The first ensures that \mathcal{E} genuinely captures the features of the original Euclidean least squares functional: any proposed lifting that failed to satisfy this requirement would not be a plausible method of extending E to the Wasserstein space. The second, convexity and continuity, is a fundamental property of E , and is clearly desirable for mathematical analysis of the regression problem. As we shall see, this requirement also plays a crucial role in the development of convex duality for the Wasserstein least squares functional, see Section 2.2.

These two requirements alone are not sufficient to uniquely specify \mathcal{E} , nor to make it useful; for example, on a compact set, the definition $\mathcal{E}(\nu_1, \dots, \nu_n) = E(\int x d\nu_1, \dots, \int x d\nu_n)$ which simply performs Euclidean least squares on the *means* of the measures satisfies R1 and R2, but it throws away too much information, since it fails to distinguish between different measures with the same centering. This example shows that \mathcal{E} can fail to be meaningful if it does not usefully discriminate between different inputs. Motivated by this observation, we define \mathcal{E} to be “as discriminating as possible” by setting

$$(11) \quad \mathcal{E}(\nu_1, \dots, \nu_n) = \sup_{\Phi: \Phi \text{ satisfies R1 \& R2}} \Phi(\nu_1, \dots, \nu_n).$$

Equivalently, \mathcal{E} is the *convex extension* or *convex hull* of the Euclidean functional E , which is the canonical way of constructing convex functions taking prescribed values at certain points (Hiriart-Urruty and Lemaréchal, 1993, IV.2.5, see also Bing et al., 2022). Crucially, since both R1 and R2 are preserved under pointwise suprema, \mathcal{E} defined by (11) itself satisfies our main requirements. Though this is good evidence that \mathcal{E} is a natural object, unfortunately, the definition in (11) is not explicit. Our

²We stress that this convexity is with respect to the *linear* structure of the space $\mathcal{P}(\mathbb{R}^d)$ (equipped with the topology of narrow convergence), that is, given $\nu_1, \dots, \nu_n, \nu'_1, \dots, \nu'_n \in \mathcal{P}_2(\mathbb{R}^d)$, we require

$$\mathcal{E}(\lambda\nu_1 + (1-\lambda)\nu'_1, \dots, \lambda\nu_n + (1-\lambda)\nu'_n) \leq \lambda\mathcal{E}(\nu_1, \dots, \nu_n) + (1-\lambda)\mathcal{E}(\nu'_1, \dots, \nu'_n) \quad \forall \lambda \in [0, 1].$$

We discuss geodesic convexity (with respect to the Wasserstein geometry) in Remark 2, below.

main theorem in this section gives two equivalent characterizations for \mathcal{E} in terms of optimal transport problems, which provides further justification for it as our primary object of study.

To state these, we need two pieces of notation. First, given $\nu_1, \dots, \nu_n \in \mathcal{P}_2(\mathbb{R}^d)$, write $\Pi(\nu_1, \dots, \nu_n) \in \mathcal{P}_2((\mathbb{R}^d)^n)$ for the set of multi-marginal couplings: joint distributions whose d -dimensional marginals agree with ν_1, \dots, ν_n , respectively. Second, given a Borel probability measure Q on \mathcal{F} and $\mathbf{x} \in \mathbb{R}^p$, denote by $Q_{\mathbf{x}}$ the probability measure on \mathbb{R}^d obtained as the pushforward of Q by the map $f \mapsto f(\mathbf{x})$.³

The following result shows that (11) can be equivalently expressed either as a multi-marginal optimal transport problem over $\Pi(\nu_1, \dots, \nu_n)$, or as an optimization problem over probability measures on \mathcal{F} .

Theorem 1. *Adopt either Assumption 1 or Assumption 2. Let \mathcal{E} be the convex extension of E defined via (11), and let $\nu_1, \dots, \nu_n \in \mathcal{P}_2(\mathbb{R}^d)$. Then*

$$(12) \quad \mathcal{E}(\nu_1, \dots, \nu_n) = \min_{P \in \Pi(\nu_1, \dots, \nu_n)} \int E(\mathbf{y}_1, \dots, \mathbf{y}_n) dP(\mathbf{y}_1, \dots, \mathbf{y}_n)$$

$$(13) \quad = \min_{Q \in \mathcal{P}(\mathcal{F})} \frac{1}{n} \sum_{i=1}^n W_2^2(\nu_i, Q_{\mathbf{x}_i}).$$

Part of the content of Theorem 1 is that the minima in both (12) and (13) are attained. In the linear case (Assumption 2), $\mathcal{P}(\mathcal{F})$ is exactly the set of laws of $\mathbb{R}^{p \times d}$ -valued random variables, recovering the basic Wasserstein least squares problem from the introduction.

The expression given by (13) is the Wasserstein least squares function promised in the introduction. Remarkably, despite the abstractness of the definition (11), the equivalent version in (13) is a direct Wasserstein space analogue of E , with the ℓ^2 distance replaced by the W_2 distance and the optimization set \mathcal{F} replaced by the set $\mathcal{P}(\mathcal{F})$ of probability measures over \mathcal{F} . The axiomatic justification of \mathcal{E} via (11) and its more interpretable expressions given by Theorem 1 together make the case that (13) is a canonical formulation of least squares regression on the Wasserstein space.

Note that, unlike the Euclidean least squares problem, the solution to (13) is not unique in general, since the objective function involves only the marginal distributions $Q_{\mathbf{x}_1}, \dots, Q_{\mathbf{x}_n}$. However, in Proposition 2 we will give a natural condition under which these marginal distributions are uniquely identified.

2.2. Convex duality. In this section, we establish that the functional \mathcal{E} , which is given by a convex minimization problem, also possesses a dual formulation as a maximization problem. This formulation is crucial to the development of the algorithms we present in Section 3 as well as our statistical results in Section 4.

Our proof is based on an extension of the strategy pioneered by [Agueh and Carlier \(2011\)](#) for showing a similar dual formulation for the Wasserstein barycenter problem.

Given $\psi : \mathcal{F} \rightarrow \mathbb{R}$ and $i \in [n]$, we denote by $S_i\psi : \mathbb{R}^d \rightarrow \mathbb{R}$ the function

$$(14) \quad S_i\psi(\mathbf{y}) = \inf_{f \in \mathcal{F}} \|\mathbf{y} - f(\mathbf{x}_i)\|^2 - \psi(f).$$

³We equip \mathcal{F} with the compact-open topology, for which the pointwise evaluation maps are measurable.

Theorem 2. *Adopt either Assumption 1 or Assumption 2. If $\nu_1, \dots, \nu_n \in \mathcal{P}_2(\mathbb{R}^d)$, then*

$$(15) \quad \mathcal{E}(\nu_1, \dots, \nu_n) = \sup \left\{ \frac{1}{n} \sum_{i=1}^n \int S_i \psi_i d\nu_i : \psi_1, \dots, \psi_n \in C(\mathcal{F}), \sum_{i=1}^n \psi_i = 0 \right\}.$$

Note that for any $\psi \in C(\mathcal{F})$, the function $S_i \psi$ satisfies $S_i \psi(\mathbf{y}) \leq C(1 + \|\mathbf{y}\|^2)$ for some $C > 0$, and since $\nu_i \in \mathcal{P}_2(\mathbb{R}^d)$, this ensures that the integral appearing in (15) is well defined in $[-\infty, \infty)$.

2.3. Wasserstein linear least squares. In this section, we work under Assumption 2, where the set \mathcal{F} consists of *linear* functions from \mathbb{R}^p to \mathbb{R}^d , in which case the Wasserstein least squares problem furnishes a canonical linear regression methodology for the Wasserstein space.

We identify the set \mathcal{F} with the set of real $p \times d$ matrices, with $\mathbf{B} \in \mathbb{R}^{p \times d}$ giving rise to the linear function $\mathbf{x} \mapsto \mathbf{B}^\top \mathbf{x}$.

For convenience, we restate Theorem 1 explicitly for the linear case.

Theorem 3. *The convex extension of the Euclidean least squares functional*

$$E(\mathbf{y}_1, \dots, \mathbf{y}_n) = \min_{\mathbf{B} \in \mathbb{R}^{p \times d}} \frac{1}{n} \sum_{i=1}^n \|\mathbf{y}_i - \mathbf{B}^\top \mathbf{x}_i\|^2$$

is given by

$$(16) \quad \begin{aligned} \mathcal{E}(\nu_1, \dots, \nu_n) &= \min_{P \in \Pi(\nu_1, \dots, \nu_n)} \int_{(\mathbb{R}^d)^n} \min_{\mathbf{B} \in \mathbb{R}^{p \times d}} \frac{1}{n} \sum_{i=1}^n \|\mathbf{y}_i - \mathbf{B}^\top \mathbf{x}_i\|^2 dP(\mathbf{y}_1, \dots, \mathbf{y}_n) \\ (17) \quad &= \min_{Q \in \mathcal{P}(\mathbb{R}^{p \times d})} \frac{1}{n} \sum_{i=1}^n \min_{\substack{\mathbf{Y}_i \sim \nu_i \\ \mathbf{B} \sim Q}} \mathbb{E} \|\mathbf{Y}_i - \mathbf{B}^\top \mathbf{x}_i\|^2. \end{aligned}$$

Since the inner minimization in (16) is the standard linear regression problem, it can be solved explicitly. Collecting the covariates into the design matrix $\mathbf{X} \in \mathbb{R}^{n \times p}$ and writing $\mathbf{Y} = (\mathbf{y}_1 | \dots | \mathbf{y}_n)^\top \in \mathbb{R}^{n \times d}$, we recall that the minimal norm solution for Euclidean least squares is

$$(18) \quad \mathbf{B}^* = (\mathbf{X}^\top \mathbf{X})^+ \mathbf{X}^\top \mathbf{Y} \in \operatorname{argmin}_{\mathbf{B} \in \mathbb{R}^{p \times d}} \frac{1}{n} \sum_{i=1}^n \|\mathbf{y}_i - \mathbf{B}^\top \mathbf{x}_i\|^2.$$

When $(\mathbf{y}_1, \dots, \mathbf{y}_n) \sim P$, this induces a corresponding distribution for \mathbf{Y} and thereby for \mathbf{B}^* via (18). We therefore have the following alternative expression for (16).

Proposition 1. *In the same setting as Theorem 3,*

$$(19) \quad \mathcal{E}(\nu_1, \dots, \nu_n) = \min_{P \in \Pi(\nu_1, \dots, \nu_n)} \int_{(\mathbb{R}^d)^n} \frac{1}{n} \sum_{i=1}^n \|\mathbf{y}_i - (\mathbf{B}^*)^\top \mathbf{x}_i\|^2 dP(\mathbf{y}_1, \dots, \mathbf{y}_n)$$

$$(20) \quad = \min_{P \in \Pi(\nu_1, \dots, \nu_n)} \int_{(\mathbb{R}^d)^n} \frac{1}{n} \|\mathbf{Y}\|_F^2 - \frac{1}{n} \|((\mathbf{X}^\top \mathbf{X})^+)^{1/2} \mathbf{X}^\top \mathbf{Y}\|_F^2 dP$$

In particular, since $\int \|\mathbf{Y}\|_F^2 dP$ depends only on the marginals ν_1, \dots, ν_n , solutions to (16) agree with those of

$$(21) \quad \max_{P \in \Pi(\nu_1, \dots, \nu_n)} \int_{(\mathbb{R}^d)^n} \|((\mathbf{X}^\top \mathbf{X})^+)^{1/2} \mathbf{X}^\top \mathbf{Y}\|_F^2 dP.$$

We stress again that, in (21), the coupling P determines the distribution of \mathbf{Y} . Recall that in Euclidean linear least squares, the quantity $\|((\mathbf{X}^\top \mathbf{X})^+)^{1/2} \mathbf{X}^\top \mathbf{Y}\|_F^2$ measures the *explained variance*, the variance in the responses attributable to the covariates. This expression gives a natural geometric interpretation to the Wasserstein linear least squares problem: it seeks a coupling between ν_1, \dots, ν_n that maximizes the predictive power of the linear model as measured by explained variance.

We can also exploit the linear structure to obtain stronger duality results under Assumption 2.

Theorem 4. *Adopt Assumption 2. If $\nu_1, \dots, \nu_n \in \mathcal{P}_2(\mathbb{R}^d)$, then the supremum in (15) is attained.*

Examining the optimality conditions of (15), we obtain a characterization of optimal primal and dual solutions for Wasserstein least squares.

Theorem 5. *Let $\nu_1, \dots, \nu_n \in \mathcal{P}_2(\mathbb{R}^d)$, and let Q be an optimal solution to (17). Then there exist convex functions $\varphi_1, \dots, \varphi_n$ such that:*

- (1) *For each $i \in [n]$, the pair (φ_i, φ_i^*) are optimal Brenier potentials for $(Q_{\mathbf{x}_i}, \nu_i)$; i.e., φ_i satisfies*

$$(22) \quad W_2^2(\nu_i, Q_{\mathbf{x}_i}) = \int (\|\cdot\|^2 - 2\varphi_i^*) d\nu_i + \int (\|\cdot\|^2 - 2\varphi_i) dQ_{\mathbf{x}_i}$$

- (2) *The functions satisfy*

$$(23) \quad \frac{1}{n} \sum_{i=1}^n \varphi_i(\mathbf{B}^\top \mathbf{x}_i) \leq \frac{1}{n} \sum_{i=1}^n \frac{\|\mathbf{B}^\top \mathbf{x}_i\|^2}{2},$$

with equality Q -a.s.

Conversely, if Q is such that there exist $\varphi_1, \dots, \varphi_n$ satisfying the above conditions, then Q is an optimal solution to (13).

In light of Theorem 5, we call any collection $(\varphi_1, \dots, \varphi_n)$ satisfying conditions 1 and 2 above *optimal dual solutions* to the Wasserstein least squares problem.

Theorem 5 also gives a criterion under which the marginal distributions of an optimal solution are uniquely identified.

Proposition 2. *Suppose that ν_1, \dots, ν_n are absolutely continuous with respect to the Lebesgue measure. If Q and Q' are any two optimal solutions to (13), then $Q_{\mathbf{x}_i} = Q'_{\mathbf{x}_i}$ for each $i \in [n]$.*

Proof. Let (ψ_1, \dots, ψ_n) solve (15), and let $\varphi_1, \dots, \varphi_n$ be constructed by (76). Then Theorem 5 shows that (φ_i, φ_i^*) are optimal Brenier potentials for both $(Q_{\mathbf{x}_i}, \nu_i)$ and $(Q'_{\mathbf{x}_i}, \nu_i)$ for each $i = 1, \dots, n$. In particular, since ν_i is absolutely continuous, this fact implies that both $Q_{\mathbf{x}_i}$ and $Q'_{\mathbf{x}_i}$ are equal to $(\nabla \varphi_i^*)_{\#} \nu_i$, hence they agree. \square

Finally, Theorem 5 gives a characterization of optimality exactly equivalent to the normal equations in linear regression.

Theorem 6. *Let $\nu_1, \dots, \nu_n \in \mathcal{P}_2(\mathbb{R}^d)$ and let Q be an optimal solution to (17). Then there exist convex functions $\varphi_1, \dots, \varphi_n$ such that (φ_i, φ_i^*) are optimal Brenier potentials for $(Q_{\mathbf{x}_i}, \nu_i)$ for each $i \in [n]$, and*

$$(24) \quad \frac{1}{n} \sum_{i=1}^n \mathbf{x}_i (\nabla \varphi_i(\mathbf{B}^\top \mathbf{x}_i))^\top = \Sigma_{XX} \mathbf{B} \quad \forall \mathbf{B} \in \text{supp}(Q).$$

In particular, φ_i is differentiable on $\text{supp}(Q_{\mathbf{x}_i})$.

Since φ_i is differentiable on $\text{supp}(Q_{\mathbf{x}_i})$ and φ_i is an optimal Brenier potential, if we write $\nabla\varphi_i(\mathbf{B}^\top \mathbf{x}_i) = \mathbf{Y}_i$, then $\mathbf{Y}_i \sim \nu_i$ when $\mathbf{B} \sim Q$. Writing $\nabla\varphi_i(\mathbf{B}^\top \mathbf{x}_i) = \mathbf{Y}_i$ and defining Σ_{YX} and Σ_{XX} as above, we observe that $\mathbf{Y}_i \sim \nu_i$ and that (24) is equivalent to

$$(25) \quad \Sigma_{YX} = \Sigma_{XX} \mathbf{B} \quad \text{a.s.}$$

However, in contrast to the Euclidean case, (25) alone does not specify the law of \mathbf{B} , since the law of Σ_{XY} depends on P , the coupling that solves (16).

The proof of Theorem 6 reveals that the gradient of the Wasserstein least squares objective vanishes precisely when the normal equations hold. The following lemma (proved in Section F) makes this explicit and is the key ingredient for the algorithms of Section 3.

Lemma 1. *Let Q be absolutely continuous. The W_2 -gradient of $G(Q) = \frac{1}{n} \sum_{i=1}^n W_2^2(Q_{\mathbf{x}_i}, \nu_i)$ with respect to Q is the map $\mathbb{W}_Q G(Q) \in L^2(\mathbb{R}^{p \times d}, \mathbb{R}^{p \times d}; Q)$ with assignment rule*

$$(26) \quad \mathbf{B} \mapsto -\frac{1}{n} \sum_{i=1}^n (\mathbf{x}_i (\nabla\varphi_i(\mathbf{B}^\top \mathbf{x}_i))^\top - \mathbf{x}_i \mathbf{x}_i^\top \mathbf{B})$$

for every $\mathbf{B} \in \text{supp}(Q)$, where φ_i are the optimal Brenier potentials for $(Q_{\mathbf{x}_i}, \nu_i)$. In particular, $\mathbb{W}_Q G(Q) = 0$ Q -a.s. if and only if the normal equations (24) hold.

Remark 1. *In the case where all the covariates are equal, (17) is a barycenter problem in Wasserstein space (Agueh and Carlier, 2011). In this case, (16) is the well known multimarginal formulation of the barycenter problem, and Theorems 4 and 5 recover the duality results for barycenters obtained by Agueh and Carlier (Agueh and Carlier, 2011). Our statistical results for Wasserstein least squares regression will supply new convergence results for barycenters as corollaries, see Section 4.1.*

3. GRADIENT DESCENT ALGORITHMS

A canonical approach for designing algorithms to solve optimization problems in Wasserstein space is to discretize the gradient flow of the associated objective function along Wasserstein geodesics; see Chapter 6 of Chewi et al. (2025) for a sampler of applications. We apply this strategy to the Wasserstein least squares objective introduced in Section 2.3; the full first-order geometry of G is developed in Section F. The two algorithms derived below are the computational workhorses of the experiments in Section 5.

Recall that the W_2 -gradient flow of G , the $\mathcal{P}_{2,\text{a.c.}}(\mathbb{R}^{p \times d})$ -variable objective function of (17), with starting measure Q is the curve of measures $(Q^t)_{t \geq 0}$ that solves the system

$$(27) \quad \begin{cases} \dot{Q}^t = -\mathbb{W}_{Q^t} G(Q^t) \\ Q^0 = Q, \end{cases}$$

The Wasserstein gradient descent scheme for G with starting measure $Q \in \mathcal{P}_2(\mathbb{R}^{p \times d})$, the corresponding discretization of (27), is

$$(28) \quad \begin{cases} Q^{k+1} := \exp_{Q^k}(-\tau \mathbb{W}_{Q^k} G(Q^k)) \quad \forall k > 0 \text{ and } k \in \mathbb{N}, \\ Q^0 := Q. \end{cases}$$

where $\exp_{Q^k} : T_{Q^k}\mathcal{P}_2(\mathbb{R}^{p \times d}) \rightarrow \mathcal{P}_2(\mathbb{R}^{p \times d})$ is the exponential map with assignment rule

$$(29) \quad \exp_{Q^k}(v) := (\text{Id} + v)_\# Q^k \quad \forall v \in T_{Q^k}\mathcal{P}(\mathbb{R}^{p \times d}).$$

Lemma 1 gives

$$(30) \quad \nabla_{\dot{Q}^t} G(Q^t) = -\frac{1}{n} \sum_{i=1}^n (\mathbf{x}_i (\nabla \varphi_i^t(\mathbf{B}^\top \mathbf{x}_i))^\top - \mathbf{x}_i \mathbf{x}_i^\top \mathbf{B}),$$

which means that the main difficulty of solving (17) via a gradient descent scheme boils down to having access to $\{\nabla \varphi_i^t\}_{i=1}^n$, the collection of Brenier maps from $Q_{\mathbf{x}_i}^t$ to ν_i at each $t \geq 0$.

We study two cases where the optimal transport between $Q_{\mathbf{x}_i}$ and ν_i is explicit: the Gaussian (Algorithm 1) and the 1-d responses (Algorithm 2) cases.

Remark 2 (Non-geodesic convexity of G). *The non-geodesic convexity of G^4 is the central difficulty for gradient descent: without convexity, standard descent arguments do not guarantee convergence to a global minimum.*

Indeed, Wasserstein barycenters are a special case of Wasserstein least squares—obtained by taking a constant design $\mathbf{x}_i \equiv c$, so that every response is fitted against the same marginal Q_c (see Section 4.1)—and Chewi et al. (2020, Section B.2) construct explicit counterexamples showing that the Wasserstein barycenter functional fails to be geodesically convex.

This non-convexity is precisely the motivation for Chewi et al. (2020) and Altschuler et al. (2021) to replace convexity by a Polyak–Lojasiewicz condition (Karimi et al., 2016) in order to recover convergence rates for barycenter gradient descent. We leave a parallel analysis for the full Wasserstein least squares functional to future work.

At a deeper level, the non-convexity stems from the fact that $(\mathcal{P}_2(\mathbb{R}^{p \times d}), W_2)$ is a CBB(0) space—a metric space of non-negative Alexandrov curvature (Alexander et al., 2024; Ambrosio et al., 2008; Sturm, 2006)—in which squared-distance functions are geodesically concave, so each summand of G is generally geodesically concave rather than convex.

3.1. Bures-Wasserstein gradient descent for the linear case. In Section G, we show that when each of the responses is Gaussian, then the solution to the Wasserstein least squares problem can be taken to be Gaussian as well. The reduction rests on parametrizing Gaussian measures $Q \in \mathcal{P}_2(\mathbb{R}^{p \times d})$ by their vectorized mean $m_Q \in \mathbb{R}^{dp}$ and covariance $\Sigma_Q \in \mathbf{S}_{++}^{dp}$, where the $\text{vec}(\cdot)$ operator identifies coefficient matrices \mathbf{B}^\top with vectors in \mathbb{R}^{dp} . In these coordinates, Section G derives the closed-form marginal covariances $\Sigma_{Q_{\mathbf{x}_i}}$, Brenier maps between $Q_{\mathbf{x}_i}$ and ν_i , and the Bures-Wasserstein gradient of G (all collected in Lemma 9), along with first-order optimality conditions for the Gaussian problem. Following the view adopted by Altschuler et al. (2021) and Lambert et al. (2022), we may therefore exploit this fact to study the Gaussian Wasserstein least squares problem as an optimization over the Bures-Wasserstein manifold.

⁴A function f on a metric space (X, d) is *geodesically convex* if $f(\gamma(t)) \leq (1-t)f(\gamma(0)) + tf(\gamma(1))$ for every constant-speed geodesic $\gamma : [0, 1] \rightarrow X$ and $t \in [0, 1]$ (see Chewi et al., 2025, Section 5.2).

With these tools in hand, we specialize the Wasserstein gradient flow (27) to Gaussian responses $\nu_i \in \mathcal{P}_2(\mathbb{R}^d)$ with mean zero and covariance Σ_{ν_i} . The flow takes the form

$$(31) \quad \begin{cases} \dot{Q}^t = \frac{1}{n} \sum_{i=1}^n \mathbf{x}_i \mathbf{x}_i^\top (\cdot) (\Sigma_{Q_i^t} \# \Sigma_{\nu_i} - I_d) \\ Q^0 = \mathcal{N}_{dp}(0, \Sigma_{Q^0}). \end{cases}$$

We show in Section G that both (31) and its discrete counterpart (28) propagate within the class of Gaussian measures, and admit explicit expressions in terms of the covariance $(\Sigma_{Q^t})_{t \geq 0}$ alone.

Proposition 3. *The following two properties hold for the Wasserstein least squares functional with mean-zero Gaussian data:*

- (1) *The Bures-Wasserstein gradient flow that solves (31) is the curve of Gaussian measures $(Q^t = \mathcal{N}_{dp}(0, \Sigma_{Q^t}))_{t \geq 0}$, where $(\Sigma_t)_{t \geq 0}$ is a solution of the Lyapunov equation*

$$(32) \quad \dot{\Sigma}_{Q^t} = M_t \Sigma_{Q^t} + \Sigma_{Q^t} M_t$$

$$\text{and } M_t := \left(\frac{1}{n} \sum_{i=1}^n \mathbf{x}_i \mathbf{x}_i^\top \otimes (\Sigma_{Q_{x_i}^t} \# \Sigma_{\nu_i} - I_d) \right).$$

- (2) *A sequence $(Q^k)_{k \in \mathbb{N}}$ produced by (28) at each iteration, has covariances $(\Sigma_{Q^k})_{k \in \mathbb{N}}$ given by each iteration of Algorithm 1.*

Algorithm 1 Bures–Wasserstein Gradient Descent

Input: Step size $\tau > 0$; design points $\{\mathbf{x}_i\}_{i=1}^n$; initial covariance Σ_{Q^0} ; target covariances $\{\Sigma_{\nu_i}\}_{i=1}^n$.

Output: Final covariance matrix Σ_{Q^K} .

1: **Initialize:** Σ_{Q^0}

2: **for** $k = 0, 1, \dots, K - 1$ **do**

$$3: \quad M_k \leftarrow \tau \left(\sum_{i=1}^n \frac{1}{n} \mathbf{x}_i \mathbf{x}_i^\top \otimes (\Sigma_{Q_{x_i}^k} \# \Sigma_{\nu_i} - I_d) \right) + I_{dp}$$

$$4: \quad \Sigma_{Q^{k+1}} \leftarrow M_k \Sigma_{Q^k} M_k$$

5: **end for**

6: **return** Σ_{Q^K}

3.2. Wasserstein least squares when $d = 1$. When $d = 1$ we can find a solution to the Wasserstein least squares problem via a gradient descent (GD) algorithm since at each step we have a concrete expression for the Brenier maps involved. Specifically,

$$(33) \quad \nabla \varphi_{Q_{x_i} \rightarrow \nu_i} := f_i^{-1} \circ g_{x_i}$$

with f_i and g_{x_i} being respectively the cumulative distribution functions of ν_i and Q_{x_i} .

We begin the operationalization of the gradient descent scheme by looking at the particle interpretation of (27), meaning, any $\beta \sim Q^0 \in \mathcal{P}_2(\mathbb{R}^p)$ induces a solution $(\beta^t)_{t \geq 0}$ of the following ODE

$$(34) \quad \begin{cases} \dot{\beta}^t &= \frac{1}{n} \sum_{i=1}^n (f_i^{-1} \circ g_{x_i}^t (\mathbf{x}_i^\top \beta^t) - \mathbf{x}_i^\top \beta^t) \mathbf{x}_i \\ \beta^0 &= \beta \end{cases}$$

where $\beta_t \sim Q_t$ for every $t \geq 0$. This is a McKean–Vlasov ODE (which depends on the distribution of the solution via the cumulative distribution function $g_{\mathbf{x}_i}^t$).

To implement (34), we employ the corresponding mean-field interacting particle system. Let $\{\beta_j^0\}_{j=1}^M$ be a collection of M i.i.d. random variables coming from Q^0 . Set $\widehat{Q}^0 := \sum_{l=1}^M \delta_{\beta_l^0}$ and $\widehat{g}_{\mathbf{x}_i}^0$ to be the cdf of $(\cdot^\top \mathbf{x}_i)_\# \widehat{Q}^0$. Then we define $(\widehat{Q}^t)_{t \geq 0}$, the particle gradient flow estimate of $(Q^t)_{t \geq 0}$, to be the curve of empirical measures formed with the solutions $\{(\beta_j^t)_{t \geq 0}\}_{j=1}^M$ of the M -particle system

$$(35) \quad \begin{cases} \dot{\beta}_j^t &= \frac{1}{n} \sum_{i=1}^n (f_i^{-1} \circ \widehat{g}_{\mathbf{x}_i}^t (\mathbf{x}_i^\top \beta_j^t) - \mathbf{x}_i^\top \beta_j^t) \mathbf{x}_i, \\ \widehat{Q}^t &= \frac{1}{M} \sum_{l=1}^M \delta_{\beta_l^t}, \\ \beta_j^0 &= \beta_j, \end{cases}$$

where $\widehat{g}_{\mathbf{x}_i}^t$ is the cdf of $\widehat{Q}_{\mathbf{x}_i}^t$.

Algorithm 2 Particle gradient descent for Wasserstein least squares ($d = 1$)

Input: Design matrix $\mathbf{X} = (\mathbf{x}_1, \dots, \mathbf{x}_n)^\top \in \mathbb{R}^{n \times p}$, target distributions $\{\nu_i\}_{i=1}^n$ with CDFs $\{f_i\}_{i=1}^n$

Input: Number of particles M , step size $\tau > 0$, number of iterations T

Output: Particles $\{\beta_j\}_{j=1}^M \subset \mathbb{R}^p$ representing the approximate minimizer Q^T

```

1: Initialize:  $\{\beta_j^0\}_{j=1}^M \subset \mathbb{R}^p$  ▷ Particle representation of  $Q^0$ 
2: for  $k = 0, 1, \dots, T - 1$  do
3:   for  $i = 1, \dots, n$  do
4:      $\mathbf{z}_{i,j}^k \leftarrow \mathbf{x}_i^\top \beta_j^k$  for  $j = 1, \dots, M$  ▷ Pushforward samples
5:      $\widehat{g}_{\mathbf{x}_i}^k \leftarrow$  empirical CDF of  $\{\mathbf{z}_{i,j}^k\}_{j=1}^M$ 
6:      $\nabla \varphi_{Q_{\mathbf{x}_i}^k \rightarrow \nu_i} \leftarrow f_i^{-1} \circ \widehat{g}_{\mathbf{x}_i}^k$  ▷ Brenier map
7:      $T_{i,j}^k \leftarrow \nabla \varphi_{Q_{\mathbf{x}_i}^k \rightarrow \nu_i}(\mathbf{z}_{i,j}^k)$  for  $j = 1, \dots, M$  ▷ Transported samples
8:   end for
9:   for  $j = 1, \dots, M$  do
10:     $\beta_j^{k+1} \leftarrow \beta_j^k + \frac{\tau}{n} \sum_{i=1}^n (T_{i,j}^k - \mathbf{z}_{i,j}^k) \mathbf{x}_i$  ▷ Gradient step
11:   end for
12: end for
13: return  $\{\beta_j^T\}_{j=1}^M$ 

```

Remark 3 (Convergence). *Neither Algorithm 1 nor Algorithm 2 comes with a formal convergence guarantee at this stage. Nevertheless, Theorem 8 and Proposition 4 in Section F establish that G is η -smooth along Wasserstein geodesics and that the iterates (28) reach an ε -critical point in $O(\varepsilon^{-2})$ steps. Though we are not able to rule out the possibility of spurious stationary points, our empirical experiments (see Section 5) suggest that these algorithms work well in practice.*

Remark 4 (Polynomial time algorithms in fixed dimension). *When ν_1, \dots, ν_n are finitely supported on at most m atoms, the derivation of the multimarginal formulation in the proof of Theorem 1 shows that the optimal Q is also finitely supported, on at most m^n atoms, and can be found by linear programming; of course, this algorithm runs in polynomial time only if $n = O(1)$. However, in fixed dimension (i.e., if both p and d are constant), it is possible to exploit the geometric structure of the Wasserstein least squares problem to obtain algorithms with $\text{poly}(n, m)$ running*

time (with exponent depending on p and d) by using the techniques of [Altschuler and Boix-Adserà \(2021\)](#). Though the resulting algorithm runs in polynomial time, it is far less practical than the gradient flow algorithms we employ.

4. ESTIMATION VIA WASSERSTEIN LEAST SQUARES

In this section, we propose a statistical model for the Wasserstein linear regression problem. As we shall see, the lifted objective defined in Section 2 will furnish a natural estimator for this setting.

We retain the same notational convention as above: given a probability measure $Q \in \mathcal{P}(\mathbb{R}^{p \times d})$ and $\mathbf{x} \in \mathbb{R}^p$, we write $Q_{\mathbf{x}} \in \mathcal{P}(\mathbb{R}^d)$ for the push-forward of Q under the map $\mathbf{B} \mapsto \mathbf{B}^\top \mathbf{x}$.

Let $\{(\mathbf{x}_i, \nu_i)\}_{i=1}^n$ be a collection of n covariate/response pairs in $\mathbb{R}^p \times \mathcal{P}_2(\mathbb{R}^d)$. We consider the following *template deformation model* ([Boissard et al., 2015](#); [Ghodrati and Panaretos, 2022](#); [Le Gouic et al., 2023](#); [Zemel and Panaretos, 2019](#)) for Wasserstein linear regression:

$$\text{(WLR)} \quad \nu_i = (\nabla \phi_i)_\# Q_{\mathbf{x}_i}^* \quad i = 1, \dots, n,$$

where $Q^* \in \mathcal{P}(\mathbb{R}^{p \times d})$ is a fixed, unknown distribution, and where $\{\phi_i\}_{i=1}^n$ are i.i.d. random functions⁵ on \mathbb{R}^d satisfying the following conditions:

- (C1) The functions ϕ_i are almost surely convex, twice differentiable, and satisfy $\phi_i(0) = 0$ and $\mathbb{E}[\|\nabla \phi_i(0)\|^2] \leq d\sigma^2$.
- (C2) For each $\mathbf{y} \in \mathbb{R}^d$, the function ϕ_i satisfies $\mathbb{E}[\nabla \phi_i(\mathbf{y})] = \mathbf{y}$.
- (C3) There exist positive constants α, β such that $\alpha \mathbf{I} \preceq \nabla^2 \phi_i \preceq \beta \mathbf{I}$ almost surely.

The random maps $\nabla \phi_i$ represent the source of noise in the model. Indeed, under our conditions, the random maps $\nabla \phi_i$ may be viewed as *mean-zero perturbations in the Wasserstein space*: condition **C1** implies that $\nabla \phi_i$ is an *optimal* transport map, and condition **C2** says that $\mathbb{E}[\nabla \phi_i]$ is the identity function on \mathbb{R}^d . The responses ν_i in **(WLR)** are therefore equal to $Q_{\mathbf{x}_i}^*$ up to corruptions which, on average, leave the measure unchanged. More rigorously, this interpretation can be justified by the fact that the above conditions guarantee that $Q_{\mathbf{x}_i}^*$ is the Fréchet mean of the random measure $(\nabla \phi_i)_\# Q_{\mathbf{x}_i}^*$:

$$(36) \quad Q_{\mathbf{x}_i}^* = \operatorname{argmin}_{P \in \mathcal{P}(\mathbb{R}^d)} \mathbb{E}[W_2^2((\nabla \phi_i)_\# Q_{\mathbf{x}_i}^*, P)].$$

We refer to the works cited above for a discussion of the statistical interpretation of **(36)** as an average on the Wasserstein space.

At the level of random variables, **(WLR)** can be written as

$$\text{(WLR')} \quad \nu_i = \operatorname{Law}(\mathbf{Y}_i \mid \phi_i), \quad \text{where } \mathbf{Y}_i = \nabla \phi_i((\mathbf{B}^*)^\top \mathbf{x}_i).$$

In this formulation, $\mathbf{B}^* \sim Q^*$ is a random matrix independent of ϕ_i . Written in this way, we see that **(WLR)** models the situation in which the response is the *law* of a linear projection of a random variable \mathbf{B}^* , corrupted by (possibly nonlinear) noise. In particular, taking $\phi_i(\mathbf{y}) = \|\mathbf{y}\|^2/2 + \langle \mathbf{y}, \varepsilon_i \rangle$ for i.i.d. mean-zero random vectors ε_i , we see that **(WLR)** includes the random-effects model **(4)**.

⁵We view ϕ_i as a random element of the space of C^2 convex functions, equipped with the C_{loc}^2 topology, so all the objects discussed below are measurable.

Since it is impractical to assume that the statistician can observe a probability distribution ν_i directly, we complete our model by assuming that the statistician has access to *estimators* $\widehat{\nu}_i$ of ν_i . In the simplest case, we assume that these estimators correspond to simply observing m i.i.d. samples from ν_i :

$$(37) \quad \widehat{\nu}_i = \sum_{j=1}^m \delta_{Y_{i,j}}, \quad Y_{i,j} \sim \nu_i \text{ i.i.d.}$$

We discuss alternative options, where $\widehat{\nu}_i$ is potentially a nonparametric estimator of ν_i , in Remark 6, below.

The observed data is the n pairs $\{(\mathbf{x}_i, \widehat{\nu}_i)\}_{i=1}^n$. Under this model, we will study the performance of the Wasserstein least squares estimator, as defined in Section 2:

$$(38) \quad \widehat{Q} \in \operatorname{argmin}_{Q \in \mathcal{P}_2(\mathbb{R}^p \times d)} \frac{1}{n} \sum_{i=1}^n W_2^2(\widehat{\nu}_i, Q_{\mathbf{x}_i}).$$

Note that this estimator is similar to the definition of an empirical Wasserstein barycenter (Le Gouic et al., 2023). This connection is not superficial, and we shall see in Section 4.1 that our techniques give new convergence bounds in this setting as well.

In order to assess the performance of \widehat{Q} as an estimator of Q^* , we will evaluate its *in-sample error* (Hastie et al., 2009, Chapter 7):

$$(39) \quad \mathbb{E}\left[\sum_{i=1}^n \frac{1}{n} W_2^2(\widehat{Q}_{\mathbf{x}_i}, Q_{\mathbf{x}_i}^*)\right].$$

We will also assume a standard incoherence condition on the fixed design (Candès and Recht, 2009; Hoaglin and Welsch, 1978):

$$(40) \quad \mathbf{x}_i^\top (\mathbf{X}^\top \mathbf{X})^+ \mathbf{x}_i \leq \mu \frac{p}{n} \quad \forall i \in [n]$$

for some $\mu \in \mathbb{R}$. Our main statistical theorem is:

Theorem 7. *Assume Conditions C1 to C3, and that the covariates satisfy the incoherence condition (40). Suppose further that the latent responses are uniformly bounded:*

$$(41) \quad \|\mathbf{B}^\top \mathbf{x}_i\| \leq M \quad \forall i \in [n], \quad Q^* \text{-almost surely.}$$

and that $\widehat{\nu}_i$ is an empirical measure from m i.i.d. samples from ν_i . Let $R = M \max(1, \beta \sqrt{\mu p})$. Then the in-sample error of the estimator (38) satisfies

$$(42) \quad \mathbb{E}\left[\frac{1}{n} \sum_{i=1}^n W_2^2(\widehat{Q}_{\mathbf{x}_i}, Q_{\mathbf{x}_i}^*)\right] \lesssim R^2 \frac{\beta}{\alpha} \sqrt{\frac{pd}{n}} + \frac{R^2}{\alpha} r_m + \sigma^2 \frac{pd}{n},$$

where

$$(43) \quad r_m := \begin{cases} m^{-2/d} & \text{if } d > 4 \\ m^{-1/2} \log m & \text{if } d = 4 \\ m^{-1/2} & \text{if } d < 4. \end{cases}$$

Remark 5. *It is easy to see that the rate of estimation guaranteed by Theorem 7 is minimax optimal up to a logarithmic factor in its dependence on m . Indeed, the rate r_m is optimal for the problem of estimating a compactly supported probability measure on \mathbb{R}^d in Wasserstein distance from m i.i.d. samples, up to the log m factor*

when $d = 4$ (Singh and Póczos, 2018), and our model includes that one as a special case. The term $\sigma^2 \frac{pd}{n}$ is the familiar minimax rate for linear regression (see, e.g., Rigollet and Hütter (2023)), which is also a special case of our model. This term is therefore also impossible to improve. However, we do not know whether the $n^{-1/2}$ dependence in the first term is optimal.

Remark 6. In many applications, the error in Theorem 7 is dominated by the slow r_m term, which arises due to the slow convergence of $\widehat{\nu}_i$ to ν_i in Wasserstein distance, which are an unavoidable feature of empirical estimators for Wasserstein distances in general (see, e.g., Fournier and Guillin, 2015; Manole and Niles-Weed, 2024; Weed and Bach, 2019). This rate can be ameliorated by imposing smoothness assumptions on ν_i and replacing the empirical estimator (37) by a suitable nonparametric estimator.

For example, Niles-Weed and Berthet (2022) and Divol (2021) show that if ν_i is a probability measure on $[0, 1]^d$ or the d -dimensional flat torus with s -smooth density for any $d \geq 3$, then a suitable wavelet or kernel density estimator $\widehat{\nu}_i$ satisfies

$$(44) \quad \mathbb{E}W_2(\widehat{\nu}_i, \nu_i) \lesssim m^{-(s+1)/(2s+d)}.$$

In this setting, for any compact set Ω , we obtain by the triangle inequality

$$\begin{aligned} \mathbb{E} \sup_{\mu \in \mathcal{P}(\Omega)} |W_2^2(\mu, \widehat{\nu}_i) - W_2^2(\mu, \nu_i)| &\leq \mathbb{E} \sup_{\mu \in \mathcal{P}(\Omega)} (W_2(\mu, \widehat{\nu}_i) + W_2(\mu, \nu_i))W_2(\widehat{\nu}_i, \nu_i) \\ &\lesssim m^{-(s+1)/(2s+d)}, \end{aligned}$$

and so the term r_m in Theorem 7 may be replaced by $m^{-(s+1)/(2s+d)}$. This is an improvement for any $d \geq 5$ and $s \geq \frac{2d-1}{d-4}$.

4.1. Application to Wasserstein barycenters. The results of the previous section can be reinterpreted to get a new bound for the estimation of Wasserstein barycenters in $\mathcal{P}_2(\mathbb{R}^d)$ under the template deformation model. In what follows, set $S := \mathcal{P}_2(\mathbb{R}^d)$, Ω a probability measure in $\mathcal{P}_2(S)$, and

$$(45) \quad \mathbf{b}^* \in \operatorname{argmin}_{\mathbf{b} \in S} \mathbb{E}_{\nu \sim \Omega} [W_2^2(\mathbf{b}, \nu)].$$

Recall that in a *template deformation model for the barycenter* \mathbf{b}^* one observes independent copies of measures ν on the support of Ω and assumes they are a push-forward measure of \mathbf{b}^* through a noisy random distortion $T \in \mathcal{A} := L^2(\mathbb{R}^d, \mathbb{R}^d; \mathbf{b}^*)$ (Boissard et al., 2015; Le Gouic et al., 2023; Zemel and Panaretos, 2019). In other words,

$$(46) \quad \nu = T_{\#} \mathbf{b}^*, \quad T \sim P \in \mathcal{P}_2(\mathcal{A})$$

where $P \in \mathcal{P}_2(\mathcal{A})$. We shall note that equations (45) and (46) coincide with equations (36) and (WLR) respectively when P is a probability measure supported on the functions satisfying conditions C1 to C3 and if we set $p = 1$, $\mathbf{x}_i = 1$ for every $\nu_i \in \operatorname{supp}(\Omega)$. Then we can understand the problem of estimating W_2 -barycenters through the lens of Theorem 7.

Corollary 1. Let $\Omega \in \mathcal{P}_2(S)$ have a barycenter \mathbf{b}^* with $\operatorname{supp}(\mathbf{b}^*) \subset B_M$. Assume we observe n measures ν_i which come from the template deformation model (46) where each $T = \nabla \phi_i$ satisfies conditions C1 to C3. Set

$$\widehat{\mathbf{b}} := \operatorname{argmin}_{\mathbf{b}} \frac{1}{n} \sum_{i=1}^n W_2^2(\mathbf{b}, \nu_i).$$

Then

$$(47) \quad \mathbb{E} \left[W_2^2(\widehat{\mathbf{b}}, \mathbf{b}^*) \right] \lesssim M^2 \frac{\beta^3}{\alpha} \sqrt{\frac{d}{n}} + \frac{\sigma^2 d}{n}.$$

Remark 7 (Subtleties of the template deformation model, and a comparison to the lower bound of [Hundrieser et al. \(2024\)](#)). *In our model, we require that φ satisfy Condition C2, which reads*

$$(48) \quad \mathbb{E}[\nabla\varphi(\mathbf{y})] = \mathbf{y} \quad \text{for all } \mathbf{y} \in \mathbb{R}^d.$$

This agrees with the definition proposed by [Boissard et al. \(2015\)](#) and [Zemel and Panaretos \(2019\)](#). However, it is stronger than the assumption made by [Le Gouic et al. \(2023\)](#), who require only that

$$(49) \quad \mathbb{E}[\nabla\varphi(\mathbf{y})] = \mathbf{y} \quad \text{for } \mathbf{b}^*\text{-almost every } \mathbf{y} \in \mathbb{R}^d.$$

In the language of [Zemel and Panaretos \(2019\)](#), this condition is equivalent to requiring that \mathbf{b}^ is a Karcher mean. The arguments of [Zemel and Panaretos \(2019, Theorem 2\)](#) show that, under Condition C3, these two assumptions agree if \mathbf{b}^* is absolutely continuous, with density positive on a convex subset of \mathbb{R}^d .*

However, a construction of [Hundrieser et al. \(2024\)](#) shows that there is a significant difference between (48) and (49) in general. Section 3.5 of that work constructs an example showing that it is possible to construct φ satisfying Condition C3 with $\beta/\alpha = O(1)$ and (49)—but not (48)—for which no estimate like (47) can hold. In their example, the barycenter is supported on two Diracs.

This rate should be understood in comparison with the rate derived in Corollary 4.4 of [Le Gouic et al. \(2023\)](#). Our rate is neither a generalization nor a special case of theirs. The rate in [Le Gouic et al. \(2023\)](#) holds for measures supported in Hilbert spaces, while ours only works for measures supported in finite-dimensional vector spaces. Even then, when both rates hold, theirs converges considerably faster in terms of sample size. Perhaps more importantly, in terms of [Zemel and Panaretos \(2019\)](#), the results in [Le Gouic et al. \(2023\)](#) are stronger since they only require \mathbf{b}^* to be a Karcher mean. Meanwhile, our result is valid only when \mathbf{b}^* is a Fréchet mean. However, they require that condition C3 hold with $\beta - \alpha < 1$, which is significantly more stringent than our assumption. For the case of general $\alpha, \beta > 0$ covered by Corollary 1, the best known rates, due to [Ahidar-Coutrix et al. \(2020\)](#), are exponentially slower.

5. EXPERIMENTS

We begin with a large-scale real-data application (Section A contains full pre-processing details and supplementary figures), then turn to two synthetic settings that demonstrate the structural virtues of the Wasserstein least squares framework; complete experimental specifications are in Section B.

5.1. Modeling BMI with Wasserstein least squares. We examine data coming from the RAND Health and Retirement Study (HRS) Longitudinal File 2022 ([RAND Center for the Study of Aging, 2025](#)), a nationally representative longitudinal survey comprising 16 biennial waves (1992–2022) with approximately 45,000 U.S. respondents aged 50 and older. The HRS is a longitudinal panel: in each wave of the study, individuals are asked about personal, demographic, and

health information, yielding a data footprint which can be used to ask questions related to aging both at an *individual* and *population* level.

One such question is obesity, commonly measured through body mass index (BMI), a widely used epidemiological metric with established associations to metabolic disease, longevity, and healthcare burden (Gutin, 2018). In this experiment we aim to characterize how a person’s BMI changes across decades by using distributional data. Capturing this calls for an approach that is at once a distributional regression and a model of individual random variation, in the spirit of the linear mixed effects framework (Laird and Ware, 1982). Based on (WLR) and (WLR’), Wasserstein least squares is both.

Prior work has fitted linear mixed effects models in which age, birth cohort, and gender are covariates and individual heterogeneity is encoded as a random effect on the regression coefficients (Yang et al., 2021). We adopt the same model structure but fit entirely from distributional data. That is, we do *not* use longitudinal per-individual data when computing our estimator. This per-individual data collected as part of the survey can then be used to validate our findings. For the purposes of our analysis, each observation is therefore the BMI distribution of a demographic *cell*—a group of respondents sharing the same birth cohort (5-year bins: 1930–34 through 1955–59), survey wave, and gender—yielding $n = 164$ cells after quality filtering. Details can be found in Appendix A.

Under the template deformation model (WLR) paradigm, this translates into describing the cell distributions ν_i through the quadratic design vectors

$$(50) \quad \mathbf{x}_i = (1, \tilde{a}_i, \tilde{a}_i^2, \tilde{c}_i, \tilde{g}_i)^\top,$$

where \tilde{a}_i , \tilde{c}_i , and $\tilde{g}_i \in \{-1, +1\}$ are normalized age, birth cohort, and gender (+1 = female), so that

$$(51) \quad \nu_i = \text{Law}(\nabla\phi_i((\mathbf{B}^*)^\top \mathbf{x}_i)), \quad \mathbf{B}^* \sim Q^* \in \mathcal{P}_2(\mathbb{R}^P).$$

The quadratic age term captures the empirical rise in BMI until approximately age 70, followed by a plateau or decline (Yang et al., 2021). The symmetric gender coding ensures β_0 represents the predicted distribution at the mean age and cohort, averaged across genders.

We represent \hat{Q} , the Wasserstein least squares estimator for this data, as a cloud of $M = 20,000$ particles fit via Algorithm 2, and compare against Global Fréchet regression (Petersen and Müller, 2019) on the same cells. The central inferential goal is the probability of crossing BMI = 30 (Centers for Disease Control and Prevention, 2024) and how that probability updates as successive measurements accumulate, a question we assess directly against the individual HRS trajectories.

Results and analysis. Both methods achieve similar in-sample fit: Wasserstein $R^2 \approx 0.90$ for the quadratic Wasserstein least squares and Fréchet models alike, and leave-one-out cross-validation errors differing by a mean W_2 gap of just 0.025 BMI units. This is expected since the two methods produce identical marginal predictions at the observed cells in expectation. Their architectures diverge in how they represent the *joint* distribution of coefficients (Figure 1) and, consequently, in their capacity for conditional inference (Figure 2).

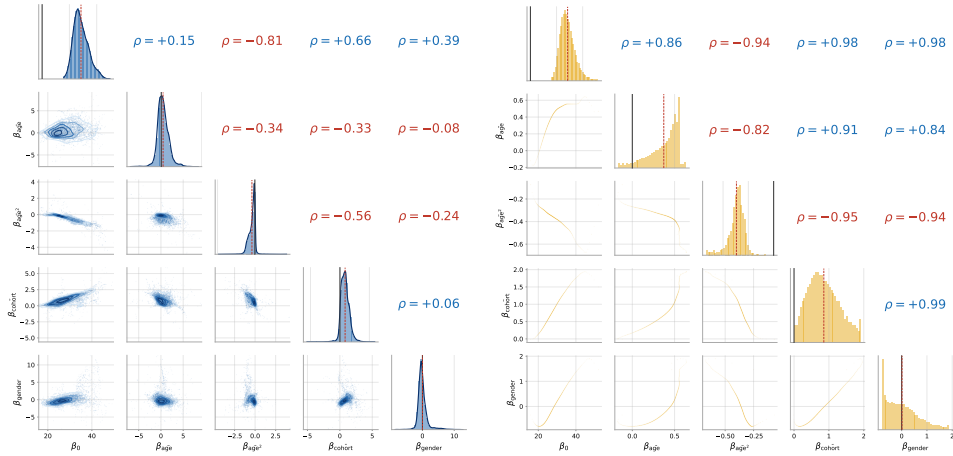
Both models also agree at the level of mean effects on the primary demographic trends: a baseline BMI of approximately 28.5 kg/m²; a positive cohort effect

($\hat{\beta}_{\text{cohort}} \approx 0.88$, consistent with the global rise of obesity (World Health Organization, 2000)); and a concave age trajectory ($\hat{\beta}_{\text{age}^2} \approx -0.37$), rising to a peak in early retirement before declining. These headline figures are consistent across the two methods precisely because they reflect the dominant variation in the data and are well-captured by any reasonable regression model. The differences emerge when we look beyond these mean effects.

The Wasserstein least squares estimator returns a full joint distribution \hat{Q} over the coefficient vector

$$\boldsymbol{\beta} = (\beta_0, \beta_{\text{age}}, \beta_{\text{age}^2}, \beta_{\text{cohort}}, \beta_{\text{gender}})^\top.$$

Figure 1 (left) shows its corner plot: diagonal panels display the marginal distribution of each coefficient, and off-diagonal panels reveal genuine correlations among demographic effects. On the other hand, as we describe in Section A, Fréchet regression also implicitly yields a joint distribution over the coefficient vector: the predicted distribution corresponding to a covariate vector \boldsymbol{x} has quantile function $p \mapsto \boldsymbol{x}^\top \hat{\boldsymbol{\beta}}(p)$ for $p \in (0, 1)$, where $\hat{\boldsymbol{\beta}}(p)$ is a least-squares estimate constructed from the quantile functions of the responses. At the level of random variables, this also gives rise to a joint distribution over the coefficient vector, namely $\text{Law}(\hat{\beta}_0(U), \hat{\beta}_{\text{age}}(U), \hat{\beta}_{\text{age}^2}(U), \hat{\beta}_{\text{cohort}}(U), \hat{\beta}_{\text{gender}}(U))$, for $U \sim \text{Unif}([0, 1])$. Fig. 1 (right) shows the corresponding corner plot.



(A) Wasserstein least squares: genuine joint distribution \hat{Q} . (B) Fréchet: one-dimensional deterministic curve.

FIGURE 1. Corner plots of estimated coefficient distributions on HRS BMI data (quadratic model, $n = 164$ cells). Diagonal: marginal distributions; lower triangle: pairwise scatter plots; upper triangle: Pearson correlations. **Wasserstein least squares** (left) recovers a genuine multivariate distribution with $p = 5$ independent degrees of freedom. **Fréchet** (right) collapses to a curve in \mathbb{R}^5 parametrized by the single scalar p , forcing all pairs into near-perfect correlation and suppressing all subpopulation heterogeneity.

Several features stand out in the Wasserstein least squares analysis. Approximately 10% of the particle mass satisfies $\beta_{\text{age}^2} > 0$, identifying a subpopulation whose BMI trajectory is convex — accelerating rather than plateauing with age. The raw HRS trajectories confirm this: roughly 10% of individuals in the 1940–44 female cohort exhibit a genuine BMI minimum followed by a late-life upturn (Section A). In the estimator obtained from Fréchet regression, $\widehat{\beta}_{\text{age}^2}(p)$ is negative for all p , implying that *zero* individuals have convex trajectories. Similarly, the gender coefficient in Wasserstein least squares carries a standard deviation of 1.69 — more than twice the Fréchet estimate of 0.64 — reflecting that the male–female BMI gap varies substantially across subpopulations, a feature that independent quantile mapping compresses away.

More broadly, since the joint distribution obtained in Fréchet regression is parametrized by this single scalar, the coefficients are perfectly correlated and the support of the joint distribution is a one-dimensional curve in \mathbb{R}^p . Concretely, knowing the intercept β_0 from the Fréchet fit determines every other coefficient; the conditional variance of any slope given β_0 is essentially zero. This is a structural consequence of pointwise quantile regression since Fréchet regression has exactly one degree of freedom in its coefficient distribution. Wasserstein least squares, by contrast, retains all $p = 5$ degrees of freedom, enabling the model to capture localized demographic heterogeneity that is invisible to Fréchet regression.

The consequences of this structural difference become most visible when attempting to make conditional predictions. For Wasserstein least squares, conditioning on observed BMI ≈ 31 at age 50 is simple particle selection: retain

$$\mathcal{M}_{50} = \{m : |\mathbf{x}(50)^\top \boldsymbol{\beta}_m - 31| \leq 2\}$$

and propagate those particles forward with age.⁶ Even at this single-conditioning stage, the Wasserstein least squares intervals are wide (≈ 8 – 12 BMI units at the 80% level), correctly reflecting the genuine biological uncertainty: individuals at the same current BMI may follow vastly different long-term trajectories. By contrast, the perfect correlations implicit in the Fréchet regression estimator yield near-degenerate intervals. Empirically, Wasserstein least squares achieves 87.7% coverage at the nominal 99% prediction interval; Fréchet achieves only 45.6% (Section A).

Introducing a second observation at age 60 further filters the particle set, separating three outcome groups: continued weight gain ($\text{BMI}_{60} > 33$), stable obesity ($\text{BMI}_{60} \in [29, 33]$), and improvement ($\text{BMI}_{60} < 29$). Figure 2 shows the result. Wasserstein least squares differentiates all three scenarios: the prediction bands separate clearly, widen appropriately as the retained sample shrinks ($n = 1,029$, 1,729, and 195 particles respectively), and the improved trajectory descends below the obesity threshold with a median that tracks the empirical data.

Fréchet regression again produces near degenerate intervals; in the third scenario, it produces nothing, because every quantile-level trajectory consistent with

⁶Here m indexes the $M = 20,000$ particles $\{\boldsymbol{\beta}_m\}$, each a draw from the fitted distribution \widehat{Q} over the coefficient vector $\boldsymbol{\beta}$. The covariate vector $\mathbf{x}(a)$ encodes age a together with the cohort and gender of the cell of interest (see (50)), so $\mathbf{x}(50)^\top \boldsymbol{\beta}_m$ is the BMI predicted by particle m at age 50. The set \mathcal{M}_{50} therefore collects all particles whose age-50 prediction falls within ± 2 BMI units of the target value of 31; the ≤ 2 tolerance window is chosen to retain a sufficient number of particles for reliable downstream inference.

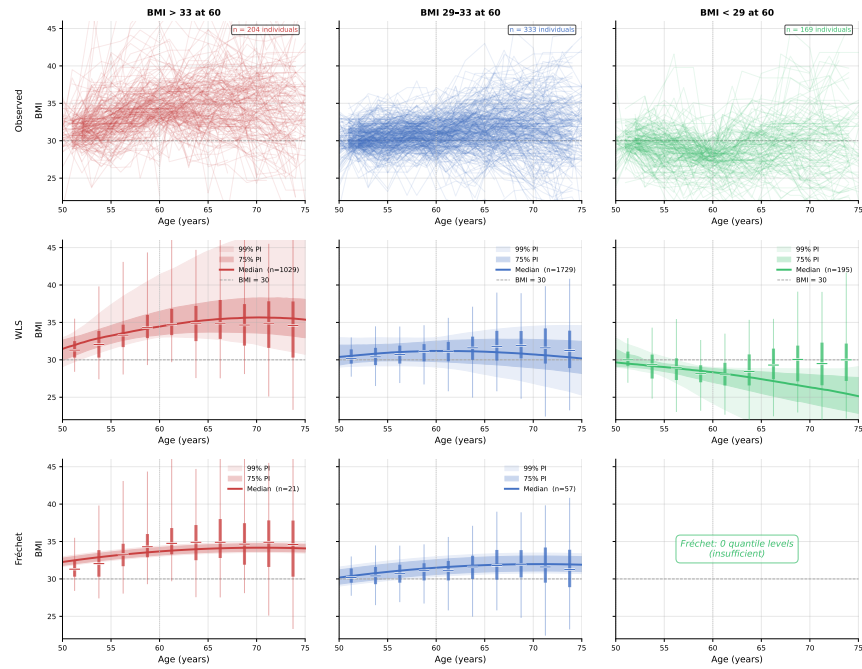


FIGURE 2. **Sequential conditioning (BMI $\in [29, 33]$ at age 50; three age-60 scenarios), cohorts 1935–39 and 1940–44, both sexes.** Columns: worsening (BMI > 33 , red), stable (BMI 29–33, blue), improved (BMI < 29 , green). Rows: observed trajectories (top), Wasserstein least squares (middle), Fréchet (bottom). Shaded bands: 75% and 99% prediction intervals; box plots: matched empirical distribution. Wasserstein least squares differentiates all three scenarios with well-separated, meaningful prediction bands. Fréchet produces results only for worsening and stable; the improved scenario is structurally impossible under the fitted model.

$\text{BMI}_{50} \approx 31$ also predicts $\text{BMI}_{60} \geq 29$. A non-negligible fraction of HRS respondents lowers their BMI between ages 50 and 60, yet the Fréchet model cannot represent this outcome at all. This failure is a direct consequence of the one-dimensional structure of the Fréchet coefficient distribution. Wasserstein least squares, by retaining the full joint distribution of Q^* , remains capable of expressing the full heterogeneity of the data.

5.2. Synthetic experiments. We validate Wasserstein least squares on two controlled settings that illustrate the model’s capacity to recover linear distributional structure from noisy observations. In both settings, each observed distribution $\nu_i = (\nabla\phi_i)_{\#}Q_{\mathbf{x}_i}^*$ arises from the template deformation model (**WLR**): a random convex map $\nabla\phi_i$ satisfying C1–C3 pushes the true template $Q_{\mathbf{x}_i}^*$ forward, adding noise whose form is unknown to the estimator. Figure 3 illustrates this process for five noise families; the deviation $T(y) - y$ (bottom row) confirms that each map stays close to the identity on average, satisfying condition C2.

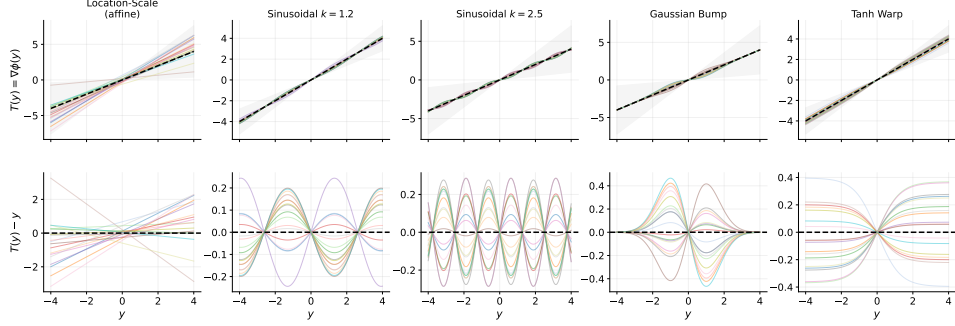


FIGURE 3. Random transport maps $\nabla\phi_i$ from five noise families (coloured) applied to the template $Q_{\mathbf{x}}^*$ (black dashed). Top row: the maps $T(y)$; shaded band shows the C3 curvature bounds. Bottom row: deviation $T(y) - y$ from the identity, illustrating C2 ($\mathbb{E}[T(y)] = y$).

The two templates are: (i) *Univariate* ($d = 1, n = 50$), with $Q_{\mathbf{x}}^* = \mathcal{N}(t, 1 + t^2)$ and covariate $\mathbf{x} = (1, t)^\top$, $t \sim \mathcal{U}[-2, 2]$; the variance is U-shaped, growing quadratically in $|t|$. (ii) *Bivariate Gaussian* ($d = 2, n = 50$), with $Q_{\mathbf{x}}^* = \mathcal{N}(\mu(t), \Sigma(t))$ where $\Sigma(t) = A + t(B + B^\top) + t^2C$ traces a quadratic arc on the cone of symmetric positive definite matrices. Full specifications and numerical summaries are in Section B.

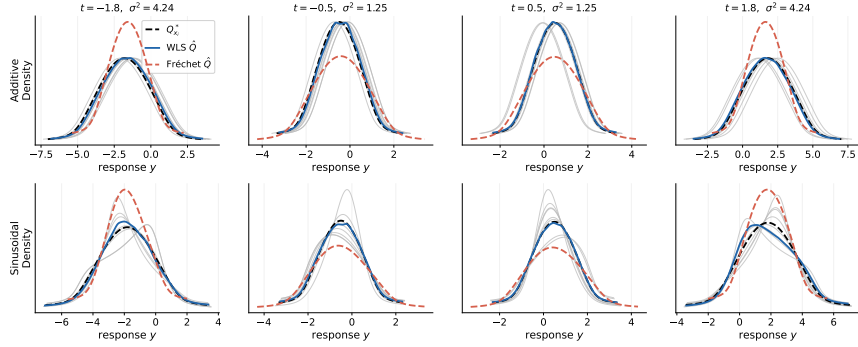


FIGURE 4. Univariate: estimated densities at $t \in \{-1.8, -0.5, 0.5, 1.8\}$. True template $Q_{\mathbf{x}_i}^*$ (black dashed), noisy observations ν_i (grey), Wasserstein least squares (blue), Fréchet (red dashed). Wasserstein least squares recovers the true template across the covariate range under additive noise. The U-shaped variance (univariate), Fréchet regression underestimates spread at the extremes.

Both templates share a feature that illuminates the modeling scope of Wasserstein least squares. In the univariate Gaussian case, Fréchet regression (Petersen and Müller, 2019, §6.2) corresponds to the model $Q_x \sim \mathcal{N}(\mu_0 + \beta x, (\sigma_0 + \gamma x)^2)$. The Wasserstein least squares model corresponds to $Q_x \sim \mathcal{N}(\mu_0 + \beta x, \sigma_0^2 + \gamma^2 x^2 + 2\rho x)$

for any $|\rho| \leq \sigma_0\gamma$, which is strictly more flexible: completing the square gives $\sigma_0^2 + \gamma^2x^2 + 2\rho x = (a + \gamma x)^2 + b$ where $a = \rho/\gamma$ and $b = \sigma_0^2 - \rho^2/\gamma^2 \geq 0$, yielding one extra degree of freedom over Fréchet.

At the level of random variables, this extra freedom is $\text{Cov}(B_0, B_1) = \rho$: the Fréchet parametrization is precisely the boundary case $\rho = \sigma_0\gamma$, which forces B_0 and B_1 to be perfectly dependent ($\text{Corr}(B_0, B_1) = 1$). Our template $\sigma^2(t) = 1 + t^2$ corresponds to $\rho = 0$, independent random coefficients, which is natural in many applications but cannot be expressed in the Fréchet family.

In the bivariate case, the same principle operates at the level of covariance matrices: Fréchet predictions are confined to the convex hull of the training responses and cannot reach the quadratic arc traced by $\Sigma(t)$. We compare against two Fréchet baselines: *Fréchet-GD*, which applies the iterative descent algorithm of [Xu and Li \(2025\)](#), and *Fréchet-OLS*, a closed-form ordinary least squares fit on the covariance entries (details in Section B).

Figure 4 shows the fitted distributions at four covariate values; Wasserstein least squares tracks the true template across the full range of t . Figure 5 focuses on the bivariate covariance trajectory: the true path bends, and Wasserstein least squares follows it faithfully in log-Euclidean coordinates.

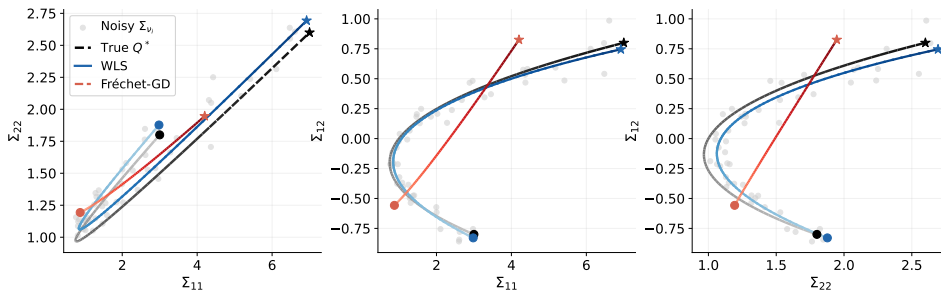


FIGURE 5. Covariance trajectory $t \mapsto \Sigma(t)$ projected onto three coordinate pairs of the SPD cone. Wasserstein least squares (blue) traces the curved true path (black); Fréchet-GD (red) follows a straight line. Bivariate Gaussian experiment: Wasserstein least squares recovers the quadratic covariance trajectory $\Sigma(t) = A + t(B + B^\top) + t^2C$. The log-Euclidean view (right) makes the curvature explicit; Fréchet regression’s linear weighting prevents it from reaching beyond the convex hull of the training responses.

ACKNOWLEDGMENTS

The authors would like to thank Aram-Alexandre Pooladian, Jacob Shkrob, and Shay Sadosky for helpful discussions. The second author was supported in part by NSF grant DMS-2339829.

REFERENCES

Martial Agueh and Guillaume Carlier. Barycenters in the Wasserstein space. *SIAM Journal on Mathematical Analysis*, 43(2):904–924, 2011. doi: 10.1137/100805741.

- Adil Ahidar-Coutrix, Thibaut Le Gouic, and Quentin Paris. Convergence rates for empirical barycenters in metric spaces: curvature, convexity and extendable geodesics. *Probability Theory and Related Fields*, 177(1–2):323–368, 2020. doi: 10.1007/s00440-019-00950-0.
- Stephanie Alexander, Vitali Kapovitch, and Anton Petrunin. *Alexandrov Geometry: Foundations*, volume 236 of *Graduate Studies in Mathematics*. American Mathematical Society, Providence, RI, 2024. ISBN 978-1-4704-7536-9.
- Charalambos D. Aliprantis and Kim C. Border. *Infinite Dimensional Analysis: A Hitchhiker’s Guide*. Springer, Berlin, 3 edition, 2006. doi: 10.1007/3-540-29587-9.
- Jason M. Altschuler and Enric Boix-Adserà. Wasserstein barycenters can be computed in polynomial time in fixed dimension. *Journal of Machine Learning Research*, 22(44):1–19, 2021. URL <https://jmlr.org/papers/v22/20-588.html>.
- Jason M. Altschuler, Sinho Chewi, Patrik R. Gerber, and Austin J. Stromme. Averaging on the Bures–Wasserstein manifold: dimension-free convergence of gradient descent. In *Advances in Neural Information Processing Systems*, volume 34, pages 22132–22145, 2021.
- Luigi Ambrosio, Nicola Gigli, and Giuseppe Savaré. *Gradient Flows in Metric Spaces and in the Space of Probability Measures*. Lectures in Mathematics ETH Zürich. Birkhäuser, Basel, 2 edition, 2008. ISBN 978-3-7643-8721-1.
- Richard E. Barlow, David J. Bartholomew, Joan M. Bremner, and Hugh D. Brunk. *Statistical Inference under Order Restrictions: The Theory and Application of Isotonic Regression*. Wiley Series in Probability and Mathematical Statistics. John Wiley & Sons, London, 1972.
- Rudolf Beran and Peter Hall. Estimating coefficient distributions in random coefficient regressions. *The Annals of Statistics*, 20(4):1970–1984, 1992. doi: 10.1214/aos/1176348898.
- Rajendra Bhatia, Tanvi Jain, and Yongdo Lim. On the Bures–Wasserstein distance between positive definite matrices. *Expositiones Mathematicae*, 37(2):165–191, 2019. doi: 10.1016/j.exmath.2018.01.002.
- Xin Bing, Florentina Bunea, and Jonathan Niles-Weed. Estimation and inference for the Wasserstein distance between mixing measures in topic models, 2022. Forthcoming, Bernoulli.
- Emmanuel Boissard, Thibaut Le Gouic, and Jean-Michel Loubes. Distribution’s template estimate with Wasserstein metrics. *Bernoulli*, 21(2):740–759, 2015. doi: 10.3150/13-BEJ585.
- Nicolas Boumal. *An Introduction to Optimization on Smooth Manifolds*. Cambridge University Press, 2023. doi: 10.1017/9781009166164.
- Charlotte Bunne, Stefan G. Stark, Gabriele Gut, Jacobo Sarabia del Castillo, Mitch Levesque, Kjong-Van Lehmann, Lucas Pelkmans, Andreas Krause, and Gunnar Rätsch. Learning single-cell perturbation responses using neural optimal transport. *Nature Methods*, 20(11):1759–1768, 2023. doi: 10.1038/s41592-023-01969-x.
- Emmanuel J. Candès and Benjamin Recht. Exact matrix completion via convex optimization. *Foundations of Computational Mathematics*, 9(6):717–772, 2009. doi: 10.1007/s10208-009-9045-5.
- Centers for Disease Control and Prevention. About adult BMI, 2024. URL <https://www.cdc.gov/bmi/about/index.html>. Accessed: 2026-02-03.
- Yaqing Chen, Zhenhua Lin, and Hans-Georg Müller. Wasserstein regression. *Journal of the American Statistical Association*, 118(542):869–882, 2023. doi:

10.1080/01621459.2021.1956937.

- Sinho Chewi, Tyler Maunu, Philippe Rigollet, and Austin J. Stromme. Gradient descent algorithms for Bures–Wasserstein barycenters. In *Proceedings of the 33rd Conference on Learning Theory*, volume 125 of *Proceedings of Machine Learning Research*, pages 1276–1304. PMLR, 2020.
- Sinho Chewi, Jonathan Niles-Weed, and Philippe Rigollet. *Statistical Optimal Transport*, volume 2364 of *Lecture Notes in Mathematics*. Springer, Cham, 2025. ISBN 978-3-031-85159-9. doi: 10.1007/978-3-031-85160-5. École d’Été de Probabilités de Saint-Flour XLIX – 2019.
- Lénaïc Chizat, Pierre Roussillon, Flavien Léger, François-Xavier Vialard, and Gabriel Peyré. Faster Wasserstein distance estimation with the Sinkhorn divergence. In *Advances in Neural Information Processing Systems*, volume 33, pages 2257–2269, 2020.
- Angus Deaton. Panel data from time series of cross-sections. *Journal of Econometrics*, 30(1–2):109–126, 1985. doi: 10.1016/0304-4076(85)90134-4.
- Vincent Divol. A short proof on the rate of convergence of the empirical measure for the Wasserstein distance, 2021.
- Jiaojiao Fan, Isabel Haasler, Johan Karlsson, and Yongxin Chen. On the complexity of the optimal transport problem with graph-structured cost. In *Proceedings of the 25th International Conference on Artificial Intelligence and Statistics*, volume 151 of *Proceedings of Machine Learning Research*, pages 9147–9165. PMLR, 2022.
- Nicolas Fournier and Arnaud Guillin. On the rate of convergence in Wasserstein distance of the empirical measure. *Probability Theory and Related Fields*, 162(3–4):707–738, 2015. doi: 10.1007/s00440-014-0583-7.
- Matthias Gelbrich. On a formula for the L^2 Wasserstein metric between measures on Euclidean and Hilbert spaces. *Mathematische Nachrichten*, 147:185–203, 1990. doi: 10.1002/mana.19901470121.
- Laya Ghodrati and Victor M. Panaretos. Distribution-on-distribution regression via optimal transport maps. *Biometrika*, 109(4):957–974, 2022. doi: 10.1093/biomet/asac005.
- Iliya Gutin. In BMI we trust: reframing the body mass index as a measure of health. *Social Theory & Health*, 16(3):256–271, 2018. doi: 10.1057/s41285-017-0055-0.
- Trevor Hastie, Robert Tibshirani, and Jerome Friedman. *The Elements of Statistical Learning: Data Mining, Inference, and Prediction*. Springer Series in Statistics. Springer, New York, 2 edition, 2009. doi: 10.1007/978-0-387-84858-7.
- Jean-Baptiste Hiriart-Urruty and Claude Lemaréchal. *Convex Analysis and Minimization Algorithms I: Fundamentals*, volume 305 of *Grundlehren der mathematischen Wissenschaften*. Springer, Berlin, 1993. doi: 10.1007/978-3-662-02796-7.
- David C. Hoaglin and Roy E. Welsch. The hat matrix in regression and ANOVA. *The American Statistician*, 32(1):17–22, 1978. doi: 10.1080/00031305.1978.10479237.
- Stefan Hoderlein, Jussi Klemelä, and Enno Mammen. Analyzing the random coefficient model nonparametrically. *Econometric Theory*, 26(3):804–837, 2010. doi: 10.1017/S0266466609990119.
- Tailen Hsing and Randall Eubank. *Theoretical Foundations of Functional Data Analysis, with an Introduction to Linear Operators*. Wiley Series in Probability and Statistics. John Wiley & Sons, Chichester, 2015. doi: 10.1002/9781118762547.

- Shayan Hundrieser, Benjamin Eltzner, and Stephan F. Huckemann. A lower bound for estimating Fréchet means, 2024.
- Amirhossein Karimi and Tryphon T. Georgiou. Regression analysis of distributional data through multi-marginal optimal transport, 2021.
- Amirhossein Karimi, Luigia Ripani, and Tryphon T. Georgiou. Statistical learning in Wasserstein space. *IEEE Control Systems Letters*, 5(3):899–904, 2021. doi: 10.1109/LCSYS.2020.3006837.
- Hamed Karimi, Julie Nutini, and Mark Schmidt. Linear convergence of gradient and proximal-gradient methods under the Polyak–lojasiewicz condition. In *Machine Learning and Knowledge Discovery in Databases (ECML PKDD)*, volume 9851 of *Lecture Notes in Computer Science*, pages 795–811. Springer, 2016. doi: 10.1007/978-3-319-46128-1_50.
- Nan M. Laird and James H. Ware. Random-effects models for longitudinal data. *Biometrics*, 38(4):963–974, 1982. doi: 10.2307/2529876.
- Marc Lambert, Sinho Chewi, Francis Bach, Silvère Bonnabel, and Philippe Rigollet. Variational inference via Wasserstein gradient flows. In *Advances in Neural Information Processing Systems*, volume 35, 2022.
- Hugo Lavenant. Lifting functionals defined on maps to measure-valued maps via optimal transport. *Annali della Scuola Normale Superiore di Pisa, Classe di Scienze*, 2024. doi: 10.2422/2036-2145.202309_034. Published online.
- Thibaut Le Gouic, Quentin Paris, Philippe Rigollet, and Austin J. Stromme. Fast convergence of empirical barycenters in Alexandrov spaces and the Wasserstein space. *Journal of the European Mathematical Society*, 25(6):2229–2250, 2023. doi: 10.4171/jems/1234.
- Nicholas T. Longford. *Random Coefficient Models*, volume 11 of *Oxford Statistical Science Series*. Clarendon Press, Oxford University Press, New York, 1993. ISBN 0-19-852264-9.
- Tudor Manole and Jonathan Niles-Weed. Sharp convergence rates for empirical optimal transport with smooth costs. *The Annals of Applied Probability*, 34(1B):1108–1135, 2024. doi: 10.1214/23-AAP1986.
- Tudor Manole, Sivaraman Balakrishnan, Jonathan Niles-Weed, and Larry Wasserman. Plugin estimation of smooth optimal transport maps. *The Annals of Statistics*, 52(3):966–998, 2024. doi: 10.1214/24-AOS2379.
- Hans-Georg Müller. Peter Hall, functional data analysis and random objects. *The Annals of Statistics*, 44(5):1867–1887, 2016. doi: 10.1214/16-AOS1492.
- Jonathan Niles-Weed and Quentin Berthet. Minimax estimation of smooth densities in Wasserstein distance. *The Annals of Statistics*, 50(3):1519–1540, 2022. doi: 10.1214/21-AOS2161.
- Victor M. Panaretos and Yoav Zemel. *An Invitation to Statistics in Wasserstein Space*. SpringerBriefs in Probability and Mathematical Statistics. Springer, Cham, 2020. doi: 10.1007/978-3-030-38438-8.
- Alexander Petersen and Hans-Georg Müller. Fréchet regression for random objects with Euclidean predictors. *The Annals of Statistics*, 47(2):691–719, 2019. doi: 10.1214/17-AOS1624.
- Alexander Petersen, Xi Liu, and Afshin A. Divani. Wasserstein F-tests and confidence bands for the Fréchet regression of density response curves. *The Annals of Statistics*, 49(1):590–611, 2021. doi: 10.1214/20-AOS1971.

- Alexander Petersen, Chao Zhang, and Piotr Kokoszka. Modeling probability density functions as data objects. *Econometrics and Statistics*, 21:159–178, 2022. doi: 10.1016/j.ecosta.2021.04.004.
- J. O. Ramsay and B. W. Silverman. *Functional Data Analysis*. Springer Series in Statistics. Springer, New York, 2 edition, 2005. ISBN 978-0-387-40080-8.
- RAND Center for the Study of Aging. RAND HRS longitudinal file 2022 (v1). Technical report, Institute for Social Research, University of Michigan, Ann Arbor, MI, 2025. URL <https://hrsdata.isr.umich.edu/data-products/rand-hrs-longitudinal-file-2022>. Funded by the National Institute on Aging (NIA U01AG009740) and the Social Security Administration.
- Philippe Rigollet and Jan-Christian Hütter. High-dimensional statistics, 2023. Lecture notes for MIT 18.657.
- R. Tyrrell Rockafellar. *Convex Analysis*. Number 28 in Princeton Mathematical Series. Princeton University Press, Princeton, NJ, 1970.
- Giuseppe Savaré and Giacomo Enrico Sodini. A simple relaxation approach to duality for optimal transport problems in completely regular spaces. *Journal of Convex Analysis*, 29(1):1–12, 2022.
- Shashank Singh and Barnabás Póczos. Minimax distribution estimation in Wasserstein distance, 2018.
- Wookyeong Song, Hang Zhou, Yidong Zhou, and Hans-Georg Müller. Non-Euclidean data analysis with metric statistics. *Harvard Data Science Review*, February 2026. URL <https://hdsr.mitpress.mit.edu/pub/fig0cphkz>.
- Stephen M. Stigler. *The History of Statistics: The Measurement of Uncertainty Before 1900*. Belknap Press of Harvard University Press, Cambridge, MA, 1986. ISBN 0-674-40340-1.
- Karl-Theodor Sturm. On the geometry of metric measure spaces. I. *Acta Mathematica*, 196(1):65–131, 2006. doi: 10.1007/s11511-006-0002-8.
- James W. Vaupel, Kenneth G. Manton, and Eric Stallard. The impact of heterogeneity in individual frailty on the dynamics of mortality. *Demography*, 16(3): 439–454, 1979. doi: 10.2307/2061224.
- Marno Verbeek. *A Guide to Modern Econometrics*. John Wiley & Sons, Hoboken, NJ, 5 edition, 2017. ISBN 978-1-119-40115-5.
- Roman Vershynin. *High-Dimensional Probability: An Introduction with Applications in Data Science*, volume 47 of *Cambridge Series in Statistical and Probabilistic Mathematics*. Cambridge University Press, 2018. doi: 10.1017/9781108231596.
- Cédric Villani. *Optimal Transport: Old and New*, volume 338 of *Grundlehren der mathematischen Wissenschaften*. Springer, Berlin, 2009. doi: 10.1007/978-3-540-71050-9.
- Zachary J. Ward, Sara N. Bleich, Angie L. Cradock, Jessica L. Barrett, Catherine M. Giles, Chasmine Flax, Michael W. Long, and Steven L. Gortmaker. Projected U.S. state-level prevalence of adult obesity and severe obesity. *New England Journal of Medicine*, 381(25):2440–2450, 2019. doi: 10.1056/NEJMsa1909301.
- Jonathan Weed and Francis Bach. Sharp asymptotic and finite-sample rates of convergence of empirical measures in Wasserstein distance. *Bernoulli*, 25(4A): 2620–2648, 2019. doi: 10.3150/18-BEJ1065.
- World Health Organization. Obesity: Preventing and managing the global epidemic. report of a WHO consultation. Technical Report 894, World Health

- Organization, Geneva, 2000. PMID: 11234459.
- Haoshu Xu and Hongzhe Li. Wasserstein F-tests for Fréchet regression on Bures–Wasserstein manifolds. *Journal of Machine Learning Research*, 26(77):1–123, 2025. URL <http://jmlr.org/papers/v26/24-0493.html>.
- Yang Claire Yang, Christine E. Walsh, Moira P. Johnson, Daniel W. Belsky, Max Reason, Patrick Curran, Allison E. Aiello, Marianne Chanti-Ketterl, and Kathleen Mullan Harris. Life-course trajectories of body mass index from adolescence to old age: racial and educational disparities. *Proceedings of the National Academy of Sciences*, 118(17):e2020167118, 2021. doi: 10.1073/pnas.2020167118.
- Yoav Zemel and Victor M. Panaretos. Fréchet means and Procrustes analysis in Wasserstein space. *Bernoulli*, 25(2):932–976, 2019. doi: 10.3150/17-BEJ1009.

APPENDIX A. EXPERIMENT: RETIREMENT DATA (FULL ANALYSIS)

Body Mass Index (BMI) is a widely used, simple, and cost-effective metric for population health, offering insights into metabolic disease associated with obesity, longevity, and a variety of healthcare burdens (Gutin, 2018). To demonstrate the practical and theoretical advantages of the Wasserstein least squares framework in the analysis of distributional responses, we examine the BMI data from the RAND Health and Retirement Study (HRS) Longitudinal File 2022 (Version 1) [RAND Center for the Study of Aging \(2025\)](#). We compare our approach to Global Fréchet regression [Petersen and Müller \(2019\)](#) and illustrate how our framework translates standard linear modeling methods—including coefficient interpretation and analysis of variance—directly into the space of probability distributions.

Modelling and pre-processing. The HRS is a nationally representative longitudinal survey of U.S. citizens aged 50 and older and their spouses, sponsored by the National Institute on Aging and conducted biennially by the University of Michigan since 1992. The study comprises 16 biennial waves spanning 1992 to 2022, with approximately 45,000 unique respondents. For each respondent and wave, the database provides self-reported height and weight from which BMI is computed as weight (kg) divided by height squared (m^2) [Centers for Disease Control and Prevention \(2024\)](#).

We adopt a “macroscopic” distributional approach where each observation is the BMI distribution of a specific demographic “cell”. A cell is defined as the set of participants in the study who share three demographic variables: birth cohort, survey wave, and gender. Respondents are assigned to six 5-year birth cohorts based on birth year: 1930–1934, 1935–1939, 1940–1944, 1945–1949, 1950–1954, and 1955–1959.

Individual BMI observations are filtered to the range $[15, 55]$ kg/m^2 to exclude implausible values. Cells with fewer than 200 valid observations are excluded to ensure reliable density estimation. For each retained cell (c, w, g) corresponding to cohort c , wave w , and gender g , we compute a representative age as $a_{c,w} = y_w - (c + 2.5)$, where y_w denotes the calendar year of wave w and $c + 2.5$ is the cohort midpoint. The final sample comprises $n = 164$ cells with ages ranging from approximately 35 to 90 years.

From the cell-level BMI observations, we construct continuous density estimates as follows. For each cell i , the raw BMI values $\{b_{i,1}, \dots, b_{i,n_i}\}$ are smoothed using kernel density estimation with a Gaussian kernel and bandwidth selected via

Scott’s rule, yielding continuous density estimates ν_i evaluated on a grid of 200 equally-spaced points spanning $[15, 55]$ kg/m². Each density is normalized so that it integrates to 1.

To capture the structural evolution of these BMI profiles, we model the cell-level distributions ν_i using a Wasserstein linear regression framework (**WLR**), meaning

$$\nu_i = \text{law}(\mathbf{Y}_i), \quad \text{where } \mathbf{Y}_i = \nabla\phi_i((\mathbf{B}^*)^\top \mathbf{x}_i) \quad \text{and} \quad \mathbf{B}^* \sim Q^* \in \mathcal{P}_2(\mathbb{R}^p).$$

This formulation mimics the dynamics of a classical linear mixed-effects model when interpreted at the particle level. For any individual particle comprising the distribution of a demographic cell, the linear predictor $(\mathbf{B}^*)^\top \mathbf{x}_i$ acts as a shared, group-specific random effect. We interpret the convex gradient $\nabla\phi_i$ as a functional error term capturing variation unexplained by the covariates.

Based on the insights of previous population-level studies of BMI [Yang et al. \(2021\)](#), we consider two specifications for the design matrix \mathbf{X} . Let \bar{a} and s_a denote the sample mean and standard deviation of cell ages, and let \bar{c} and s_c denote the analogous quantities for cohort midpoints. Define the normalized covariates

$$\tilde{a}_i = \frac{a_i - \bar{a}}{s_a}, \quad \tilde{c}_i = \frac{c_i - \bar{c}}{s_c}, \quad \tilde{g}_i = \begin{cases} -1 & \text{if male} \\ +1 & \text{if female.} \end{cases}$$

The **linear model** uses a design matrix $\mathbf{X} \in \mathbb{R}^{n \times 4}$ with rows

$$(52) \quad \mathbf{x}_i = (1, \tilde{a}_i, \tilde{c}_i, \tilde{g}_i)^\top$$

corresponding to an intercept, normalized age, normalized cohort, and gender indicator.

The **quadratic model** uses a design matrix $\mathbf{X} \in \mathbb{R}^{n \times 5}$ with rows

$$(53) \quad \mathbf{x}_i = (1, \tilde{a}_i, \tilde{a}_i^2, \tilde{c}_i, \tilde{g}_i)^\top$$

incorporating a quadratic age term to capture the empirical observation that BMI tends to increase with age until approximately 70 years, then plateaus or declines.

We normalized the continuous covariates to ensure the coefficients are on comparable scales and to facilitate interpretation. The intercept β_0 represents the predicted BMI distribution at the mean age and cohort, averaged across genders. The symmetric gender coding centers this covariate at zero, so that β_{gender} captures the half-difference between female and male BMI distributions.

Model fitting and selection metrics. To analyze the relationship between demographic covariates and BMI profiles, we fit two types of vector-covariate, distribution-response regression models to the data: Wasserstein least squares and Global Fréchet regression.

For the Wasserstein least squares approach, we evaluate several model specifications on the n demographic cells, utilizing their covariate vectors $\{\mathbf{x}_i\}_{i=1}^n$ and target BMI distributions $\{\nu_i\}_{i=1}^n$. These specifications vary primarily in two ways: we include an additional quadratic age covariate (age²) in most models to capture nonlinear aging dynamics, and we scale the number of particles representing the fit to either $M = 2,000$ or $M = 20,000$, depending on the distributional resolution required for the analysis.

We compute the fit of the least squares estimator \hat{Q} using the procedure outlined in [Algorithm 2](#). The estimator is represented as an empirical measure of

M particles $\{\beta_j\}_{j=1}^M \subset \mathbb{R}^p$, which we update via gradient descent with a learning rate $\tau_k = 0.1/(1 + 0.001k)$, a momentum coefficient $\rho = 0.9$, and a mini-batch size $B = 5$ over $T = 2,000$ iterations. The resulting particle cloud provides a nonparametric estimate of the distribution over the coefficient vectors $\beta = (\beta_0, \beta_{\text{age}}, \beta_{\text{age}^2}, \beta_{\text{cohort}}, \beta_{\text{gender}})^\top$.

From this, we extract summary statistics including marginal distributions, pairwise correlations, and the covariance matrix

$$\Sigma_\beta = \frac{1}{M-1} \sum_{j=1}^M (\beta_j - \bar{\beta})(\beta_j - \bar{\beta})^\top,$$

where $\bar{\beta} = \frac{1}{M} \sum_{i=1}^M \beta_i$.

As a benchmark for Wasserstein least squares, we fit the Global Fréchet regression model (Petersen and Müller, 2019) to the same distributional data. Let $S_{\nu_i} : (0, 1) \rightarrow \mathbb{R}$ denote the quantile function of the observed BMI distribution ν_i for cell i . We evaluate these quantile functions on a uniform grid of $L = 500$ probability levels $\{p_\ell\}_{\ell=1}^L$ spanning $[0.001, 0.999]$. For each quantile level $p \in (0, 1)$, we first compute the unconstrained least squares estimate:

$$(54) \quad \tilde{\beta}(p) = (\beta_0(p), \dots, \beta_{\text{gender}}(p))^\top = (\mathbf{X}^\top \mathbf{X})^{-1} \mathbf{X}^\top S(p),$$

where $S(p) = (S_{\nu_1}(p), \dots, S_{\nu_n}(p))^\top \in \mathbb{R}^n$ is the vector of observed quantiles at level p , and $\mathbf{X} \in \mathbb{R}^{n \times 5}$ is the design matrix with rows \mathbf{x}_i^\top .

The unconstrained predicted quantile function for a covariate vector \mathbf{x} is $\tilde{S}_\mathbf{x}(p) = \mathbf{x}^\top \tilde{\beta}(p)$. However, this prediction may not be monotonically increasing in p , violating the definition of a quantile function. Following the computational procedure in Section 6.1 of Petersen and Müller (2019), we project onto the space of valid quantile functions via isotonic regression:

$$(55) \quad \hat{S}_\mathbf{x} = \underset{q: q(p_1) \leq \dots \leq q(p_L)}{\operatorname{argmin}} \sum_{\ell=1}^L \left(q(p_\ell) - \tilde{S}_\mathbf{x}(p_\ell) \right)^2.$$

This projection is computed efficiently using the Pool-Adjacent-Violators Algorithm (PAVA) (Barlow et al., 1972)⁷.

To evaluate the goodness-of-fit and generalizability of our models, we conduct a comparative performance analysis using the Wasserstein coefficient of determination R^2 , introduced in section 6.4 of Petersen and Müller (2019), and leave-one-out cross-validation (LOO-CV).

As summarized in Table 1, the inclusion of the quadratic age term (\tilde{a}^2) improves model fit for both methodologies.

⁷An important subtlety arises regarding monotonicity in Fréchet regression. The unconstrained coefficients $\tilde{\beta}(p)$ from (54) define a curve $p \mapsto \tilde{\beta}(p)$ in coefficient space \mathbb{R}^p . When visualizing the joint distribution of coefficient pairs $(\tilde{\beta}_k(p), \tilde{\beta}_j(p))$ as p varies and where $j, k \in \{0, \text{age}, \text{age}^2, \text{cohort}, \text{gender}\}$, one might observe non-injective curves as in Figure 8. This non-injectivity might suggest that the predicted quantile functions $\tilde{S}_\mathbf{x}(p) = \mathbf{x}^\top \tilde{\beta}(p)$ could violate monotonicity for certain covariate vectors \mathbf{x} . In our BMI application, we verified empirically that $\tilde{S}_\mathbf{x}(p)$ is monotonic for all observed covariate vectors \mathbf{x}_i , rendering the PAVA projection step unnecessary in practice. Nevertheless, for general applications where monotonicity violations may occur, the isotonic regression step described in Petersen and Müller (2019) remains essential.

Model	R^2
Wasserstein least squares (Linear)	0.7254
Wasserstein least squares (Quadratic)	0.8958
Fréchet (Linear)	0.7536
Fréchet (Quadratic)	0.8932

TABLE 1. Wasserstein R^2 for distributional regression models on BMI data ($n = 164$ cells). Computed as $R^2 = 1 - \sum_i W_2^2(\nu_i, \hat{Q}_{\mathbf{x}_i}) / \sum_i W_2^2(\nu_i, \bar{\nu})$ following Petersen and Müller (2019), where $\bar{\nu}$ is the Wasserstein barycenter. Linear models use covariates $\mathbf{x} = (1, \tilde{a}, \tilde{c}, \tilde{g})^\top$; quadratic models add \tilde{a}^2 . Both quadratic models explain $\approx 89\%$ of distributional variance; Wasserstein least squares (0.8958) and Fréchet (0.8932) are indistinguishable at this aggregate level.

Furthermore, the R^2 metrics reveal that at the macroscopic level of explained variability, neither Wasserstein least squares nor Global Fréchet regression strictly dominates.

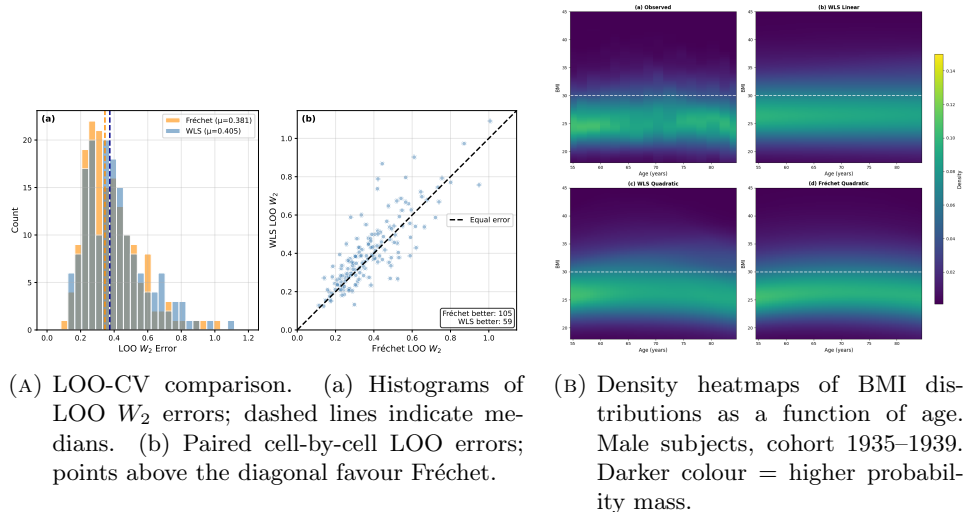
To assess out-of-sample predictive performance, we perform LOO-CV across the filtered sample of $n = 164$ demographic cells. Given the computationally intensive nature of LOO-CV, we fitted the Wasserstein least squares model for this specific evaluation using an Adam optimizer with gradient clipping and early stopping ($M = 2000$ particles, patience = 100). Table 2 reports the mean and standard deviation of the W_2 distances. Fréchet regression exhibits slightly lower LOO error than Wasserstein least squares, suggesting a marginally higher out-of-sample stability.

However, a paired cell-by-cell comparison of the LOO errors provides a more nuanced picture (Figure 6a). Histograms of the LOO W_2 errors show highly overlapping distributions, with the median error for Fréchet at 0.345 and Wasserstein least squares at 0.370, closely trailing. When comparing performance on identical cells, Fréchet achieves a lower LOO error in 61% (100/164) of the cells. Ultimately, the mean difference in LOO error between the two approaches is a mere 0.025 BMI units.

Taken together, the quantitative R^2 and LOO-CV metrics, along with qualitative visual assessments, tell a consistent empirical story: when interpolating within the observed covariate space, Wasserstein least squares and Global Fréchet regression exhibit equivalent performance. This interpolation parity is evident in Fig. 6b, which shows the density heatmaps of the fitted BMI distributions ν_i for a representative demographic slice (males in the 1935–1939 birth cohort). Here, the distributions output by Wasserstein least squares and Fréchet regression are virtually indistinguishable. Both frameworks capture the nonlinear age dynamics present in the observed data. Since neither model significantly outperforms the other in raw interpolating power, the choice between them hinges on their structural properties.

Model	LOO W_2
Fréchet (Quadratic)	0.3813 ± 0.1618
Wasserstein least squares (Quadratic)	0.4060 ± 0.1874

TABLE 2. Leave-one-out cross-validation results for distributional regression on BMI data ($n = 164$ cells; errors reported as mean \pm std of W_2 distance). Fréchet achieves a marginally lower mean error (0.381 vs. 0.406), a gap of 0.025 W_2 units on average; the two error distributions overlap substantially (Fig. 6a).



(A) LOO-CV comparison. (a) Histograms of LOO W_2 errors; dashed lines indicate medians. (b) Paired cell-by-cell LOO errors; points above the diagonal favour Fréchet. (B) Density heatmaps of BMI distributions as a function of age. Male subjects, cohort 1935–1939. Darker colour = higher probability mass.

FIGURE 6. Predictive parity between Wasserstein least squares and Fréchet regression on the BMI data. *Left*: LOO W_2 error histograms (top) and paired cell-level comparison (bottom); the median difference is 0.025 BMI units and 61% of cells favour Fréchet, confirming that neither method dominates on raw out-of-sample fit. *Right*: Fitted density heatmaps for male subjects, cohort 1935–1939; both models produce virtually identical distributions across the age range. The two methods are interchangeable for interpolation; structural differences emerge only when conditioning on individual-level observations (see Figs. 1 and 2).

Coefficient measures, covariances, and joint probability distributions of the coefficients for the fitted models. While both models interpolate effectively, their mathematical architectures differ in how they handle population heterogeneity. Wasserstein least squares extends the logic of linear mixed-effects modeling into a nonparametric setting by estimating a joint probability measure, \hat{Q} , over the multidimensional coefficient space \mathbb{R}^p . In contrast, Global Fréchet regression constructs its distributional response by independently regressing each quantile level p .

Wasserstein least squares ($M = 20,000$ particles)					
Coefficient	Mean	SD	2.5%	97.5%	$\widehat{P}(\beta_j > 0)$
β_0	28.479	5.468	19.513	41.057	100.0%
β_{age}	0.451	1.412	-1.909	3.663	60.7%
β_{age^2}	-0.393	0.490	-1.347	0.143	9.9%
β_{cohort}	0.877	0.718	-0.225	2.414	94.0%
β_{gender}	0.020	1.693	-2.084	5.057	38.6%
Fréchet ($K = 500$ quantile levels)					
Coefficient	Mean	SD	2.5%	97.5%	$\widehat{P}(\beta_j > 0)$
β_0	28.483	5.699	19.458	41.930	100.0%
β_{age}	0.372	0.176	-0.072	0.554	95.2%
β_{age^2}	-0.368	0.082	-0.602	-0.250	0.0%
β_{cohort}	0.854	0.452	0.110	1.814	99.6%
β_{gender}	0.014	0.636	-0.789	1.505	45.2%

TABLE 3. Coefficient summaries for the Wasserstein least squares and Fréchet regression fits on HRS BMI data. **Wasserstein least squares:** each row summarises the marginal distribution of the j -th coordinate of \widehat{Q} across $M = 20,000$ particles $(\beta_m)_{m=1}^M$ computed via Algorithm 2; Mean, SD, and prediction interval are empirical particle statistics. $\widehat{P}(\beta_j > 0)$ is the fraction of particles with positive j -th coordinate. **Fréchet:** each row summarises the j -th coordinate of the OLS coefficient vector $\widehat{\beta}(p)$ across $K = 500$ quantile levels $p \in (0, 1)$; Mean, SD, and interval are taken over quantile levels. Covariates are normalized.

Table 3 and Figure 7 illustrate the practical consequences of this divergence. At a macro level, both methods agree on the baseline BMI ($\beta_0 \approx 28.5$) and identify the same primary population trends: later birth cohorts exhibit higher BMI ($\beta_{\text{cohort}} > 0$), and aging generally follows a negative quadratic trajectory ($\beta_{\text{age}^2} < 0$).

However, the marginal distributions reveal that Wasserstein least squares permits a broader range of structural variation. For example, Fréchet regression yields a quadratic age effect that is strictly negative across all quantiles ($P(\beta_{\text{age}^2} > 0) = 0$). Wasserstein least squares, conversely, indicates that while the average effect is concave, approximately 10% of the mass allows for near-zero or slightly positive curvature. Likewise, Wasserstein least squares yields a substantially wider spread for the linear age and gender coefficients (e.g., a gender standard deviation of 1.69 versus 0.64).

Structurally, this flexibility enables Wasserstein least squares to model scenarios in which different segments of the BMI distribution experience demographic gradients in different ways, a localized heterogeneity that independent quantile mapping tends to constrain.

The structural difference between the two frameworks becomes most pronounced while examining the joint distribution of the regression coefficients (Figure 8). Since Global Fréchet regression constructs its estimates by independently evaluating each

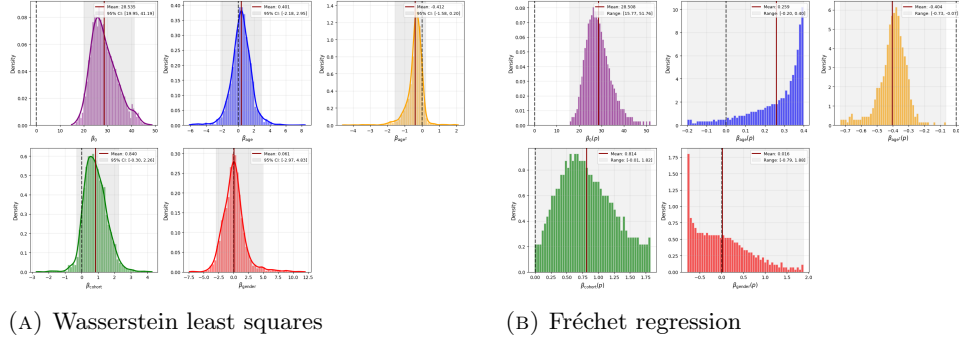


FIGURE 7. Comparison of coefficient distributions from Wasserstein least squares and Fréchet regression. **(a)** Marginal distributions of the random coefficient vector $\beta \sim \widehat{Q}$ estimated via Wasserstein least squares. Each panel shows the empirical distribution of one coefficient component from the $M = 2000$ particle representation of \widehat{Q} . Histogram with kernel density estimate overlay; vertical black dashed line at zero; The red vertical line indicates the mean; the gray shaded region shows the range from the 2.5-th to the 97.5-th quantile on each distribution. **(b)** Marginal distributions of coefficient functions $\beta_k(p)$ from Fréchet regression as in equation (54). Unlike Wasserstein least squares, Fréchet yields pointwise estimates $\beta_k(p)$ for each quantile level $p \in [0.001, 0.999]$.

probability level $p \in (0, 1)$, the resulting coefficient functions $\beta_k(p)$ are strictly parameterized by this single scalar. This induces near-perfect correlations across all coefficient pairs. Wasserstein least squares, by contrast, estimates a full multidimensional measure \widehat{Q} that captures the covariance structure among the demographic variables.

This architectural difference has severe implications for conditional inference, exposing a critical limitation of the pointwise Fréchet approach, as demonstrated by our variance partition analysis (Figure 9).

In a classical multivariate setting, we can compute the conditional standard deviation of the demographic effects given a specific baseline BMI (β_0) using the Schur complement:

$$\Sigma_{\text{rest}|\beta_0} = \Sigma_{22} - \Sigma_{21}\Sigma_{11}^{-1}\Sigma_{12}.$$

For Wasserstein least squares, this conditional variance remains substantial. It reflects the biological reality that subpopulations sharing the same baseline BMI profile can still exhibit highly varied physiological responses to aging and generational shifts. For Fréchet regression, the conditional standard deviation collapses to approximately zero. Because its coefficients are perfectly correlated by the quantile index p , knowing the intercept deterministically dictates the exact slopes for age, cohort, and gender. This artificial rigidity structurally prevents the Fréchet model from capturing independent, localized demographic heterogeneity.

Because Wasserstein least squares preserves the full joint distribution of the coefficients, it can explore rare population dynamics. Fréchet regression’s quantile-based construction forces certain structural assumptions—such as a strictly positive

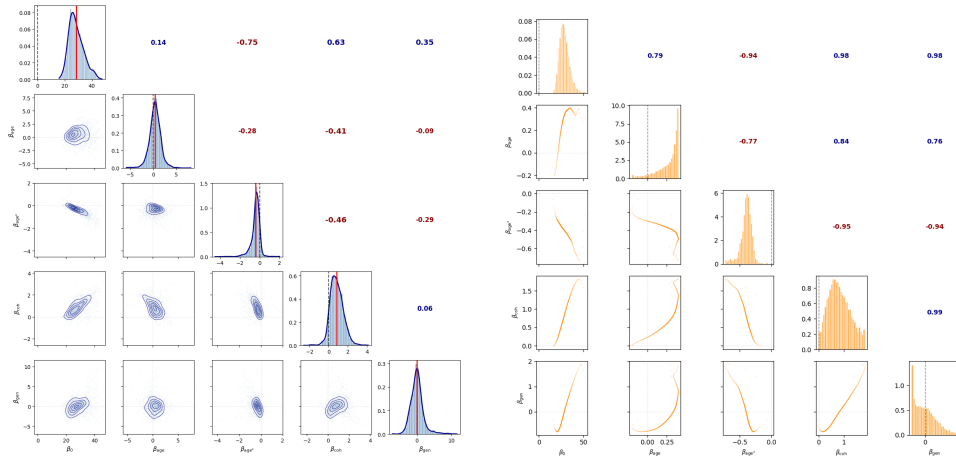


FIGURE 8. Comparison of joint distribution structures between Wasserstein least squares and Fréchet regression. **To the left:** Corner plot showing the joint distribution structure of $\beta \sim \hat{Q}$. Diagonal panels: marginal distributions (histogram with KDE) for each coefficient; black vertical line at zero, red vertical line at the mean. Lower triangle: bivariate scatter plots showing pairwise joint distributions with contour lines from kernel density estimation. Upper triangle: Pearson correlation coefficients ρ_{ij} between coefficient pairs; Blue text indicates positive correlation, red indicates negative. **To the right:** corner plots showing the joint distribution structure of the regression coefficients $\beta = (\beta_0, \beta_{\text{age}}, \beta_{\text{age}^2}, \beta_{\text{cohort}}, \beta_{\text{gender}})^T$ for Fréchet regression. Diagonal panels show marginal distributions; lower triangles show pairwise scatter plots; upper triangles show Pearson correlations.

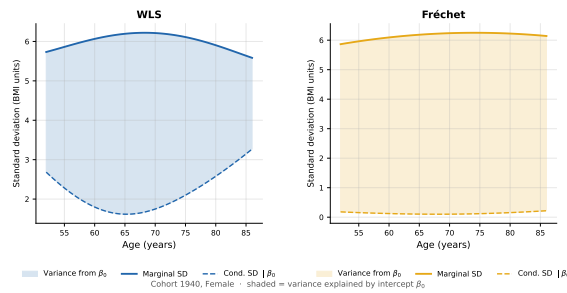


FIGURE 9. Marginal versus conditional standard deviation (cohort 1940, female). The shaded region represents the variance explained by knowing β_0 .

cohort effect—across the entire distribution. In contrast, interrogating the Wasserstein least squares particle cloud reveals distinct minority trajectories.

For instance, while the vast majority of the modeled population exhibits a late-life plateau or decline in BMI, approximately 10% of the Wasserstein least squares particles yield a positive quadratic age coefficient ($\beta_{\text{age}^2} > 0$). Within the model framework, this corresponds to a subpopulation experiencing accelerating BMI growth in later years (Figure 10).

To quantify how prevalent this convex pattern is in the data, we fit an individual quadratic regression $\text{BMI}_i(t) = a_i + b_it + c_it^2$ to each trajectory in the 1940–44 female cohort and classify it as *convex* if $c_i > 0$, the fitted minimum (at $t^* = -b_i/2c_i$) occurs strictly within the observed age window, and the predicted BMI at the last observation exceeds that minimum by at least 3.5 units. Under this definition, approximately 10.0% of individuals (197 out of 1,964 with at least four observations) exhibit a genuine upturn; the remaining 90.0% are concave or monotone. Figure 11 visualizes the two groups: the majority (blue) follows the familiar plateau-and-decline pattern, while the minority (orange) shows a clear BMI minimum in mid-follow-up, followed by a rise at older ages.

Similarly, the model identifies a reverse cohort effect for roughly 10% of the particles ($\beta_{\text{cohort}} < 0$), suggesting a subset of individuals for whom more recent birth cohorts actually exhibit lower BMI scores (Figure 12).

Crucially, these minority coefficients do not appear as uniformly distributed noise within the Wasserstein least squares framework. When mapped onto the joint distribution of the intercept and linear age effect ($\beta_0, \beta_{\text{age}}$), the particles exhibiting these extreme β_{age^2} and β_{cohort} values cluster in specific regions (Figure 13). This localized clustering points toward a complex demographic profile. For instance, the cluster of particles with $\beta_{\text{age}^2} > 0$ formed around $(30, -1)$ suggests that a subgroup of retirees with a high starting BMI exhibits a convex weight trajectory, meaning these individuals experience accelerating weight gain toward the later years of their lives.

While establishing these minority trajectories as distinct biological phenomena requires subsequent empirical verification, identifying them illustrates a practical utility of the Wasserstein least squares framework. By extending the machinery of classical linear regression to the Wasserstein space, Wasserstein least squares provides an interpretability tool alongside its predictive capabilities. It allows researchers to observe localized structural heterogeneity directly from the model outputs, offering a principled way to generate hypotheses from complex distributional data.

Conditional trajectory and obesity persistence. The obesity epidemic represents one of the most pressing public health crises of our time (Ward et al., 2019). From an epidemiological perspective, modeling longitudinal BMI trajectories is critical, particularly regarding the persistence of obesity, which the Centers for Disease Control and Prevention (CDC) defines as $\text{BMI} \geq 30$ (Centers for Disease Control and Prevention, 2024). Population-level interventions rely on understanding not just average weight gain, but the genuine probability that individuals at the threshold will either cross into severe obesity or return to healthier baseline levels over time. It is in this predictive, conditional context that the structural advantages of Wasserstein least squares over Fréchet regression become apparent.

To demonstrate this clinical utility, we compute conditional BMI trajectories and obesity probabilities for both models. For Wasserstein least squares, consider the coefficient distribution \hat{Q} represented via $M = 20,000$ particles $\{\beta^{(m)}\}_{m=1}^M$. To

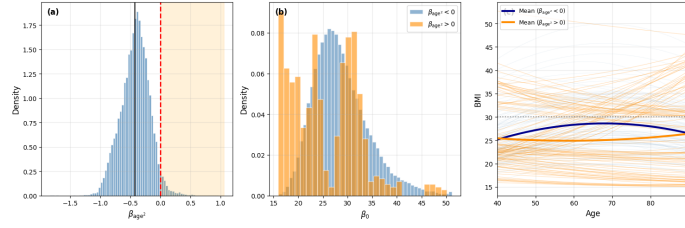


FIGURE 10. Analysis of particles with $\beta_{\text{age}^2} > 0$ (accelerating BMI growth). Using $M = 20,000$ particles, approximately 10% exhibit positive quadratic age coefficients, representing individuals whose BMI continues to accelerate with age rather than plateau or decline. (a) Marginal distribution of β_{age^2} ; vertical dashed line indicates zero, solid line shows the mean. Shaded region highlights particles with $\beta_{\text{age}^2} > 0$. (b) Conditional distribution of β_0 (intercept) given the sign of β_{age^2} . (c) BMI trajectories for cohort 1940, female. Blue curves show 100 sampled trajectories with $\beta_{\text{age}^2} < 0$ (typical); orange curves show trajectories with $\beta_{\text{age}^2} > 0$ (accelerating). Thick lines indicate conditional means. Horizontal line marks the obesity threshold (BMI = 30).

compute trajectories conditional on BMI ≈ 31 at age 50, we identify the subset of particles satisfying the conditioning criterion

$$(56) \quad \mathcal{M}_{50} = \{m : |\mathbf{x}(50)^\top \boldsymbol{\beta}^{(m)} - 31| \leq 2\},$$

where $\mathbf{x}(a) = (1, \tilde{a}, \tilde{a}^2, \tilde{c}, \tilde{g})^\top$ denotes the covariate vector at age a with normalized components $\tilde{a} = (a - \bar{a})/s_a$, $\tilde{c} = (c - \bar{c})/s_c$, and $\tilde{g} \in \{-1, +1\}$ for gender. The conditional mean trajectory at age a is then

$$(57) \quad \hat{\mu}(a) = \frac{1}{|\mathcal{M}_{50}|} \sum_{m \in \mathcal{M}_{50}} \mathbf{x}(a)^\top \boldsymbol{\beta}^{(m)},$$

and the $C\%$ prediction interval is given by the $(100 - C)/2$ th and $(100 + C)/2$ th percentiles of the distribution $\{\mathbf{x}(a)^\top \boldsymbol{\beta}^{(m)}\}_{m \in \mathcal{M}_{50}}$. The probability of obesity at age a , conditional on BMI at age 50, is computed as the proportion of conditional particles exceeding the threshold:

$$(58) \quad \text{P}(\text{BMI} \geq 30 \mid a, \text{BMI}_{50} \approx 31) = \frac{|\{m \in \mathcal{M}_{50} : \mathbf{x}(a)^\top \boldsymbol{\beta}^{(m)} \geq 30\}|}{|\mathcal{M}_{50}|}.$$

For Fréchet regression, the coefficient vectors $\{\boldsymbol{\beta}(p)\}_{p \in \mathcal{P}}$ are indexed by quantile level $p \in (0, 1)$, discretized over a fine grid \mathcal{P} . Conditioning proceeds analogously by identifying quantile levels that produce the target BMI at age 50

$$(59) \quad \mathcal{P}_{50} = \{p \in \mathcal{P} : |\mathbf{x}(50)^\top \boldsymbol{\beta}(p) - 31| \leq 2\}.$$

Mean trajectories and prediction intervals are computed over this subset, and the conditional obesity probability takes the form

$$(60) \quad \text{P}(\text{BMI} \geq 30 \mid a, \text{BMI}_{50} \approx 31) = \frac{|\{p \in \mathcal{P}_{50} : \mathbf{x}(a)^\top \boldsymbol{\beta}(p) \geq 30\}|}{|\mathcal{P}_{50}|}.$$

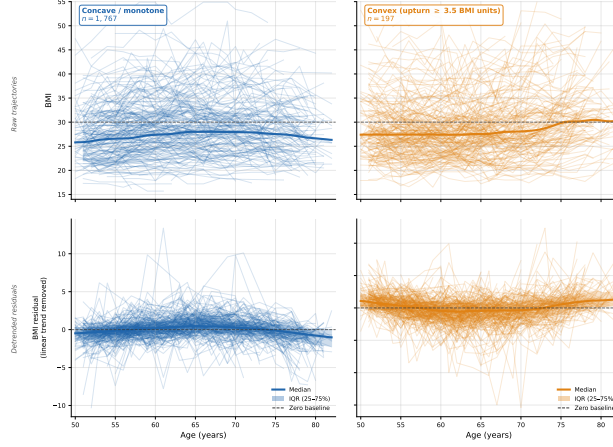


FIGURE 11. **Concave/monotone vs. convex BMI trajectories, cohort 1940–44, female.** *Top row:* individual observed BMI trajectories (thin lines) with group median (thick line); dashed line at BMI = 30. *Bottom row:* detrended residuals after removing each individual’s personal linear trend, with smoothed median and interquartile range (IQR) band (25th–75th percentile); dashed line at zero (no curvature). *Left (blue):* the 90% majority whose trajectories are concave or monotone. *Right (orange):* the 10% minority classified as convex ($n = 197$ out of 1,964 with ≥ 4 observations) — BMI reaches a minimum in mid-follow-up and rises again at older ages (upturn ≥ 3.5 BMI units above the fitted vertex). The residuals confirm that the upward curvature in the convex group is a systematic feature, not an artifact of baseline level differences.

To incorporate a second observation, we further restrict to particles satisfying conditions at both ages. For instance, to condition on $\text{BMI}_{50} \approx 31$ and $\text{BMI}_{60} > 31$, we define

$$(61) \quad \mathcal{M}_{50,60} = \{m : |\mathbf{x}(50)^\top \boldsymbol{\beta}^{(m)} - 31| \leq 2 \text{ and } \mathbf{x}(60)^\top \boldsymbol{\beta}^{(m)} > 31\}.$$

Trajectories and prediction intervals are computed over $\mathcal{M}_{50,60}$ using the same formulas as above. The conditional obesity probability with sequential conditioning becomes

$$(62) \quad \text{P}(\text{BMI} \geq 30 \mid a, \text{BMI}_{50}, \text{BMI}_{60} \in \mathcal{C}) = \frac{|\{m \in \mathcal{M}_{50,60} : \mathbf{x}(a)^\top \boldsymbol{\beta}^{(m)} \geq 30\}|}{|\mathcal{M}_{50,60}|},$$

where \mathcal{C} denotes the conditioning set for BMI at age 60. In our analysis, we consider $\mathcal{C} = (33, \infty)$ for continued weight gain, $\mathcal{C} = (31, \infty)$ for sustained obesity, and $\mathcal{C} = (-\infty, 30)$ for return below the obesity threshold.

The practical consequences of these different conditioning architectures can be understood in two complementary ways: the forecasted BMI trajectories (Figure 14) and the corresponding age-dependent probability of obesity (Figure 15).

When conditioning on a single observation at the threshold (BMI = 31 at age 50), Wasserstein least squares yields wide 80% prediction intervals spanning roughly 8

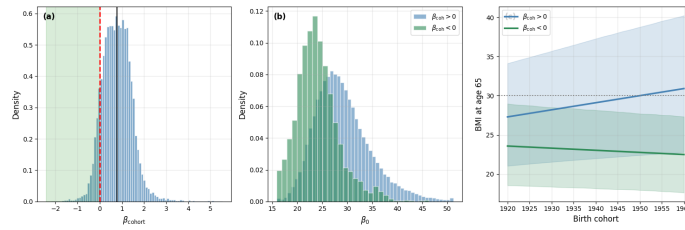


FIGURE 12. Analysis of particles with $\beta_{\text{cohort}} < 0$ (reverse cohort effect). Using $M = 20,000$ particles, approximately 6% exhibit negative cohort coefficients, representing individuals for whom later birth cohorts have lower BMI—opposite of the typical obesity epidemic trend. (a) Marginal distribution of β_{cohort} ; vertical dashed line indicates zero. Shaded region highlights particles with $\beta_{\text{cohort}} < 0$. (b) Conditional distribution of β_0 (intercept) given the sign of β_{cohort} . (c) Mean predicted BMI at age 65 as a function of birth cohort for female respondents, stratified by the sign of β_{cohort} . Shaded bands show 80% prediction intervals. For typical particles ($\beta_{\text{cohort}} > 0$), later cohorts have higher BMI; for the minority with $\beta_{\text{cohort}} < 0$, the trend reverses. Horizontal line marks the obesity threshold.

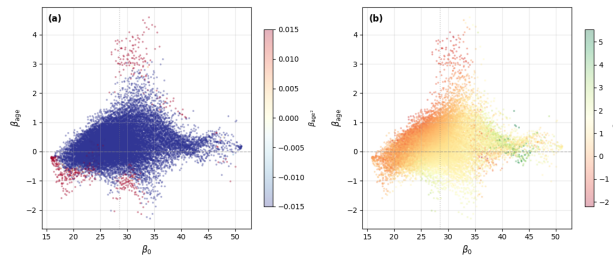


FIGURE 13. Joint distribution of coefficients colored by extreme values ($M = 20,000$ particles). (a) Scatter plot of $(\beta_0, \beta_{\text{age}})$ colored by β_{age}^2 . Particles with $\beta_{\text{age}}^2 > 0$ (red/orange) tend to cluster in specific regions of the $(\beta_0, \beta_{\text{age}})$ space, revealing the correlation structure among coefficients. (b) Same scatter plot colored by β_{cohort} . Particles with $\beta_{\text{cohort}} < 0$ (red) show distinct patterns in the joint distribution.

to 12 BMI units. This is not a lack of precision but a reflection of genuine biological uncertainty; as observed, the empirical distribution of the trajectories fans out in a manner similar to the prediction interval.

Consequently, the conditional probability of obesity (Panel 1 of Figure 15) produces smooth, clinically meaningful curves. An individual with a BMI of 31 at age 50 faces a steady decline in obesity risk, reaching roughly 50% by age 90, indicating that individuals with the same current BMI may follow vastly different long-term trajectories.

In contrast, conditioning the Fréchet model on the same single observation exhibits a highly constrained behavior. Because the target BMI selects only a narrow cluster of quantile levels (roughly 39 to 48 out of 500), and each level defines a deterministic trajectory, the resulting prediction intervals are exceptionally narrow. This forces the conditional obesity probabilities (Panel 2 of Figure 15) into near-binary states with sharp transition zones. The apparent predictive precision in this case is largely a structural consequence of pointwise quantile regression, which inherently limits the representation of individual-level variance within the forecasted paths.

This structural divergence is further highlighted when sequential conditioning is introduced to update longitudinal predictions. For Wasserstein least squares, incorporating a second measurement at age 60 refines the forecast. As seen in the right panel of Figure 14, stratifying the age 60 observations into three outcomes (continued weight gain, stable obesity, or returning below the threshold) differentiates future trajectories and narrows the prediction intervals.

The probability curves adjust accordingly (Panel 3 of Figure 15): a second measurement below the obesity threshold shifts the predicted outcome, dropping the long-run obesity probability toward zero. This indicates that Wasserstein least squares accommodates sequential updating, where the initial predictive variance is reduced as new observations are incorporated.

By contrast, applying this sequential conditioning illustrates a structural constraint within the Fréchet framework. By age 60, only 7 to 38 quantile levels satisfy the criteria for the stable or weight-gain scenarios. Notably, for the subset representing a return below the obesity threshold ($\text{BMI} < 30$ at age 60), zero quantile levels survive. Because every Fréchet trajectory that predicts $\text{BMI} \approx 31$ at age 50 in this specific fit also predicts $\text{BMI} \geq 30$ at age 60, this particular sequence of observations cannot be represented under the fitted model.

To empirically evaluate the predictive structures of both models, we compare their conditional forecasts against the observed trajectories of the corresponding HRS cohorts (males and females born 1935–1939 and 1940–1944 with $\text{BMI} \in [29, 33]$ at age 50). Table 4 summarizes the empirical coverage of the prediction intervals averaged across age bins 50 to 75.

Wasserstein least squares, which retains 2,953 posterior draws after conditioning, yields an empirical coverage of 0.877 for its 99% PI and 0.579 for its 75% PI. In contrast, the Fréchet model selects 78 quantile-level vectors, resulting in empirical coverages of 0.456 and 0.355 for the 99% and 75% PIs, respectively. The larger negative gap between empirical and nominal coverage in the Fréchet model indicates that its constrained trajectories do not fully encompass the observed spread of individual outcomes.

This difference in coverage is visually apparent in Figure 16. The Wasserstein least squares prediction intervals gradually widen with age, remaining generally centered on the empirical box plots and accommodating the varying long-term trajectories of individuals starting from a similar baseline.

By contrast, the Fréchet intervals are substantially narrower and tend to drift above the empirical distributions at older ages. Because the pointwise quantile regression framework largely pre-determines a quantile’s future path once its level is fixed at age 50, it structurally understates the inherent variability in long-term BMI progression.

Method	PI level	n_{ptcl}	n_{real}	Mean emp. coverage	Gap
Wasserstein least squares	99%	2953	632	0.877	-0.113
Wasserstein least squares	75%	2953	632	0.579	-0.171
Fréchet	99%	78	632	0.456	-0.534
Fréchet	75%	78	632	0.355	-0.395

TABLE 4. **Empirical PI coverage for single conditioning** (BMI $\in [29, 33]$ at age 50, cohorts 1935–39 and 1940–44, both sexes; trajectory shown for the 1935–39 female reference group). For each method, we report the mean empirical coverage across age bins 50–75 for the 75% and 99% prediction intervals, together with the gap (empirical – nominal). Wasserstein least squares retains heterogeneous posterior draws, whereas Fréchet selects quantile-level coefficient vectors; the large negative gap for Fréchet reflects that a handful of near-deterministic quantile trajectories cannot represent the spread of individual outcomes.

Building on the single conditioning results, we extend our empirical evaluation to sequential conditioning. We assess how well both models capture the observed trajectories of individuals measured at both age 50 (BMI $\in [29, 33]$) and age 60 across three distinct clinical scenarios: worsening (BMI > 33), stable (BMI $\in [29, 33]$), and improved (BMI < 29). Table 5 details the empirical coverage for these subgroups. While Wasserstein least squares exhibits some under-coverage relative to nominal levels, it consistently maintains higher coverage than the Fréchet model.

For the worsening and stable scenarios, Fréchet’s coverage drops significantly, with its 99% PIs capturing only 17.3% and 44.5% of the empirical data, respectively. This large negative gap indicates that a small subset of deterministic quantile trajectories struggles to encompass the natural variance of observed longitudinal outcomes. Furthermore, for the improved scenario, Fréchet retains zero quantile levels, meaning coverage cannot even be calculated.

These coverage metrics translate directly to the forecasted trajectories shown in Figure 17. The top row demonstrates that Wasserstein least squares successfully differentiates the three conditional pathways. The resulting prediction intervals adapt logically to the second observation; whether the trajectory worsens, remains stable, or improves, the Wasserstein least squares intervals remain broad enough to generally bracket the empirical box plots of the real HRS cohort. For the improved scenario, Wasserstein least squares does produce a median trajectory that descends below the obesity threshold, but its predicted path is monotonically decreasing, failing to capture the convexity visible in the empirical trajectories, where BMI typically bottoms out and then rises again at older ages; an observation actually supported by our model (see Fig. 10 panel (c), where the sampled trajectories with $\beta_{\text{age}^2} > 0$ predict a behavior similar to the improved case). This limitation is at least partly a data artifact: observations become sparser at older ages as cohort members attrit from the study, so the linear model is effectively pulled toward the more data-rich middle-age trajectories, biasing the predicted trend at the tail of the follow-up window.

Scenario	Method	PI level	n_{ptcl}	n_{real}	Mean emp. coverage	Gap
BMI > 33 at 60	Wasserstein least squares	99%	1029	204	0.692	-0.298
	Wasserstein least squares	75%	1029	204	0.417	-0.333
	Fréchet	99%	21	204	0.173	-0.817
	Fréchet	75%	21	204	0.138	-0.612
BMI 29–33 at 60	Wasserstein least squares	99%	1729	333	0.709	-0.281
	Wasserstein least squares	75%	1729	333	0.489	-0.261
	Fréchet	99%	57	333	0.445	-0.545
	Fréchet	75%	57	333	0.351	-0.399
BMI < 29 at 60	Wasserstein least squares	99%	195	169	0.491	-0.499
	Wasserstein least squares	75%	195	169	0.244	-0.506

TABLE 5. **Empirical PI coverage for double conditioning** (BMI $\in [29, 33]$ at age 50, three age-60 scenarios, cohorts 1935–39 and 1940–44, both sexes; trajectory shown for the 1935–39 female reference group). Fréchet quantile-level coefficients are shown only when at least 15 levels survive the conditioning step; in the improved scenario, no Fréchet levels are eligible (all trajectories predict BMI ≥ 29 at age 60) and are therefore omitted. Wasserstein least squares under-covers relative to its nominal level because the prediction band captures uncertainty about the population-level template Q^* , not individual random variability.

The bottom row of Figure 17 illustrates the structural constraints of applying sequential conditioning within the pointwise Fréchet framework. For both the worsening and stable scenarios, the surviving quantile levels yield prediction bands that are substantially narrower than those of Wasserstein least squares, often failing to capture the spread of the empirical data. For the improved scenario, the model cannot generate a prediction at all. Because every Fréchet trajectory that places a patient near the obesity threshold at age 50 strictly predicts an elevated BMI at age 60, the framework mathematically precludes the empirical reality of a patient successfully reducing their BMI over that specific decade.

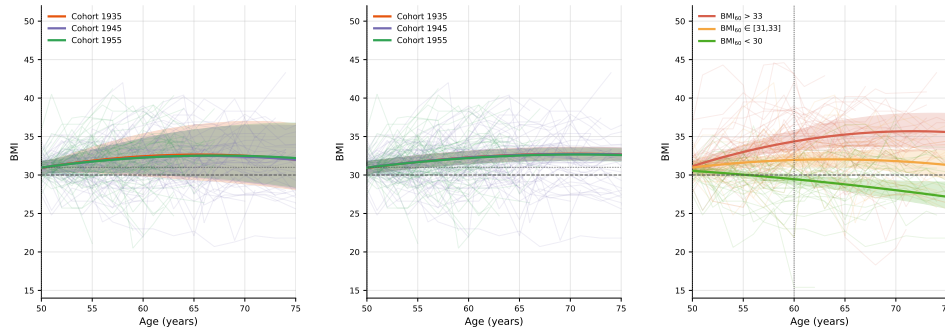


FIGURE 14. **Observed BMI trajectories (thin lines) overlaid on model-implied 80% prediction bands (shaded) for individuals at the obesity threshold (BMI = 31 at age 50), ages 50–75.** Prediction bands are the 10th–90th percentile of $\{x(\text{age})^\top \beta_m\}_{m=1}^{M'}$, where β_m are the $M' \leq M$ particles (Wasserstein least squares) or quantile-level coefficient vectors (Fréchet) that survive the conditioning criterion $\hat{y}(50) \in [30, 32]$. Dashed horizontal line: obesity threshold (BMI = 30); dotted horizontal line: conditioning level (BMI = 31); dotted vertical line: conditioning age (50). **(Left) Wasserstein least squares** ($M = 20,000$ particles, three birth cohorts, female respondents): orange = cohort 1935, purple = cohort 1945, green = cohort 1955. The 80% prediction bands are wide (≈ 8 – 12 BMI units). Conditioning on a single BMI observation does not uniquely identify the coefficient vector, so the joint distribution \hat{Q} retains substantial spread. Observed trajectories largely fall within the prediction intervals. **(Center) Fréchet** (same conditioning): After conditioning on BMI = 31 at age 50, only 39–48 quantile-level coefficient vectors $\hat{\beta}(p)$ satisfy the criterion, and since all coefficients are determined by the same quantile level p , The entire trajectory is nearly fixed. The near-degenerate prediction bands contrast with the heterogeneous spread of observed individual paths, revealing that Fréchet’s apparent precision is a structural artifact rather than genuine predictive accuracy. **(Right) Wasserstein least squares with sequential conditioning** (cohort 1945, female; dotted vertical lines at ages 50 and 60): starting from BMI ≈ 31 at age 50, a second observation at age 60 focuses predictions. Red: BMI₆₀ > 33 (continued weight gain, $n = 541$ particles, $n_{\text{obs}} = 42$); orange: BMI₆₀ $\in [31, 33]$ (stable obesity, $n = 697$, $n_{\text{obs}} = 34$); green: BMI₆₀ < 30 (returned below threshold, $n = 132$, $n_{\text{obs}} = 32$). The three groups trace clearly separated trajectories with substantially narrowed prediction bands, demonstrating that Wasserstein least squares uncertainty is meaningful and resolves as additional observations accumulate.

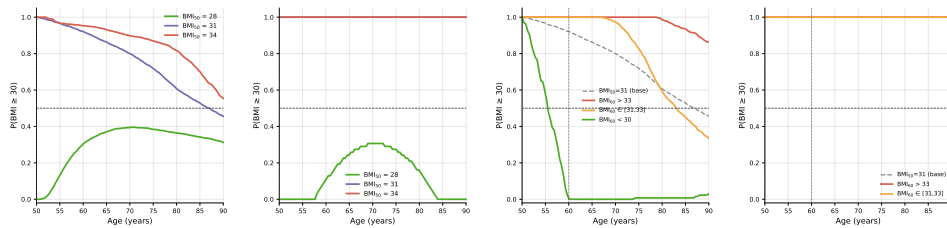


FIGURE 15. **Probability of obesity ($\text{BMI} \geq 30$) as a function of age for females in cohort 1945, comparing Wasserstein least squares and Fréchet regression under single and sequential conditioning. (Panel 1) Wasserstein least squares, single conditioning.** Conditioning on BMI at age 50 produces smooth, clinically meaningful probability curves. Individuals starting below the threshold ($\text{BMI}_{50} = 28$, green) show a modest, gradually rising probability of obesity, peaking at 30%–40% in their seventies before declining. Those just above ($\text{BMI}_{50} = 31$, purple) begin at certainty and see their probability decline steadily, reaching roughly 50% by age 90, reflecting long-run uncertainty. Individuals well into obesity ($\text{BMI}_{50} = 34$, red) maintain high probability ($> 80\%$) throughout, with a gradual decline toward 60% at age 90. The smooth transitions arise because the Wasserstein least squares posterior retains heterogeneity among the coefficient draws that survive conditioning: individuals with the same current BMI may follow different future trajectories. **(Panel 2) Fréchet, single conditioning.** Near-binary probabilities (close to 0 or 1) with sharp transition zones. In Fréchet regression, the fitted object is a collection of $K = 500$ quantile-level coefficient vectors $\hat{\beta}_k$, one per quantile level k/K ; conditioning on an observed BMI range selects only those quantile levels whose predicted value falls within the observed range. Since each $\hat{\beta}_k$ traces a deterministic trajectory, the selected quantile levels are clustered ($n \approx 28$ – 62 levels survive), implying near-certain future BMI predictions given a single current measurement. This is a structural feature of pointwise quantile regression rather than a reflection of the underlying biological uncertainty. **(Panel 3) Wasserstein least squares, sequential conditioning.** Starting from $\text{BMI}_{50} \approx 31$ (gray dashed, base), a second observation at age 60 differentiates long-run outcomes. When $\text{BMI}_{60} > 33$ (red), the obesity probability rises toward 100% and remains persistently high. When $\text{BMI}_{60} \in [31, 33]$ (orange), the probability stays elevated but begins to decline after age 70, reaching roughly 60% at age 80. When $\text{BMI}_{60} < 30$ (green), the probability drops toward zero—a second healthy-range measurement effectively reclassifies the long-run prognosis. **(Panel 4) Fréchet, sequential conditioning.** Applying the same double conditioning to the Fréchet quantile-level coefficients leaves only 7–38 quantile levels for the $\text{BMI}_{60} > 33$ and $\text{BMI}_{60} \in [31, 33]$ scenarios; the improved scenario retains zero levels, as every quantile-level trajectory that predicts $\text{BMI}_{50} \approx 31$ also predicts $\text{BMI}_{60} \geq 30$, making a healthy second observation structurally impossible under the fitted model. Horizontal dashed line: $P = 0.5$; vertical dotted lines: conditioning ages (50 and 60).

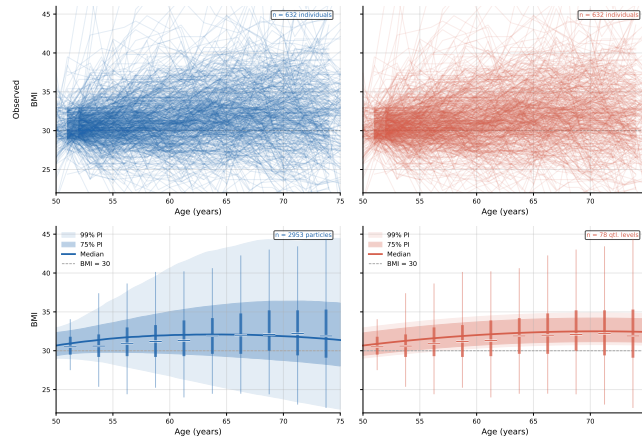


FIGURE 16. **Predicted BMI trajectories under single conditioning ($\text{BMI} \in [29, 33]$ at age 50), cohorts 1935–39 and 1940–44, both sexes.** The top row shows individual observed BMI trajectories from the matched HRS cohort for Wasserstein least squares (left, blue) and Fréchet (right, red). The bottom row shows the Wasserstein least squares (left) and Fréchet (right) prediction intervals together with empirical box plots of the real cohort’s BMI distribution at each age bin. Box plots show the interquartile range (thick segment), 2.5th–97.5th percentile whiskers, and median tick; trajectory shown for the 1935–39 female reference group. **Wasserstein least squares** (left) retains $n = 2,953$ posterior draws after conditioning, producing smooth 75% and 99% prediction intervals that grow as age increases and remain well-centered on the empirical distribution. The band reflects genuine uncertainty: individuals with $\text{BMI} \approx 31$ at age 50 may follow very different trajectories, as evidenced by both the width of the intervals and the spread of the real box plots. **Fréchet** (right) selects $n = 78$ quantile-level coefficient vectors after conditioning, producing prediction intervals that are substantially narrower than those of Wasserstein least squares and that drift above the empirical box plots at older ages. This reflects the near-deterministic nature of the individual quantile trajectories under pointwise quantile regression: once a quantile level is pinned at age 50, its future path is largely pre-determined, understating the true variability in long-run BMI outcomes.

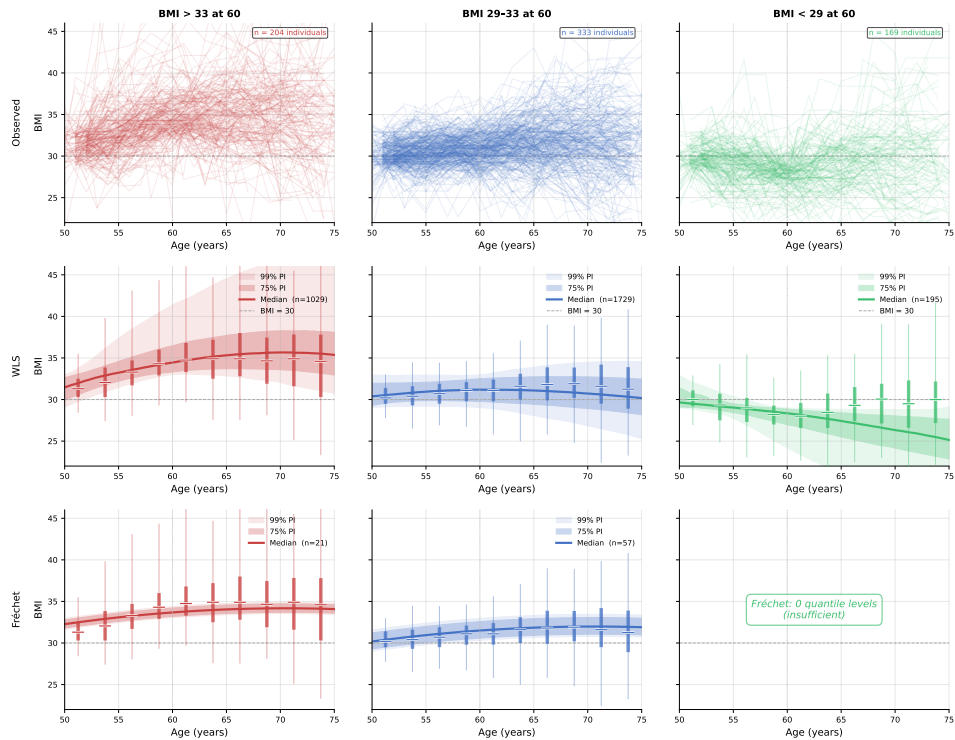


FIGURE 17. **Predicted BMI trajectories under sequential conditioning ($\text{BMI} \in [29, 33]$ at age 50 followed by three scenarios at age 60), cohorts 1935–39 and 1940–44, both sexes.** Columns correspond to three second-observation scenarios: worsening ($\text{BMI} > 33$ at 60, red), stable ($\text{BMI} 29\text{--}33$ at 60, blue), and improved ($\text{BMI} < 29$ at 60, green). The top row shows individual observed trajectories from the matched HRS cohort; the middle row shows Wasserstein least squares predictions; the bottom row shows Fréchet. Shaded bands are 75% (darker) and 99% (lighter) prediction intervals; the solid line is the predicted median. Thin box plots show the empirical BMI distribution of matched real individuals at each age bin (IQR as thick segment, 2.5th–97.5th percentile whiskers). Vertical dotted lines mark the two conditioning ages (50 and 60). Trajectory shown for the 1935–39 female reference group. **Wasserstein least squares** successfully differentiates all three scenarios. The worsening trajectory maintains a median BMI well above 30 throughout follow-up ($n = 1,029$ posterior draws); the stable scenario shows a modestly elevated trajectory ($n = 1,729$); the improved scenario produces a median that crosses below 30 within a few years and remains low, though with wide prediction intervals reflecting the small retained sample ($n = 195$). **Fréchet** produces meaningful results only for the worsening ($n = 21$ quantile levels) and stable ($n = 57$) scenarios. Both intervals are narrower than their Wasserstein least squares counterparts, underscoring the structural limitations of pointwise quantile regression under sequential conditioning. The improved scenario retains zero quantile levels—every quantile-level trajectory that places $\text{BMI} \approx 31$ at age 50 also predicts $\text{BMI} \geq 29$ at age 60, making the improvement condition structurally empty under the Fréchet model.

APPENDIX B. SYNTHETIC DATA EXPERIMENTS

One-Dimensional Responses. We validate the Wasserstein least squares estimator under the template deformation model (WLR) with scalar responses ($d = 1$) and a two-dimensional covariate

$$\mathbf{x}_i = (1, t_i)^\top \in \mathbb{R}^2.$$

The true template is chosen as

$$Q^* = \mathcal{N}(m_Q, \Sigma_Q) \text{ on } \mathbb{R}^2, \quad m_Q = \begin{pmatrix} 0 \\ 1 \end{pmatrix}, \quad \Sigma_Q = I_2,$$

so that the marginal template at covariate $\mathbf{x} = (1, t)^\top$ is

$$(63) \quad Q_{\mathbf{x}}^* = \mathcal{N}(t, 1 + t^2), \quad t \in [-2, 2].$$

The variance $\sigma^2(t) = 1 + t^2$ is U-shaped in t . This is a deliberate stress test: the marginal variance grows quadratically with $|t|$, a non-linear feature that Fréchet regression on quantile functions cannot capture (Fig. 18). Covariates t_i are drawn

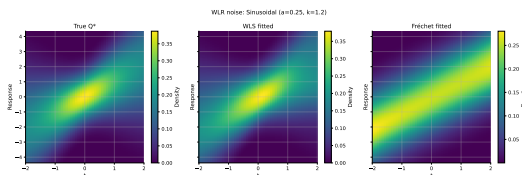


FIGURE 18. Template recovery under sinusoidal deformation ($k = 1.2$, $n = 50$). Density heatmaps of the true $Q_{\mathbf{x}}^*$ (left), Wasserstein least squares fit (center), and Fréchet fit (right) over the covariate range $t \in [-2, 2]$. Wasserstein least squares reproduces the U-shaped variance of the true template; Fréchet produces nearly uniform spread across all t .

uniformly from $[-2, 2]$; each response $\nu_i = (\nabla\phi_i)_\# Q_{\mathbf{x}_i}^*$ is approximated by an empirical measure of $m = 500$ i.i.d. draws.

We consider five families of random transport maps $\nabla\phi_i$, each satisfying conditions C1–C3 (see Table 6). The first three are affine; the last two are non-linear deformations that create non-Gaussian responses even when applied to a Gaussian template. Figure 19(a) illustrates 18 independent draws of $T(y)$ and the deviation $T(y) - y$ for each noise model.

We compare two estimators: Wasserstein least squares, estimated with the particle-based gradient descent estimator \hat{Q} defined in Algorithm 2, implemented with $M = 1,000$ particles and 1,500 gradient steps (learning rate $\tau_0 = 0.1$, exponential decay 10^{-3} , momentum 0.9, mini-batch size 5) for the visual panels of Fig. 19, and $M = 2,000$ particles and 3,000 steps for the averaged errors in Table 7; predictions $\hat{Q}_{\mathbf{x}}$ are formed via the \mathbf{x} -linear pushforward of the particle system. We also compare against Global Fréchet regression (Petersen and Müller, 2019), computed with OLS on the quantile functions, $\hat{\beta} = (X^\top X)^{-1} X^\top Q$, where Q is the $n \times K$ matrix of quantile functions evaluated on a grid of $K = 200$ quantile levels; the fitted quantile $\hat{Q}_{\mathbf{x}}$ is the ℓ^2 -projection on monotone functions (PAVA).

Figure 19(b) displays, at four covariate values $t \in \{-1.8, -0.5, 0.5, 1.8\}$, the true marginal $Q_{\mathbf{x}_i}^*$ (black dashed), six independent noisy realisations ν_i (grey),

Name	Transport map $T(y)$	Parameters	α	β
<i>Affine / near-affine models</i>				
Additive	$y + \varepsilon, \varepsilon \sim \mathcal{N}(0, \sigma^2)$	$\sigma = 0.3$	1.00	1.00
Radial scaling	$(1 + \eta)y, \eta \sim \mathcal{U}(-a, a)$	$a = 0.3$	0.70	1.30
Location-scale	$ay + b, a \sim \mathcal{N}(1, \sigma_s^2)_{>0}, b \sim \mathcal{N}(0, \sigma_s^2)$	$\sigma_s = 0.2$	0.40	1.60
<i>Non-linear models</i>				
Sinusoidal ($k = 1.2$)	$y + A \sin(ky), A \sim \mathcal{U}(-A_{\max}, A_{\max})$	$k = 1.2, A_{\max} = 0.25$	0.70	1.30
Sinusoidal ($k = 2.5$) [†]	$y + A \sin(ky), A \sim \mathcal{U}(-A_{\max}, A_{\max})$	$k = 2.5, A_{\max} = 0.30$	0.25	1.75
Gaussian Bump [†]	$y + Aye^{-y^2/(2\sigma_b^2)}, A \sim \mathcal{U}(-A_{\max}, A_{\max})$	$A_{\max} = 0.8, \sigma_b = 1.0$	0.20	1.80
Tanh warp	$y + A \tanh(ky), A \sim \mathcal{U}(-A_{\max}, A_{\max})$	$k = 0.8, A_{\max} = 0.4$	0.68	1.32

TABLE 6. **Noise models for the 1-D template deformation experiment.** Each model defines a random transport map $T(y) = \nabla \phi_i(y)$ satisfying conditions C1–C3. The curvature band $[\alpha, \beta]$ gives the almost-sure range of $T'(y) = \nabla^2 \phi_i(y)$, i.e. the C3 bounds on the slope of the transport map. Models marked [†] appear in Panel (a) of Fig. 19 only; the remaining five are used in the comparison of Table 7.

the Wasserstein least squares fit (blue), and the Fréchet fit (red dashed), for the additive and sinusoidal noise models. Several features are apparent. First, the Wasserstein least squares fit closely tracks the true density at all four covariate values and under both noise models: the estimated spread widens correctly as $|t|$ increases. Second, the Fréchet fit consistently under-estimates the spread at $|t| = 1.8$ and over-estimates it near $t = 0$; its width is nearly constant across the four panels, a direct consequence of the linear quantile model. Third, Wasserstein least squares is robust to the type of noise: the blue curves under additive and sinusoidal noise are virtually indistinguishable, confirming that the estimator does not require knowledge of the noise distribution.

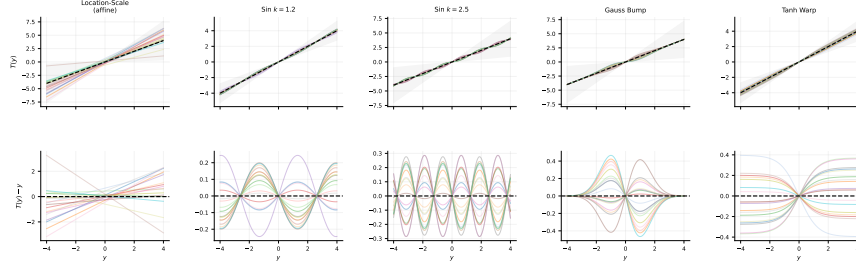
Figure 19(c) focuses on template recovery. At $t \in \{-1.8, 0.0, 1.8\}$, we plot the true Q_x^* alongside the Wasserstein least squares fits under additive (blue) and sinusoidal (green) noise, and the Fréchet fit (red dashed, common to both noise models). Both Wasserstein least squares curves agree closely with the truth, while the Fréchet curve exhibits the predicted mis-calibration: it produces roughly the same spread at all three t values, matching neither the narrow distribution at $t = 0$ nor the wide distributions at $t = \pm 1.8$. Table 7 reports the average W_2 error against $\{\nu_i\}_{1 \leq i \leq 50}$ and the error against the true template Q^* , averaged over $n_{\text{rep}} = 5$ independent replicates of size $n = 50$.

For the error versus Q^* , the Wasserstein least squares estimator achieves values between 0.039 and 0.167 across all five noise models, while Fréchet regression ranges from 0.343 to 0.364. The Wasserstein least squares improvement is roughly $5\times$ for mild (sinusoidal, additive) noise and $2\times$ for the more challenging location-scale model. Figure 19(d) provides a per-observation view: each scatter plot places the Fréchet W_2 error on the x -axis and the Wasserstein least squares W_2 error on the y -axis for the same observation; points below the diagonal correspond to observations where Wasserstein least squares achieves a smaller error. In all five noise models, all the points fall below the diagonal.

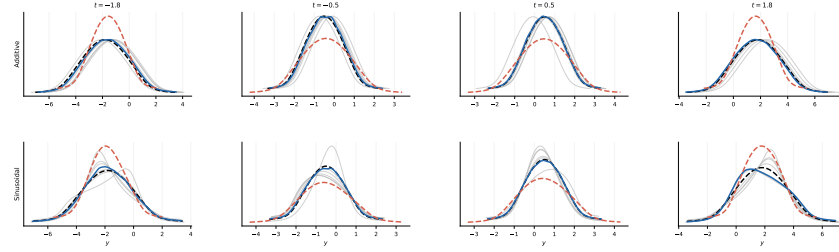
TABLE 7. **1-D template deformation: Wasserstein least squares vs. Fréchet regression.** Average W_2 error against $\{\nu_i\}_{1 \leq i \leq 50}$ and error versus the true template Q^* , mean \pm std over 5 replicates ($n = 50$ observations each); Wasserstein least squares fitted with $M = 2,000$ particles and $T = 3,000$ steps. All Wasserstein least squares errors are strictly smaller than the corresponding Fréchet errors.

Noise model	[α, β]		Average W_2 (vs ν_i)		Vs. true Q^* (W_2)	
	α	β	Wasserstein least squares	Fréchet	Wasserstein least squares	Fréchet
Additive ($\sigma = 0.3$)	1.00	1.00	0.223 \pm 0.035	0.437 \pm 0.023	0.071 \pm 0.026	0.356 \pm 0.012
Radial ($a = 0.3$)	0.70	1.30	0.270 \pm 0.026	0.420 \pm 0.039	0.143 \pm 0.055	0.356 \pm 0.009
Location-Scale ($\sigma_s = 0.2$)	0.40	1.60	0.338 \pm 0.053	0.496 \pm 0.062	0.167 \pm 0.065	0.364 \pm 0.012
Sinusoidal ($k = 1.2$)	0.70	1.30	0.085 \pm 0.008	0.357 \pm 0.007	0.039 \pm 0.011	0.343 \pm 0.001
Tanh Warp ($k = 0.8$)	0.68	1.32	0.139 \pm 0.012	0.364 \pm 0.019	0.067 \pm 0.024	0.345 \pm 0.003

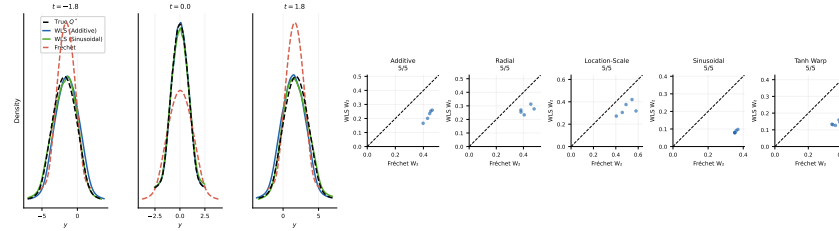
a



b



c



d

FIGURE 19. **Wasserstein least squares recovers Q^* under affine and non-linear noise; Fréchet regression is structurally misspecified.** DGP: $\nu_i = (\nabla\phi_i)\#Q_{\mathbf{x}_i}^*$, $Q_{\mathbf{x}_i}^* \sim \mathcal{N}(t, 1+t^2)$, $n = 50$, five noise models (see Table 6). **(a)** 18 draws of $T(y) = \nabla\phi_i(y)$ per model (coloured), identity (black dashed), C3 curvature band (grey fill); bottom row shows the deviation $T(y) - y$. **(b)** Densities at $t \in \{-1.8, -0.5, 0.5, 1.8\}$ for Additive and Sinusoidal ($k=1.2$) noise: true $Q_{\mathbf{x}_i}^*$ (black dashed), noisy ν_i (grey), Wasserstein least squares (blue), Fréchet (red dashed). Wasserstein least squares spread widens with $|t|$; Fréchet width is flat. **(c)** Q^* recovery at $t \in \{-1.8, 0, 1.8\}$: Wasserstein least squares under Additive (blue) and Sinusoidal (green) noise tracks the truth; Fréchet (red dashed) predicts constant spread at all t . **(d)** Per-observation W_2 scatter (Wasserstein least squares vs. Fréchet, in-sample); points below the diagonal favor Wasserstein least squares. See Table 7 for numerical summaries.

Bivariate Gaussian Responses. We extend the simulation to bivariate responses ($d = 2$) with a two-dimensional covariate $\mathbf{x}_i = (1, t_i)^\top \in \mathbb{R}^2$. This setting exercises the full multivariate structure of model (WLR): the template $Q^* \in \mathcal{P}(\mathbb{R}^{dp})$ with $p = d = 2$ must capture how a 2×2 random covariance matrix varies with the scalar predictor t .

We take $Q^* = \mathcal{N}(m_Q, \Sigma_Q)$ on \mathbb{R}^4 , with

$$m_Q = (0, 0, 0, 1)^\top, \quad \Sigma_Q = \begin{pmatrix} A & B \\ B^\top & C \end{pmatrix},$$

where

$$A = I_2, \quad B = \begin{pmatrix} 0.5 & 0.2 \\ 0.2 & 0.1 \end{pmatrix}, \quad C = \begin{pmatrix} 1.0 & 0 \\ 0 & 0.3 \end{pmatrix}.$$

Via the Kronecker marginalisation in Eq. (118), the template at $\mathbf{x} = (1, t)^\top$ is

$$(64) \quad Q_{\mathbf{x}}^* = \mathcal{N}(\mu(t), \Sigma(t)), \quad \mu(t) = \begin{pmatrix} 0 \\ t \end{pmatrix}, \quad \Sigma(t) = A + t(B + B^\top) + t^2 C.$$

The mean $\mu(t)$ shifts linearly in t , while the covariance $\Sigma(t)$ traces a *quadratic* trajectory on the cone of symmetric positive definite matrices. At $t = 0$ the marginal is circular ($A = I_2$); as $|t|$ grows, the ellipse elongates and rotates. This is again a stress test for Fréchet regression.

We use three families of random maps $\nabla\phi_i : \mathbb{R}^2 \rightarrow \mathbb{R}^2$, each satisfying C1–C3:

Name	Transport map $T(\mathbf{y})$	Parameters
Additive	$\mathbf{y} + \boldsymbol{\varepsilon}$, $\boldsymbol{\varepsilon} \sim \mathcal{N}(\mathbf{0}, \sigma^2 I_2)$	$\sigma = 0.3$
Radial scaling	$(1 + \eta)\mathbf{y}$, $\eta \sim \mathcal{U}(-a, a)$	$a = 0.3$
Random rotation–scale	$R^\top D R \mathbf{y}$, $R \sim \text{SO}(2)$, $D = \text{diag}(s_1, s_2)$	$\theta \sim \mathcal{N}(0, 0.3^2)$, $s_k \sim \mathcal{U}(0.8, 1.2)$

TABLE 8. **Noise models for the bivariate Gaussian experiment.** All maps satisfy C1 (convex, C^2), C2 ($\mathbb{E}[T(\mathbf{y})] = \mathbf{y}$), and C3 (uniform curvature bounds). Each ν_i is approximated by the sample mean and covariance of $m = 500$ i.i.d. draws from $(\nabla\phi_i)_\# Q_{\mathbf{x}_i}^*$.

We compare two estimators:

- (1) Wasserstein least squares (Bures–Wasserstein gradient descent): the closed-form Gaussian specialization of the Wasserstein least squares estimator, implemented with Algorithm 1. Fitted with $K = 300$ gradient steps from a random initialization.
- (2) Fréchet-GD: the global Fréchet regression estimator of Petersen and Müller (2019), implemented for covariance matrices via iterative descent (Algorithm 1 in Xu and Li (2025)) with localization parameter $\rho = 0.01$, step size $\eta = 0.5$, and at most 200 iterations per prediction point.

Figure 20(a) shows 2σ ellipses at four covariate values $t \in \{-1.8, -0.5, 0.5, 1.8\}$ under Additive noise. The top row displays the noisy sample clouds and three independent realizations of ν_i (grey ellipses), confirming that the individual responses are substantially noisier than the template. The bottom row overlays the fitted ellipses. The Wasserstein least squares ellipses (blue) closely match the true template (black dashed) at all four values of t : the elongation and orientation of the ellipse

evolve correctly. The Fréchet-GD ellipses (red dashed) are systematically too small at $|t| = 1.8$, where the quadratic term t^2C dominates; they recover the shape only near $t = 0$.

Figure 20(b) plots the three independent entries of $\Sigma(t)$ against t on a fine grid. The true curves (black dashed) are quadratic in t ; the Wasserstein least squares curves (blue) track them closely, while the Fréchet-GD curves (red) approximate only the linear part and underestimate variance at the extremes. The structural origin of this limitation is the same as in the one-dimensional case: Fréchet regression’s linear weighting scheme cannot produce predictions outside the convex hull of training responses.

Figure 20(c) visualises the trajectory $t \mapsto \Sigma(t)$ as a curve in the three-dimensional space of SPD entries $(\Sigma_{11}, \Sigma_{22}, \Sigma_{12})$, shown through three coordinate projections. The true trajectory (black) sweeps a quadratic arc; the Wasserstein least squares curve (blue) tracks it closely across the full range $t \in [-2, 2]$. The Fréchet-GD curve (red) remains confined near the center of the training cloud, confirming the convex-hull constraint: it cannot extrapolate the quadratic growth that drives the trajectory at $|t| = 2$.

Table 9 reports the mean average W_2 error (versus ν_i) and the error against the true template Q^* , averaged over $n_{\text{rep}} = 5$ replicates of size $n = 50$. Wasserstein least squares achieves BW errors against the true template between 0.026 and 0.059, a factor of 6–14 \times smaller than Fréchet-GD (0.362–0.369). The ranking is consistent across all three noise models, including the non-linear rotation–scale model. Panel (d) provides the per-observation view: across all three noise models and all $n \times n_{\text{rep}} = 250$ training observations, nearly every single point in the scatter falls below the diagonal, meaning Wasserstein least squares achieves a smaller in-sample BW error than Fréchet-GD on every observation.

TABLE 9. **Bivariate Gaussian template deformation: Wasserstein least squares vs. Fréchet-GD.** Bures–Wasserstein error averaged over 5 replicates ($n = 50$ each). All Wasserstein least squares errors are strictly smaller than Fréchet-GD.

Noise model	Average W_2 (vs ν_i)		Vs. true Q^* (BW)	
	Wasserstein least squares	Fréchet-GD	Wasserstein least squares	Fréchet-GD
Additive ($\sigma = 0.3$)	0.102 \pm 0.006	0.371 \pm 0.009	0.059 \pm 0.005	0.369 \pm 0.001
Radial scaling ($a = 0.3$)	0.106 \pm 0.008	0.389 \pm 0.007	0.045 \pm 0.005	0.365 \pm 0.001
Random rotation–scale ($\theta_0 = 0.3$)	0.104 \pm 0.006	0.383 \pm 0.005	0.026 \pm 0.005	0.362 \pm 0.001

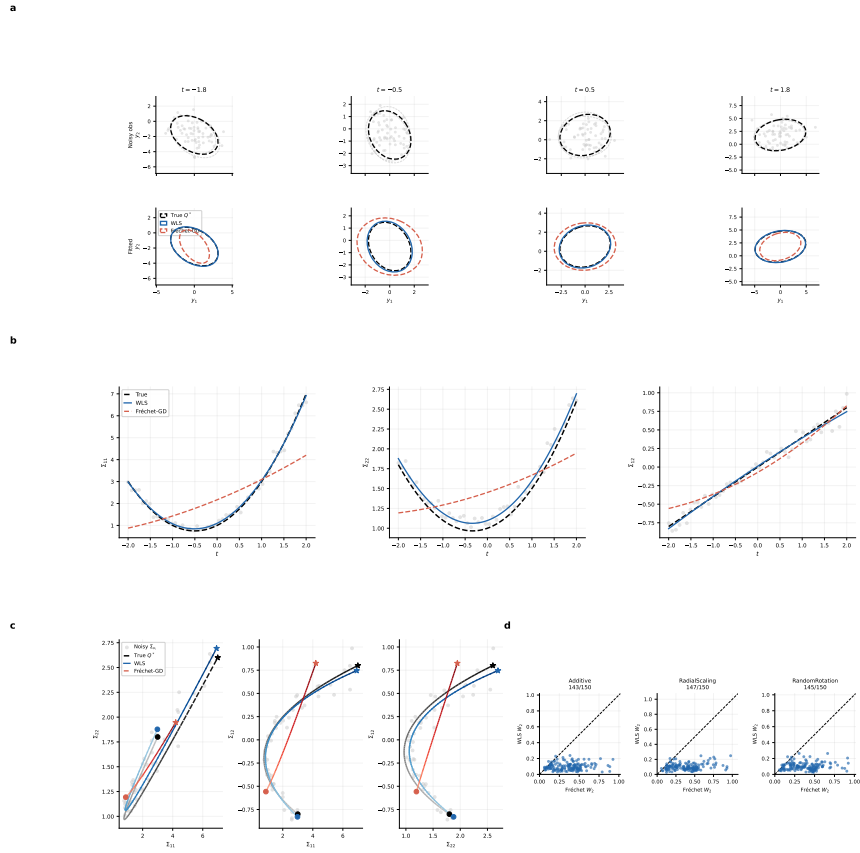


FIGURE 20. Wasserstein least squares recovers a quadratic covariance trajectory on the SPD manifold; Fréchet-GD is structurally misspecified. DGP: $\nu_i = (\nabla\phi_i)_\# Q_{x_i}^*$, $Q_{x_i}^* \sim \mathcal{N}(\mu(t), \Sigma(t))$ with $\Sigma(t) = A + t(B+B^\top) + t^2C$ (quadratic on the SPD manifold), $n = 50$, three noise models (see Table 8). **(a)** 2σ ellipses at $t \in \{-1.8, -0.5, 0.5, 1.8\}$ under Additive noise. *Top row:* noisy sample clouds and noisy ν_i ellipses (grey). *Bottom row:* true $Q_{x_i}^*$ (black dashed), Wasserstein least squares (blue), Fréchet-GD (red dashed). Wasserstein least squares ellipses track the evolving shape; Fréchet-GD ellipses are too small at extreme t . **(b)** Covariance entries Σ_{11} , Σ_{22} , Σ_{12} vs t : true curve (black dashed), Wasserstein least squares (blue), Fréchet-GD (red dashed), noisy observations (grey dots). Wasserstein least squares recovers the quadratic growth; Fréchet-GD recovers only the linear part. **(c)** Trajectory $t \mapsto (\Sigma_{11}, \Sigma_{22}, \Sigma_{12})$ projected onto three coordinate pairs in the space of SPD entries. Colour gradient encodes $t \in [-2, 2]$ (dark = $t=-2$, light = $t=2$); circles mark $t=-2$, stars mark $t=2$. Grey dots: noisy Σ_{ν_i} . The true trajectory (black) is a quadratic arc; Wasserstein least squares (blue) tracks it faithfully, while Fréchet-GD (red) collapses toward the training mean and cannot reproduce the nonlinear curvature. **(d)** Per-observation BW scatter (Wasserstein least squares vs. Fréchet-GD, in-sample); all points lie below the diagonal. See Table 9 for numerical summaries.

Rate Validation. We validate the $n^{-1/2}$ rate of Theorem 7 by isolating its n -dependent term. Taking $m = \infty$ (responses ν_i observed exactly as $K = 500$ -point quantile functions), the bound reduces to

$$(65) \quad \frac{1}{n} \sum_{i=1}^n W_2^2(\hat{Q}_{\mathbf{x}_i}, Q_{\mathbf{x}_i}^*) \lesssim \frac{1}{\sqrt{n}},$$

predicting a log–log slope of $-1/2$ in n .

We use the Bures–Wasserstein gradient estimator (Algorithm 1) rather than the particle method (Algorithm 2) so that the empirical rate reflects only the error sources controlled by Theorem 7: the statistical term $\sqrt{pd/n}$ and the within-measure term r_m (governed by m). The particle method carries a separate M -dependent discretization error whose joint scaling with n and m is a distinct question that we do not address here.

We use the template $Q_{\mathbf{x}}^* = \mathcal{N}(t, 1+t^2)$ with $\mathbf{x} = (1, t)^\top$, $t \sim \mathcal{U}[-2, 2]$ ($p = 2$, $d = 1$), and the three affine noise models from Table 6 (additive, radial, location-scale), which produce exactly Gaussian responses. We run $K = 500$ gradient descent steps and 20 independent realizations at each $n \in \{10, 25, 50, 100, 200, 500\}$.

Fig. 21 shows the median W_2^2 error and interquartile range on log–log axes together with $n^{-1/2}$ and n^{-1} reference lines. All three curves decay monotonically. The location-scale and radial models display a rate closer to n^{-1} over this range.

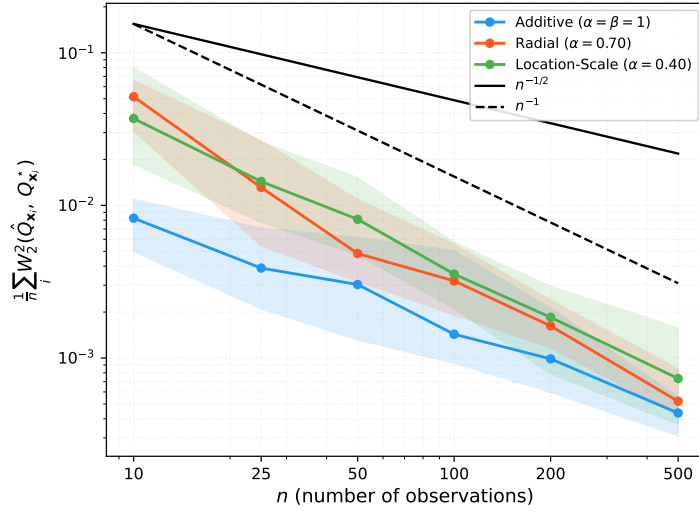


FIGURE 21. **Rate validation for Theorem 7: in-sample W_2^2 error vs. n in the $m=\infty$ regime.** Template: $Q_{\mathbf{x}_i}^* = \mathcal{N}(t_i, 1+t_i^2)$, three affine noise models (see Table 6), $n \in \{10, 25, 50, 100, 200, 500\}$, 20 seeds. Estimator: Bures–Wasserstein gradient descent ($K=500$ steps). Solid and dashed lines show $n^{-1/2}$ and n^{-1} reference slopes. All three models decay at a rate consistent with the $n^{-1/2}$ bound of Theorem 7; location-scale and radial curves display a rate closer to n^{-1} over this range.

APPENDIX C. COMPUTATIONAL COST

All times are wall-clock measurements on a 2022 MacBook Air. Fréchet regression is closed-form (OLS + optional PAVA projection) and takes less than one second in every setting.

Appendix A: Retirement data (HRS). Table 10 reports the fitting cost for the $n = 164$ demographic cells. The dominant cost is the main Wasserstein least squares quadratic fit ($M = 20,000$ particles, $T = 10,000$ iterations), which represents the highest-resolution estimate used for coefficient analysis and visualization. The LOO-CV fit uses a lighter configuration ($M = 2,000$, early stopping with patience = 100, typically converging in ~ 300 iterations).

TABLE 10. Wall-clock times — Appendix A (HRS, $n = 164$ cells, $K = 500$, $p = 5$). “WLS” = Wasserstein least squares.

Estimator	Parameters	Per fit	Total
WLS, quadratic (Particle GD)	$M = 20,000$, $T = 10,000$	≈ 11 min	≈ 11 min
WLS, LOO-CV, 164 folds (Particle GD)	$M = 2,000$, patience= 100	≈ 1 s	≈ 3 min
Fréchet, quadratic (OLS + PAVA)	$K = 500$	< 1 s	< 1 s

Appendix B: Synthetic experiments. Table 11 gives per-fit and total times for each subsection of Appendix B. “Total” refers to the full comparison run that produced the published tables and figures (number of fits in parentheses).

TABLE 11. Wall-clock times — Appendix B (synthetic experiments). “WLS” = Wasserstein least squares.

Estimator	Algorithm	Parameters	Per fit	Total
<i>One-dimensional responses ($n = 50$, $K = 200$; 5 models \times 5 reps = 25 fits)</i>				
WLS	Particle GD	$M = 2,000$, $T = 3,000$	5 s	≈ 2 min
Fréchet	OLS + PAVA	$K = 200$	< 1 s	< 1 s
<i>Bivariate Gaussian responses ($n = 50$, $d = p = 2$; 3 models \times 5 reps = 15 fits)</i>				
WLS	BW-GD (Algorithm 1)	$K = 300$, $dp = 4$	1.5 s	22 s
Fréchet-GD	Xu and Li (2025) Alg. 1	iter= 200	0.3 s	5 s
Fréchet-OLS	Closed-form	—	< 1 s	< 1 s
<i>Rate validation ($d = 1$, $p = 2$; 3 models \times 6 sizes \times 20 seeds = 360 fits)</i>				
WLS	BW-GD (Algorithm 1)	$K = 500$, $dp = 2$	0.2–2.5 s	≈ 8 min

APPENDIX D. LIFTING OF EUCLIDEAN LEAST SQUARES TO WASSERSTEIN LEAST SQUARES

Proof of Theorem 1. We apply the results of Lavenant (2024) to establish (12). In the notation of that paper, the right side of (12) is $\mathcal{T}_E(\nu_1, \dots, \nu_n)$ (Lavenant, 2024, Definition 3.6), with E defined as in (10), $Y = \mathbb{R}^d$, and $X = [n]$ equipped with the uniform probability measure m . Lavenant (2024, Proposition 3.13) shows that the minimum on the right side of (12) is attained, justifying the use of min in place of inf.

The functional E is continuous and, as $|X| < \infty$, it automatically satisfies (Lavenant, 2024, Assumption A). Therefore (Lavenant, 2024, Theorem 3.9) implies that \mathcal{T}_E satisfies requirement R1 and is the largest convex and lower-semicontinuous function dominated by

$$(66) \quad \tilde{\mathcal{T}}_E(\nu_1, \dots, \nu_n) = \begin{cases} E(\mathbf{y}_1, \dots, \mathbf{y}_n) & \text{if } \nu_i = \delta_{\mathbf{y}_i} \text{ for } i = 1, \dots, n \\ +\infty & \text{otherwise.} \end{cases}$$

Since \mathcal{E} as defined in (11) is convex, lower semi-continuous, and dominated by $\tilde{\mathcal{T}}_E$, we obtain that

$$\mathcal{E}(\nu_1, \dots, \nu_n) \leq \min_{P \in \Pi(\nu_1, \dots, \nu_n)} \int E(\mathbf{y}_1, \dots, \mathbf{y}_n) dP(\mathbf{y}_1, \dots, \mathbf{y}_n).$$

On the other hand, since \mathcal{T}_E satisfies R1 and R2 (Lavenant, 2024, Lemma 3.11 and Proposition 3.13), the reverse inequality also holds, which yields (12).

We now show that this expression agrees with (13). By Lemma 2, we may write

$$\begin{aligned} \min_{P \in \Pi(\nu_1, \dots, \nu_n)} \int \min_{f \in \mathcal{F}} \frac{1}{n} \sum_{i=1}^n \|\mathbf{y}_i - f(\mathbf{x}_i)\|_2^2 dP(\mathbf{y}_1, \dots, \mathbf{y}_n) &= \\ \min_{P \in \Pi(\nu_1, \dots, \nu_n)} \min_{\substack{P \in \mathcal{P}_2((\mathbb{R}^d)^n \times \mathcal{F}) \\ (\pi_1)_\# P = P}} \int \frac{1}{n} \sum_{i=1}^n \|\mathbf{y}_i - f(\mathbf{x}_i)\|_2^2 dP(\mathbf{y}_1, \dots, \mathbf{y}_n, f) &= \\ \min_{\substack{P \in \mathcal{P}_2((\mathbb{R}^d)^n \times \mathcal{F}) \\ (\pi_1)_\# P \in \Pi(\nu_1, \dots, \nu_n)}} \int \frac{1}{n} \sum_{i=1}^n \|\mathbf{y}_i - f(\mathbf{x}_i)\|_2^2 dP(\mathbf{y}_1, \dots, \mathbf{y}_n, f). \end{aligned}$$

where $\pi_1 : (\mathbb{R}^d)^n \times \mathcal{F} \rightarrow (\mathbb{R}^d)^n$ denotes the canonical projection.

Interchanging integration and summation, we obtain

$$\mathcal{E}(\nu_1, \dots, \nu_n) = \min_{\substack{P \in \mathcal{P}_2((\mathbb{R}^d)^n \times \mathcal{F}) \\ (\pi_1)_\# P \in \Pi(\nu_1, \dots, \nu_n)}} \frac{1}{n} \sum_{i=1}^n \int \|\mathbf{y}_i - f(\mathbf{x}_i)\|_2^2 dP(\mathbf{y}_1, \dots, \mathbf{y}_n, f).$$

We now observe that the i th integral depends only on the marginal distribution of the pair (\mathbf{y}_i, f) under P , which we denote by P_i . If we write $Q \in \mathcal{P}(\mathcal{F})$ for the distribution of f under P , then each of the n marginal measures (P_1, \dots, P_n) is a coupling between ν_i and Q . Conversely, given a collection of n couplings (P'_1, \dots, P'_n) between ν_i and some element $Q' \in \mathcal{P}(\mathcal{F})$, the gluing lemma (Villani, 2009) implies that we can combine these into a $P' \in \mathcal{P}_2((\mathbb{R}^d)^n \times \mathcal{F})$ such that $(\pi_1)_\# P' \in \Pi(\nu_1, \dots, \nu_n)$. We may therefore replace minimization over P by minimization over Q and (P_1, \dots, P_n) to obtain

$$\begin{aligned} \mathcal{E}(\nu_1, \dots, \nu_n) &= \min_{Q \in \mathcal{P}(\mathcal{F})} \min_{\substack{P_i, i=1, \dots, n \\ P_i \in \Pi(\nu_i, Q)}} \frac{1}{n} \sum_{i=1}^n \int \|\mathbf{y}_i - f(\mathbf{x}_i)\|_2^2 dP_i(\mathbf{y}_i, f) \\ &= \min_{Q \in \mathcal{P}(\mathcal{F})} \frac{1}{n} \sum_{i=1}^n \min_{P_i \in \Pi(\nu_i, Q)} \int \|\mathbf{y}_i - f(\mathbf{x}_i)\|_2^2 dP_i(\mathbf{y}_i, f) \\ &= \min_{Q \in \mathcal{P}(\mathcal{F})} \frac{1}{n} \sum_{i=1}^n W_2^2(\nu_i, Q_{\mathbf{x}_i}), \end{aligned}$$

where the last step uses the fact that $\Pi(\nu_i, Q_{\mathbf{x}_i}) = (\text{Id}, \delta_{\mathbf{x}_i})_{\#} \Pi(\nu_i, Q)$, where $\delta_{\mathbf{x}_i}$ denotes the evaluation map at \mathbf{x}_i . \square

Proof of Theorem 2. Denote the right side of (15) by $\mathcal{S}(\nu_1, \dots, \nu_n)$. We first show that $\mathcal{S} \leq \mathcal{E}$. Let $\psi_1, \dots, \psi_n \in C(\mathcal{F})$ satisfy $\sum_i \psi_i = 0$, and let $P \in \Pi(\nu_1, \dots, \nu_n)$ be arbitrary. Since $\sum_i \psi_i = 0$, we have

$$\begin{aligned} \frac{1}{n} \sum_{i=1}^n S_i \psi_i(\mathbf{y}_i) &= \frac{1}{n} \sum_{i=1}^n \inf_{f \in \mathcal{F}} \|\mathbf{y} - f(\mathbf{x}_i)\|^2 - \psi_i(f) \\ &\leq \inf_{f \in \mathcal{F}} \frac{1}{n} \sum_{i=1}^n \|\mathbf{y}_i - f(\mathbf{x}_i)\|^2 - \sum_i \psi_i(f) = E(\mathbf{y}_1, \dots, \mathbf{y}_n), \end{aligned}$$

so

$$\frac{1}{n} \sum_{i=1}^n \int S_i \psi_i d\nu_i = \int \frac{1}{n} \sum_{i=1}^n S_i \psi_i(\mathbf{y}_i) dP(\mathbf{y}_1, \dots, \mathbf{y}_n) \leq \int E dP.$$

Taking the supremum over ψ_1, \dots, ψ_n and infimum over P shows that $\mathcal{S} \leq \mathcal{E}$.

We now show that $\mathcal{S} \geq \mathcal{E}$. As in the proof of Theorem 1, we appeal to the results of Lavanant (2024): by (Lavanant, 2024, Theorem 3.9),

$$(67) \quad \mathcal{E}(\nu_1, \dots, \nu_n) = \sup_{\phi_1, \dots, \phi_n \in C_b} \left\{ \frac{1}{n} \sum_{i=1}^n \int \phi_i d\nu_i : \right. \\ \left. \frac{1}{n} \sum_{i=1}^n \phi_i(\mathbf{y}_i) \leq E(\mathbf{y}_1, \dots, \mathbf{y}_n) \quad \forall \mathbf{y}_i, i = 1, \dots, n \right\}.$$

Let ϕ_1, \dots, ϕ_n be feasible for (67). For $i = 1, \dots, n-1$, define

$$(68) \quad \psi_i(f) = \inf_{\mathbf{y}} \|\mathbf{y} - f(\mathbf{x}_i)\|^2 - \phi_i(\mathbf{y}),$$

and set $\psi_n(f) = -\sum_{i=1}^{n-1} \psi_i(f)$. Then $\psi_i \in C(\mathcal{F})$ for $i = 1, \dots, n$, and $\sum_{i=1}^n \psi_i = 0$ by construction.

We now check, for $i = 1, \dots, n-1$,

$$\begin{aligned} S_i \psi_i(\mathbf{y}_i) &= \inf_{f \in \mathcal{F}} \|\mathbf{y}_i - f(\mathbf{x}_i)\|^2 - \psi_i(f) \\ &= \inf_{f \in \mathcal{F}} \sup_{\mathbf{y}} \|\mathbf{y}_i - f(\mathbf{x}_i)\|^2 - \|\mathbf{y} - f(\mathbf{x}_i)\|^2 + \phi_i(\mathbf{y}) \\ &\geq \phi_i(\mathbf{y}_i). \end{aligned}$$

and

$$\begin{aligned} S_n \psi_n(\mathbf{y}_n) &= \inf_{f \in \mathcal{F}} \|\mathbf{y}_n - f(\mathbf{x}_n)\|^2 + \sum_{i=1}^{n-1} \psi_i(f) \\ &= \inf_{f, \mathbf{y}_1, \dots, \mathbf{y}_{n-1}} \sum_{i=1}^n \|\mathbf{y}_i - f(\mathbf{x}_i)\|^2 - \sum_{i=1}^{n-1} \phi_i(\mathbf{y}_i) \\ &\geq \phi_n(\mathbf{y}_n), \end{aligned}$$

where the final inequality follows from the fact that

$$(69) \quad \sum_{i=1}^{n-1} \phi_i(\mathbf{y}_i) \leq -\phi_n(\mathbf{y}_n) + \sum_{i=1}^n \|\mathbf{y}_i - f(\mathbf{x}_i)\|^2$$

for all $\mathbf{y}_1, \dots, \mathbf{y}_n$ and $f \in \mathcal{F}$ by assumption.

Therefore $\frac{1}{n} \sum_{i=1}^n \int S_i \psi_i d\nu_i \geq \frac{1}{n} \sum_{i=1}^n \int \phi_i d\nu_i$, and $\mathcal{S} \geq \mathcal{E}$ by (67). \square

Proof of Theorem 4. We follow the approach of [Agueh and Carlier \(2011\)](#). The proof of Theorem 2 shows that for $i = 1, \dots, n-1$ we can always consider ψ_i of the form in (68):

$$\begin{aligned} \psi_i(\mathbf{B}) &= \inf_{\mathbf{y}} \|\mathbf{y} - \mathbf{B}^\top \mathbf{x}_i\|^2 - \phi_i(\mathbf{y}) \\ &= \|\mathbf{B}^\top \mathbf{x}_i\|^2 - \sup_{\mathbf{y}} (2\mathbf{x}_i^\top \mathbf{B} \mathbf{y} - \|\mathbf{y}\|^2 + \phi_i(\mathbf{y})) \end{aligned}$$

for some $\phi_i \in C_b$. In particular, we can assume that for $i = 1, \dots, n-1$, the function $\mathbf{B} \mapsto \|\mathbf{B}^\top \mathbf{x}_i\|^2 - \psi_i(\mathbf{B})$ is convex. We may also assume by shifting by appropriate constants that $\psi_i(\mathbf{0}) = 0$ for all i .

Now let $(\psi^m)_{m \geq 1} := (\psi_1^m, \dots, \psi_n^m)_{m \geq 1}$ be a maximizing sequence for \mathcal{S} satisfying the above assumptions. For each $i \in [n]$ and $m \geq 1$, the assumption that $\psi_i^m(\mathbf{0}) = 0$ implies

$$(70) \quad S_i \psi_i^m(\mathbf{y}_i) \leq \|\mathbf{y}_i\|^2.$$

And since ψ^m is a maximizing sequence, there exists a constant C such that

$$(71) \quad \frac{1}{n} \sum_{i=1}^n \int S_i \psi_i^m d\nu_i \geq C \quad \forall i, m.$$

Since each ν_i has finite second moment, we obtain the existence of a constant C' such that

$$\begin{aligned} \int S_i \psi_i^m d\nu_i &\leq C' \\ \int S_i \psi_i^m d\nu_i &\geq nC - \sum_{j \neq i} \int S_j \psi_j^m d\nu_j \\ &\geq nC - (n-1)C' \end{aligned}$$

for all i and m .

For any $\mathbf{y}_i \in \mathbb{R}^d$ and $\mathbf{B} \in \mathbb{R}^{p \times d}$, we have

$$(72) \quad \psi_i^m(\mathbf{B}) \leq \|\mathbf{y}_i - \mathbf{B}^\top \mathbf{x}_i\|^2 - S_i \psi_i^m(\mathbf{y}_i),$$

and integrating the right side with respect to ν_i and using the boundedness of $\int S_i \psi_i^m d\nu_i$ shows that there exists a constant C'' such that the functions ψ_i^m satisfy

$$(73) \quad \psi_i^m(\mathbf{B}) \leq C''(1 + \|\mathbf{B}\|_F^2) \quad \forall i, m$$

Since we have assumed that $\psi_n^m = -\sum_{i=1}^{n-1} \psi_i^m$, we also obtain

$$(74) \quad \sum_{i=1}^{n-1} \psi_i^m(\mathbf{B}) = -\psi_n^m(\mathbf{B}) \geq -C''(1 + \|\mathbf{B}\|_F^2) \quad \forall m,$$

and therefore for $i = 1, \dots, n-1$

$$\begin{aligned} \psi_i^m(\mathbf{B}) &\geq -C''(1 + \|\mathbf{B}\|_F^2) - \sum_{\substack{j=1 \\ j \neq i}}^{n-1} \psi_j^m(\mathbf{B}) \\ &\geq -(n-1)C''(1 + \|\mathbf{B}\|_F^2) \quad \forall m. \end{aligned}$$

We conclude that, for each $i \in [n]$, the sequence $(\psi_i^m)_{m \geq 1}$ satisfies a bound of the form

$$(75) \quad |\psi_i^m(\mathbf{B})| \leq C'''(1 + \|\mathbf{B}\|_F^2) \quad \forall m.$$

Moreover, since $\mathbf{B} \mapsto \|\mathbf{B}^\top \mathbf{x}_i\|^2 - \psi_i^m(\mathbf{B})$ is convex for each $i = 1, \dots, n-1$ and $m \geq 1$, the functions ψ_i^m are uniformly equicontinuous on any convex, compact subset of $\mathbb{R}^{p \times d}$. By the Arzelà–Ascoli theorem, we may therefore extract limiting dual variables (ψ_1, \dots, ψ_n) to which a subsequence of $(\psi_1^m, \dots, \psi_n^m)$ converges uniformly on compacts. The constraint $\sum_i \psi_i = 0$ is clearly preserved in the limit, so to show that these limiting variables solve (15), we note that

$$\begin{aligned} \limsup_m S_i \psi_i^m(\mathbf{y}) &\leq \inf_{\mathbf{B}} \left\{ \limsup_m \|\mathbf{y} - \mathbf{B}^\top \mathbf{x}_i\|^2 - \psi_i^m(\mathbf{B}) \right\} \\ &= \inf_{\mathbf{B}} \|\mathbf{y} - \mathbf{B}^\top \mathbf{x}_i\|^2 - \psi_i(\mathbf{B}) \\ &= S_i \psi_i(\mathbf{y}). \end{aligned}$$

Since $\|\mathbf{y}_i\|^2 - S_i \psi_i^m(\mathbf{y}_i) \geq 0$ by (70), Fatou's lemma implies that

$$\begin{aligned} \mathcal{S}(\nu_1, \dots, \nu_n) &= \limsup_m \frac{1}{n} \sum_{i=1}^n \int S_i \psi_i^m \, d\nu_i \\ &\leq \frac{1}{n} \sum_{i=1}^n \int \limsup_m S_i \psi_i^m \, d\nu_i \\ &\leq \frac{1}{n} \sum_{i=1}^n \int S_i \psi_i \, d\nu_i, \end{aligned}$$

as claimed. \square

Proof of Theorem 5. Let ψ_1, \dots, ψ_n be solutions to (15), whose existence is guaranteed by Theorem 4. For each $i = 1, \dots, n$, define $\varphi_i : \mathbb{R}^d \rightarrow \mathbb{R}$ by

$$(76) \quad \varphi_i(\mathbf{z}) := \left(\frac{1}{2} \|\cdot\|^2 - \frac{1}{2} S_i \psi_i \right)^* (\mathbf{z}).$$

Clearly φ_i is convex.

We first claim that

$$(77) \quad \frac{1}{2} \psi_i(\mathbf{B}) \leq \frac{\|\mathbf{B}^\top \mathbf{x}_i\|^2}{2} - \varphi_i(\mathbf{B}^\top \mathbf{x}_i)$$

This follows directly from unrolling the definitions: for any $\mathbf{B} \in \mathbb{R}^{p \times d}$ and $\mathbf{y} \in \mathbb{R}^d$, (14) shows

$$\begin{aligned} \frac{1}{2} \psi_i(\mathbf{B}) &\leq \frac{1}{2} \|\mathbf{y} - \mathbf{B}^\top \mathbf{x}_i\|^2 - \frac{1}{2} S_i \psi_i(\mathbf{y}) \\ &= \frac{\|\mathbf{B}^\top \mathbf{x}_i\|^2}{2} - \left(\mathbf{y}^\top \mathbf{B}^\top \mathbf{x}_i - \left(\frac{1}{2} \|\mathbf{y}\|^2 - \frac{1}{2} S_i \psi_i(\mathbf{y}) \right) \right) \\ &\leq \frac{\|\mathbf{B}^\top \mathbf{x}_i\|^2}{2} - \left(\frac{1}{2} \|\cdot\|^2 - \frac{1}{2} S_i \psi_i \right)^* (\mathbf{z}), \end{aligned}$$

by the definition of the convex conjugate.

In particular, we obtain

$$0 = \frac{1}{2n} \sum_{i=1}^n \psi_i(\mathbf{B}) \leq \frac{1}{n} \sum_{i=1}^n \frac{\|\mathbf{B}^\top \mathbf{x}_i\|^2}{2} - \frac{1}{n} \sum_{i=1}^n \varphi_i(\mathbf{B}^\top \mathbf{x}_i),$$

proving (23).

To show that φ_i is an optimal Brenier potential and that (23) holds Q -a.s., we exploit duality. The optimality of Q and (ψ_1, \dots, ψ_n) implies

$$\begin{aligned} \frac{1}{n} \sum_{i=1}^n W_2^2(\nu_i, Q_{\mathbf{x}_i}) &= \frac{1}{n} \sum_{i=1}^n \int S_i \psi_i \, d\nu_i \\ &= \frac{1}{n} \sum_{i=1}^n \left(\int S_i \psi_i \, d\nu_i + \int \psi_i \, dQ \right) \\ (78) \quad &\leq \frac{1}{n} \sum_{i=1}^n \left(\int S_i \psi_i \, d\nu_i + \int (\|\cdot\|^2 - 2\varphi_i) \, dQ_{\mathbf{x}_i} \right), \end{aligned}$$

$$(79) \quad \leq \frac{1}{n} \sum_{i=1}^n \left(\int (\|\cdot\|^2 - 2\varphi_i^*) \, d\nu_i + \int (\|\cdot\|^2 - 2\varphi_i) \, dQ_{\mathbf{x}_i} \right)$$

where the first inequality follows from (77) and the second follows from

$$\varphi_i^* = \left(\frac{1}{2} \|\cdot\|^2 - \frac{1}{2} S_i \psi_i \right)^{**} \leq \frac{1}{2} \|\cdot\|^2 - \frac{1}{2} S_i \psi_i.$$

Kantorovich duality for optimal transport Villani (2009) then implies that (φ_i, φ_i^*) are optimal Brenier potentials and that (78) and (79) are both equalities. In particular, we see that we must have

$$(80) \quad 0 = \frac{1}{n} \sum_{i=1}^n \int (\|\cdot\|^2 - 2\varphi_i) \, dQ_{\mathbf{x}_i} = \int \frac{1}{n} \sum_{i=1}^n \|\mathbf{B}^\top \mathbf{x}_i\|^2 - 2\varphi_i(\mathbf{B}^\top \mathbf{x}_i) \, dQ(\mathbf{B}),$$

which, combined with the inequality (23), shows that the integrand must vanish Q -a.s. This establishes the forward direction of the claim.

Conversely, suppose that there exists Q and $\varphi_1, \dots, \varphi_n$ satisfying conditions 1 and 2. For $i = 1, \dots, n-1$, define

$$\psi_i(\mathbf{B}) = \|\mathbf{B}^\top \mathbf{x}_i\|^2 - 2\varphi_i(\mathbf{B}^\top \mathbf{x}_i),$$

and set $\psi_n = -\sum_{i=1}^{n-1} \psi_i$. Condition 2 guarantees that $\psi_n \leq \|\mathbf{B}^\top \mathbf{x}_n\|^2 - 2\varphi_n(\mathbf{B}^\top \mathbf{x}_n)$. Then clearly (ψ_1, \dots, ψ_n) are feasible in (15), and for $i = 1, \dots, n$,

$$\begin{aligned} S_i \psi_i(\mathbf{y}_i) &= \inf_{\mathbf{B}} \|\mathbf{y}_i - \mathbf{B}^\top \mathbf{x}_i\|^2 - \psi_i(\mathbf{B}) \\ &\geq \inf_{\mathbf{B}} \|\mathbf{y}_i - \mathbf{B}^\top \mathbf{x}_i\|^2 - \|\mathbf{B}^\top \mathbf{x}_i\|^2 + 2\varphi_i(\mathbf{B}^\top \mathbf{x}_i) \\ &= \|\mathbf{y}_i\|^2 - 2 \sup_{\mathbf{B}} (\mathbf{y}_i^\top \mathbf{B}^\top \mathbf{x}_i - \varphi_i(\mathbf{B}^\top \mathbf{x}_i)) \\ &= \|\mathbf{y}_i\|^2 - 2\varphi_i^*(\mathbf{y}_i). \end{aligned}$$

We obtain

$$\begin{aligned} \frac{1}{n} \sum_{i=1}^n W_2^2(\nu_i, Q_{\mathbf{x}_i}) &= \frac{1}{n} \sum_{i=1}^n \left(\int (\|\cdot\|^2 - 2\varphi_i^*) d\nu_i + \int (\|\cdot\|^2 - 2\varphi_i) dQ_{\mathbf{x}_i} \right) \\ &\leq \frac{1}{n} \sum_{i=1}^n \int S_i \psi_i d\nu_i + \int \frac{1}{n} \sum_{i=1}^n \|\mathbf{B}^\top \mathbf{x}_i\|^2 - 2\varphi_i(\mathbf{B}^\top \mathbf{x}_i) dQ(\mathbf{B}) \\ &= \frac{1}{n} \sum_{i=1}^n \int S_i \psi_i d\nu_i, \end{aligned}$$

where the first step follows from condition 1 and the last step follows from condition 2. The claim then follows from Theorem 4. \square

Proof of Theorem 6. Both sides of (23) are continuous, and since they are equal Q -a.e., they in fact agree everywhere on $\text{supp}(Q)$. Let $\mathbf{B} \in \text{supp}(Q)$ be arbitrary. The subdifferential of the left side of (15) at \mathbf{B} is (Hiriart-Urruty and Lemaréchal, 1993, Theorem VI.4.1.1)

$$\begin{aligned} \partial \left(\frac{1}{n} \sum_{i=1}^n \varphi_i(\cdot^\top \mathbf{x}_i) \right) (\mathbf{B}) &= \left\{ \frac{1}{n} \sum_{i=1}^n g_i : g_i \in \partial \varphi_i(\cdot^\top \mathbf{x}_i)(\mathbf{B}) \right\} \\ &= \left\{ \frac{1}{n} \sum_{i=1}^n x_i g_i^\top : g_i \in \partial \varphi_i(\mathbf{B}^\top \mathbf{x}_i) \right\}. \end{aligned}$$

On the other hand, since $\frac{1}{n} \sum_{i=1}^n \varphi_i(\cdot^\top \mathbf{x}_i) \leq \frac{1}{n} \sum_{i=1}^n \frac{\|\cdot^\top \mathbf{x}_i\|^2}{2}$ with equality at \mathbf{B} , the subdifferential of the left side at \mathbf{B} is included in the subdifferential of the right side at \mathbf{B} . Therefore

$$\left\{ \frac{1}{n} \sum_{i=1}^n x_i g_i^\top : g_i \in \partial \varphi_i(\mathbf{B}^\top \mathbf{x}_i) \right\} \subseteq \{\Sigma_{XX} \mathbf{B}\}.$$

Hence each subdifferential $\partial \varphi_i(\mathbf{B}^\top \mathbf{x}_i)$ is actually a singleton, so each φ_i is differentiable at $\mathbf{B}^\top \mathbf{x}_i$, proving (24). \square

Lemma 2. *Adopt either Assumption 1 or Assumption 2, and let $P \in \mathcal{P}_2((\mathbb{R}^d)^n)$. Then*

$$\begin{aligned} (81) \quad &\int \min_{f \in \mathcal{F}} \frac{1}{n} \sum_{i=1}^n \|\mathbf{y}_i - f(\mathbf{x}_i)\|_2^2 dP(\mathbf{y}_1, \dots, \mathbf{y}_n) \\ &= \min_{\substack{P \in \mathcal{P}_2((\mathbb{R}^d)^n \times \mathcal{F}) \\ (\pi_1)_\# P = P}} \int \frac{1}{n} \sum_{i=1}^n \|\mathbf{y}_i - f(\mathbf{x}_i)\|_2^2 dP(\mathbf{y}_1, \dots, \mathbf{y}_n, f). \end{aligned}$$

Proof. Let $\mathbf{Y} = (\mathbf{y}_1, \dots, \mathbf{y}_n) \in (\mathbb{R}^d)^n$, and write $\Phi(\mathbf{Y}, f) := \frac{1}{n} \sum_{i=1}^n \|\mathbf{y}_i - f(\mathbf{x}_i)\|_2^2$ for brevity. Then Φ is continuous, and the function

$$m(\mathbf{Y}) := \min_{f \in \mathcal{F}} \Phi(\mathbf{Y}, f)$$

is well defined (the minimum is attained under either Assumption 1 or Assumption 2) and continuous (by Berge's maximum theorem (Aliprantis and Border, 2006, Theorem 17.31) under Assumption 1 and by explicit computation under Assumption 2).

Let $\mathbf{P} \in \mathcal{P}_2((\mathbb{R}^d)^n \times \mathcal{F})$ be any admissible coupling, i.e. $(\pi_1)_\# \mathbf{P} = P$. The fact that $\Phi(\mathbf{Y}, f) \geq m(\mathbf{Y})$ for all $f \in \mathcal{F}$ implies

$$(82) \quad \int \Phi(\mathbf{Y}, f) d\mathbf{P}(\mathbf{Y}, f) \geq \int m(\mathbf{Y}) d\mathbf{P}(\mathbf{Y}, f) = \int m(\mathbf{Y}) dP(\mathbf{Y}).$$

On the other hand, suppose we can construct a Borel map $\sigma : (\mathbb{R}^d)^n \rightarrow \mathcal{F}$ such that

$$\Phi(\mathbf{Y}, \sigma(\mathbf{Y})) = m(\mathbf{Y}) \quad \forall \mathbf{Y} \in (\mathbb{R}^d)^n.$$

Then $\mathbf{P} = (\text{Id}, \sigma)_\# P$ satisfies $(\pi_1)_\# \mathbf{P} = P$ and

$$(83) \quad \int \Phi(\mathbf{Y}, f) d\mathbf{P}(\mathbf{Y}, f) = \int \Phi(\mathbf{Y}, \sigma(\mathbf{Y})) dP(\mathbf{Y}) = \int m(\mathbf{Y}) dP(\mathbf{Y}).$$

Combining (82) and (83) yields Eq. (81).

It remains to construct a suitable σ . Under Assumption 1, we note that for each \mathbf{Y} the set $\mathcal{F}_{\mathbf{Y}} := \operatorname{argmin}_{f \in \mathcal{F}} \Phi(\mathbf{Y}, f)$ is nonempty and the correspondence $\mathbf{Y} \mapsto \mathcal{F}_{\mathbf{Y}}$ is upper-hemicontinuous (again by Berge's theorem), hence the Kuratowski–Ryll–Nardzewski measurable selection theorem (Aliprantis and Border, 2006, Theorem 18.13) guarantees the existence of a Borel σ for which $\sigma(\mathbf{Y}) \in \mathcal{F}_{\mathbf{Y}}$. Under Assumption 2, we may choose the minimum-norm solution $\sigma(\mathbf{Y}) = (\mathbf{X}^\top \mathbf{X})^+ \mathbf{X}^\top \mathbf{Y} \in \mathcal{F}_{\mathbf{Y}}$, which is clearly also Borel. This proves the claim. \square

APPENDIX E. ESTIMATION OF WASSERSTEIN LEAST SQUARES

Proof of Theorem 7. We first reduce to the case where $\nabla \phi_i(0) = 0$ for all i . Write $\mathbf{v}_i := \nabla \phi_i(0)$, and define $\bar{\phi}_i(\mathbf{y}) = \phi_i(\mathbf{y}) - \langle \mathbf{v}_i, \mathbf{y} \rangle$. Condition C2 implies that $\mathbb{E}[\mathbf{v}_i] = 0$; therefore, the function $\bar{\phi}_i$ still satisfies conditions C1 to C3 as well as the further condition $\nabla \bar{\phi}_i(0) = 0$. Define $\bar{\nu}_i = (\nabla \bar{\phi}_i)_\# Q_{\mathbf{x}_i}^*$ and let $\tilde{\nu}_i$ be an empirical measure corresponding to the shifted measure $\bar{\nu}_i$. Finally, we let $\tilde{Q} = \operatorname{argmin}_{Q \in \mathcal{P}_2(\mathbb{R}^p \times d)} \frac{1}{n} \sum_{i=1}^n W_2^2(\tilde{\nu}_i, Q_{\mathbf{x}_i})$ be the analogue of (38) constructed from the shifted measures $\tilde{\nu}_i$.

The data $\tilde{\nu}_i$ and estimator \tilde{Q} correspond precisely to the model under investigation, under the added assumption that the deformations ϕ_i satisfy $\nabla \phi_i(0) = 0$ almost surely. Moreover, the following lemma shows that the expected in-sample error for the original data can be bounded by considering the same quantity for the shifted data.

Lemma 3. *The in-sample error satisfies*

$$(84) \quad \mathbb{E} \left[\frac{1}{n} \sum_{i=1}^n W_2^2(\hat{Q}_{\mathbf{x}_i}, Q_{\mathbf{x}_i}^*) \right] \lesssim \mathbb{E} \left[\frac{1}{n} \sum_{i=1}^n W_2^2(\tilde{Q}_{\mathbf{x}_i}, Q_{\mathbf{x}_i}^*) \right] + \sigma^2 \frac{pd}{n}.$$

We therefore adopt the assumption that $\nabla \phi_i(0) = 0$ almost surely in what follows, and conclude the ultimate error bound via Lemma 3. Under this reduction, $\nabla \bar{\phi}_i(0) = 0$ and $\nabla \bar{\phi}_i$ is β -Lipschitz by condition C3, so the assumption (41) that $\operatorname{supp}(Q_{\mathbf{x}_i}^*) \subset B_M$ implies $\operatorname{supp}(\bar{\nu}_i), \operatorname{supp}(\tilde{\nu}_i) \subset B_{\beta M}$ almost surely. Note that the boundedness assumption (41) is invariant under this centering reduction, since it is imposed on Q^* rather than on the deformed responses ν_i .

Let $\widehat{G} : \mathcal{P}_2(\mathbb{R}^{p \times d}) \rightarrow \mathbb{R}$ be the empirical loss

$$(85) \quad \widehat{G}(Q) := \frac{1}{n} \sum_{i=1}^n W_2^2(\widehat{\nu}_i, Q_{\mathbf{x}_i})$$

and let $G : \mathcal{P}_2(\mathbb{R}^{p \times d}) \rightarrow \mathbb{R}$ be its population counterpart

$$(86) \quad G(Q) := \frac{1}{n} \sum_{i=1}^n W_2^2(\nu_i, Q_{\mathbf{x}_i}).$$

We exploit a strong convexity inequality for the squared Wasserstein distance ([Manole et al., 2024](#), Theorem 6). For completeness, we give a proof of the particular bound we employ in Lemma 4. Since each ϕ_i is α -strongly convex, Lemma 4 yields

$$(87) \quad \frac{\alpha}{n} \sum_{i=1}^n W_2^2(\widehat{Q}_{\mathbf{x}_i}, Q_{\mathbf{x}_i}^*) \leq \int \left(\frac{1}{n} \sum_{i=1}^n \|\cdot^\top \mathbf{x}_i\|^2 - 2\phi_i(\cdot^\top \mathbf{x}_i) \right) d(Q^* - \widehat{Q}) + (G(\widehat{Q}) - G(Q^*)).$$

For any $R > 0$, let $B_R := \{\mathbf{y} \in \mathbb{R}^d : \|\mathbf{y}\| \leq R\}$ be the closed ball of radius R in \mathbb{R}^d . By Lemma 6, there exists $R > 0$ such that, under both $\mathbf{B} \sim \widehat{Q}$ and $\mathbf{B} \sim Q^*$, the support of \mathbf{XB} lies in $K := B_R^n \subseteq \mathbb{R}^{n \times d}$. Denote by \mathcal{K} the set of probability measures on $\mathbb{R}^{p \times d}$ with this property. Then since \widehat{Q} minimizes \widehat{G} , we have

$$(88) \quad G(\widehat{Q}) - G(Q^*) \leq G(\widehat{Q}) - \widehat{G}(\widehat{Q}) + \widehat{G}(Q^*) - G(Q^*) \leq 2 \sup_{Q \in \mathcal{K}} |G(Q) - \widehat{G}(Q)|.$$

For $\mathbf{Y} \in \mathbb{R}^{n \times d}$ with rows $\mathbf{y}_1^\top, \dots, \mathbf{y}_n^\top$, define the random variable

$$(89) \quad Z_{\mathbf{Y}} := \frac{1}{n} \sum_{i=1}^n \|\mathbf{y}_i\|^2 - 2\phi_i(\mathbf{y}_i)$$

Under conditions C1 and C2, $\mathbb{E}[\phi_i(\mathbf{y})] = \|\mathbf{y}\|^2/2$, so $Z_{\mathbf{Y}}$ is a mean-zero stochastic process on $\mathbb{R}^{n \times d}$, and we have

$$(90) \quad \left| \int \left(\frac{1}{n} \sum_{i=1}^n \|\cdot^\top \mathbf{x}_i\|^2 - 2\phi_i(\cdot^\top \mathbf{x}_i) \right) d(Q^* - \widehat{Q}) \right| = \left| \int Z_{\mathbf{XB}}(\widehat{Q} - Q^*)(d\mathbf{B}) \right|$$

$$(91) \quad \leq \sup_{\mathbf{B} : \mathbf{XB} \in K} |Z_{\mathbf{XB}}|.$$

Combining these estimates with (87) yields

$$(92) \quad \frac{\alpha}{n} \sum_{i=1}^n W_2^2(\widehat{Q}_{\mathbf{x}_i}, Q_{\mathbf{x}_i}^*) \lesssim \sup_{\mathbf{B} : \mathbf{XB} \in K} |Z_{\mathbf{XB}}| + \sup_{Q \in \mathcal{K}} |G(Q) - \widehat{G}(Q)|.$$

The first term is controlled by Dudley's chaining bound [Vershynin \(2018\)](#): Lemma 5 shows that

$$(93) \quad \mathbb{E} \sup_{\mathbf{B} : \mathbf{XB} \in K} |Z_{\mathbf{XB}}| \lesssim \frac{\beta R^2 \sqrt{pd}}{\sqrt{n}}.$$

A bound on the second term follows from known results in empirical convergence rates for the Wasserstein distance [Chizat et al. \(2020\)](#): by Lemma 7,

$$(94) \quad \mathbb{E} \left[\sup_{Q \in \mathcal{K}} |G(Q) - \widehat{G}(Q)| \right] \leq \frac{1}{n} \sum_{i=1}^n \mathbb{E} \left[\sup_{\mu \in \mathcal{P}(B_R)} |W_2^2(\mu, \nu_i) - W_2^2(\mu, \widehat{\nu}_i)| \right] \lesssim R^2 r_m.$$

Applying (93) and (94) to (92) and recalling Lemma 3 proves the claim. \square

Proof of Lemma 3. Given any probability measure μ with finite first moment, denote its mean by $m(\mu)$. The Wasserstein distance satisfies the following translation equivariance property. Given a vector v , let $\tau^v(x) = x + v$ be the map that translates by v . Then we have

$$(95) \quad W_2^2(\mu, \nu) = W_2^2(\tau_{\#}^{-m(\mu)}\mu, \tau_{\#}^{-m(\nu)}\nu) + \|m(\mu) - m(\nu)\|^2.$$

In (38), if we write $\widehat{m}_i := m(\widehat{\nu}_i)$ and $\mathbf{M} := m(Q)$, then the objective function may therefore be written as

$$(96) \quad \frac{1}{n} \sum_{i=1}^n W_2^2(\tau_{\#}^{-\widehat{m}_i}\widehat{\nu}_i, (\tau_{\#}^{-\mathbf{M}}Q)_{\mathbf{x}_i}) + \|\widehat{m}_i - \mathbf{M}^\top \mathbf{x}_i\|^2.$$

Reparametrizing in terms of the mean-zero measure $\tau_{\#}^{-\mathbf{M}}Q$, we can therefore equivalently consider two separate minimization problems, the first optimizing over the “shape” of Q , and the second over its mean:

$$\begin{aligned} \widehat{Q}^0 &\in \operatorname{argmin}_{Q^0 \in \mathcal{P}_2(\mathbb{R}^p \times d): \mathbb{E}_{Q^0} \mathbf{B} = 0} \frac{1}{n} \sum_{i=1}^n W_2^2(\tau_{\#}^{-\widehat{m}_i}\widehat{\nu}_i, Q_{\mathbf{x}_i}^0) \\ \widehat{\mathbf{M}} &\in \operatorname{argmin}_{\mathbf{M} \in \mathbb{R}^{p \times d}} \frac{1}{n} \sum_{i=1}^n \|\widehat{m}_i - \mathbf{M}^\top \mathbf{x}_i\|^2 \\ \widehat{Q} &:= \tau_{\#}^{\widehat{\mathbf{M}}}\widehat{Q}^0. \end{aligned}$$

By the same logic, the in-sample error satisfies

$$(97) \quad \frac{1}{n} \sum_{i=1}^n W_2^2(\widehat{Q}_{\mathbf{x}_i}, Q_{\mathbf{x}_i}^*) = \frac{1}{n} \sum_{i=1}^n W_2^2(\widehat{Q}_{\mathbf{x}_i}^0, (\tau_{\#}^{-\mathbf{M}^*}Q^*)_{\mathbf{x}_i}) + \|\widehat{\mathbf{M}}^\top \mathbf{x}_i - (\mathbf{M}^*)^\top \mathbf{x}_i\|^2$$

Applying the same decomposition to \widetilde{Q} yields $\widetilde{Q} = \tau_{\#}^{\widetilde{\mathbf{M}}}\widetilde{Q}^0$ and

$$(98) \quad \frac{1}{n} \sum_{i=1}^n W_2^2(\widetilde{Q}_{\mathbf{x}_i}, Q_{\mathbf{x}_i}^*) = \frac{1}{n} \sum_{i=1}^n W_2^2(\widetilde{Q}_{\mathbf{x}_i}^0, (\tau_{\#}^{-\mathbf{M}^*}Q^*)_{\mathbf{x}_i}) + \|\widetilde{\mathbf{M}}^\top \mathbf{x}_i - (\mathbf{M}^*)^\top \mathbf{x}_i\|^2.$$

Shape errors coincide. Since $\widehat{\nu}_i = \tau_{\#}^{\mathbf{v}_i}\widetilde{\nu}_i$, we have $\widehat{m}_i = \widetilde{m}_i + \mathbf{v}_i$ where $\widetilde{m}_i = m(\widetilde{\nu}_i)$, and therefore $\tau_{\#}^{-\widehat{m}_i}\widehat{\nu}_i = \tau_{\#}^{-\widetilde{m}_i}\widetilde{\nu}_i$. The centered data being identical implies $\widehat{Q}^0 = \widetilde{Q}^0$, so the shape errors in (98) are equal to those in the preceding display.

Mean errors. The OLS solutions satisfy $\mathbf{X}\widehat{\mathbf{M}} = \mathbf{H}\widehat{\mathbf{m}}$ and $\mathbf{X}\widetilde{\mathbf{M}} = \mathbf{H}\widetilde{\mathbf{m}}$, where $\mathbf{H} = \mathbf{X}(\mathbf{X}^\top \mathbf{X})^+ \mathbf{X}^\top$ is the hat matrix and where $\widehat{\mathbf{m}}$ and $\widetilde{\mathbf{m}}$ are $n \times d$ matrices with rows \widehat{m}_i^\top and \widetilde{m}_i^\top , respectively. Since $\widehat{\mathbf{m}} = \widetilde{\mathbf{m}} + \mathbf{V}$ (where \mathbf{V} is the $n \times d$ matrix with rows \mathbf{v}_i^\top), the inequality $\|a + b\|^2 \leq 2\|a\|^2 + 2\|b\|^2$ gives

$$\frac{1}{n} \|\mathbf{X}(\widehat{\mathbf{M}} - \mathbf{M}^*)\|^2 = \frac{1}{n} \|\mathbf{X}(\widetilde{\mathbf{M}} - \mathbf{M}^*) + \mathbf{H}\mathbf{V}\|^2 \leq \frac{2}{n} \|\mathbf{X}(\widetilde{\mathbf{M}} - \mathbf{M}^*)\|^2 + \frac{2}{n} \|\mathbf{H}\mathbf{V}\|^2.$$

For the last term, independence of ϕ_i across i and $\mathbb{E}[\mathbf{v}_i] = 0$ give $\mathbb{E}[\|\mathbf{H}\mathbf{V}\|_F^2] = \sum_{i=1}^n H_{ii} \mathbb{E}[\|\mathbf{v}_i\|^2] \leq d\sigma^2 \operatorname{Tr}(\mathbf{H}) \leq d\sigma^2 p$, where we used condition C1 and $\operatorname{Tr}(\mathbf{H}) =$

$\text{rank}(\mathbf{X}) \leq p$. Combining the equality of shape errors with the mean error bound gives

$$\mathbb{E} \left[\frac{1}{n} \sum_{i=1}^n W_2^2(\widehat{Q}_{\mathbf{x}_i}, Q_{\mathbf{x}_i}^*) \right] \leq 2 \mathbb{E} \left[\frac{1}{n} \sum_{i=1}^n W_2^2(\widetilde{Q}_{\mathbf{x}_i}, Q_{\mathbf{x}_i}^*) \right] + 2\sigma^2 \frac{pd}{n}.$$

□

Lemma 4. *Under the conditions of Theorem 7,*

$$(99) \quad \frac{\alpha}{2n} \sum_{i=1}^n W_2^2(\widehat{Q}_{\mathbf{x}_i}, Q_{\mathbf{x}_i}^*) \leq \int \left(\frac{1}{n} \sum_{i=1}^n \frac{\|\cdot^\top \mathbf{x}_i\|^2}{2} - \phi_i(\cdot^\top \mathbf{x}_i) \right) d(Q^* - \widehat{Q}) \\ + (G(\widehat{Q}) - G(Q^*)).$$

Proof. Given α -strong convexity of ϕ_i for each $i = 1, \dots, n$ we have that

$$\phi_i^*(x) + \phi_i(y) \geq \langle x, y \rangle + \frac{\alpha}{2} \|y - \nabla \phi_i^*(x)\|^2.$$

Expanding the square and rearranging

$$\frac{\|x - y\|^2}{2} - \frac{\alpha}{2} \|y - \nabla \phi_i^*(x)\|^2 \geq \frac{\|x\|^2}{2} - \phi_i^*(x) + \frac{\|y\|^2}{2} - \phi_i(y).$$

Integrating the previous expression w.r.t γ_i , the optimal coupling between ν_i and $\widehat{Q}_{\mathbf{x}_i}$, we arrive at

$$\frac{1}{2} W_2^2(\nu_i, \widehat{Q}_{\mathbf{x}_i}) - \frac{\alpha}{2} \int \|y - \nabla \phi_i^*(x)\|^2 d\gamma_i \geq \int \left(\frac{\|\cdot\|^2}{2} - \phi_i^* \right) d\nu_i + \int \left(\frac{\|\cdot\|^2}{2} - \phi_i \right) d\widehat{Q}_{\mathbf{x}_i}.$$

Noting that $W_2^2(\widehat{Q}_{\mathbf{x}_i}, Q_{\mathbf{x}_i}^*) \leq \int \|y - \nabla \phi_i^*(x)\|^2 d\gamma_i$ and summing over $1 \leq i \leq n$ gives us

$$G(\widehat{Q}) - \frac{\alpha}{2n} \sum_{i=1}^n W_2^2(\widehat{Q}_{\mathbf{x}_i}, Q_{\mathbf{x}_i}^*) \geq \frac{1}{n} \sum_{i=1}^n \int \left(\frac{\|\cdot\|^2}{2} - \phi_i^* \right) d\nu_i + \int \left(\frac{\|\cdot\|^2}{2} - \phi_i \right) d\widehat{Q}_{\mathbf{x}_i}$$

So

$$G(\widehat{Q}) - \frac{\alpha}{2n} \sum_{i=1}^n W_2^2(\widehat{Q}_{\mathbf{x}_i}, Q_{\mathbf{x}_i}^*) \geq \frac{1}{n} \sum_{i=1}^n \left[\int \left(\frac{\|\cdot\|^2}{2} - \phi_i^* \right) d\nu_i \right. \\ \left. + \int \left(\frac{\|\cdot\|^2}{2} - \phi_i \right) d\widehat{Q}_{\mathbf{x}_i} \right] \\ = G(Q^*) + \frac{1}{n} \sum_{i=1}^n \int \left(\frac{\|\cdot\|^2}{2} - \phi_i \right) d(\widehat{Q}_{\mathbf{x}_i} - Q_{\mathbf{x}_i}^*) \\ = G(Q^*) \\ + \int \left(\frac{1}{n} \sum_{i=1}^n \frac{\|\cdot^\top \mathbf{x}_i\|^2}{2} - \phi_i(\cdot^\top \mathbf{x}_i) \right) d(\widehat{Q} - Q^*).$$

Re-ordering the previous expression yields (99). □

Lemma 5. *Let $K = B_R^n \subseteq \mathbb{R}^{n \times d}$, where $B_R = \{\mathbf{y} \in \mathbb{R}^d : \|\mathbf{y}\| \leq R\}$. Then*

$$(100) \quad \mathbb{E} \sup_{\mathbf{B}: \mathbf{X}\mathbf{B} \in K} |Z_{\mathbf{X}\mathbf{B}}| \lesssim \beta R^2 \sqrt{\frac{pd}{n}}.$$

Proof. We first show that $Z_{\mathbf{Y}}$ has sub-gaussian increments: For any $\mathbf{Y}, \mathbf{Y}' \in K$, we will show

$$(101) \quad \|Z_{\mathbf{Y}} - Z_{\mathbf{Y}'}\|_{\psi_2} \leq \frac{\sigma}{n} \|\mathbf{Y} - \mathbf{Y}'\|$$

where $\sigma = \beta R$. Indeed, Condition **C3** and the assumption that $\nabla \phi_i(0) = 0$ imply that the function

$$\psi_i(\mathbf{y}) = \|\mathbf{y}\|^2 - 2\phi_i(\mathbf{y})$$

satisfies $\nabla \psi_i(0) = 0$ and $\|\nabla^2 \psi_i(\mathbf{y})\|_{\text{op}} \leq 2 \max\{1 - \alpha, \beta - 1\} =: L$. Hence the gradient of ψ_i is L Lipschitz, and in particular $\|\nabla \psi_i(\mathbf{y})\| \leq L\|\mathbf{y}\|$ for all \mathbf{y} . Therefore

$$\begin{aligned} \left| \|\mathbf{y}_i\|^2 - 2\phi_i(\mathbf{y}_i) - (\|\mathbf{y}'_i\|^2 - 2\phi_i(\mathbf{y}'_i)) \right| &= |\psi_i(\mathbf{y}_i) - \psi_i(\mathbf{y}'_i)| \\ &\leq L\|\mathbf{y}_i - \mathbf{y}'_i\| \max\{\|\mathbf{y}_i\|, \|\mathbf{y}'_i\|\} \end{aligned}$$

We obtain that $Z_{\mathbf{Y}} - Z_{\mathbf{Y}'}$ is an average of n independent, mean zero terms, and the i th term is bounded by $L\|\mathbf{y}_i - \mathbf{y}'_i\| \max\{\|\mathbf{y}_i\|, \|\mathbf{y}'_i\|\}$ almost surely. Hoeffding's lemma therefore implies that for any $\mathbf{Y}, \mathbf{Y}' \in K$, the increment $Z_{\mathbf{Y}} - Z_{\mathbf{Y}'}$ is

$$(102) \quad \frac{L^2}{4n^2} \max_{i \in [n]} \max\{\|\mathbf{y}_i\|^2, \|\mathbf{y}'_i\|^2\} \|\mathbf{Y} - \mathbf{Y}'\|^2$$

subgaussian. Condition **C3** implies that $\alpha \leq 1 \leq \beta$, so $L \leq 2\beta$, and the definition of K shows that any $\mathbf{Y} \in K$ satisfies $\max_{i \in [n]} \|\mathbf{y}_i\| \leq R$. This proves (101).

The result now follows from Dudley's entropy bound (Vershynin, 2018, Theorem 8.1.6). Equip the indexing set $T := \{\mathbf{B} \in \mathbb{R}^{p \times d} : \mathbf{X}\mathbf{B} \in K\}$ with the pseudometric $\rho(\mathbf{B}, \mathbf{B}') = \|\mathbf{X}(\mathbf{B} - \mathbf{B}')\|$. The covering numbers of (T, ρ) equal those of the image $\mathbf{X}(T) = \text{col}(\mathbf{X})^d \cap K$ under $\|\cdot\|$. This set has dimension at most pd and Frobenius diameter at most $2R\sqrt{n}$, so standard volumetric estimates give

$$(103) \quad \log N(\varepsilon, T, \rho) \leq pd \log \left(\frac{6R\sqrt{n}}{\varepsilon} \right).$$

Applying Dudley's entropy bound to the sub-gaussian process $Z_{\mathbf{X}\mathbf{B}}$ with increment parameter $\beta R/n$ from (101) yields

$$(104) \quad \mathbb{E} \sup_{\mathbf{B} \in T} |Z_{\mathbf{X}\mathbf{B}}| \lesssim \frac{\beta R}{n} \int_0^{R\sqrt{n}} \sqrt{pd \log \left(\frac{6R\sqrt{n}}{\varepsilon} \right)} d\varepsilon \lesssim \frac{\beta R^2 \sqrt{pd}}{\sqrt{n}},$$

where the last step uses the standard evaluation of the entropy integral for a pd -dimensional body of diameter $R\sqrt{n}$. \square

Lemma 6. *Assume that $\nabla \phi_i(0) = 0$ for each $i \in [n]$, that the covariates satisfy the incoherence condition*

$$(105) \quad \mathbf{x}_i^\top (\mathbf{X}^\top \mathbf{X})^+ \mathbf{x}_i \leq \frac{\mu p}{n},$$

that $\text{supp}(Q_{\mathbf{x}_i}^) \subset B_M$ for each $i \in [n]$, and that $\text{supp}(\hat{\nu}_i) \subset B_{\beta M}$ almost surely for each $i \in [n]$. Then, under both $\mathbf{B} \sim \hat{Q}$ and $\mathbf{B} \sim Q^*$, the support of $\mathbf{X}\mathbf{B}$ lies in B_R^n with $R = M \max(1, \beta\sqrt{\mu p})$.*

Proof. We handle the two cases separately.

Under $\mathbf{B} \sim Q^*$: By assumption, $\text{supp}(Q_{\mathbf{x}_i}^*) \subset B_M$, so $\|\mathbf{B}^\top \mathbf{x}_i\| \leq M$ almost surely for each $i \in [n]$.

Under $\mathbf{B} \sim \hat{Q}$: Following (18), we can write $\mathbf{B} = (\mathbf{X}^\top \mathbf{X}) \mathbf{X}^\top \mathbf{Y}$, for $(\mathbf{y}_1, \dots, \mathbf{y}_n) \sim P$ for some $P \in \Pi(\hat{\nu}_1, \dots, \hat{\nu}_n)$. Writing $\mathbf{H} = \mathbf{X}(\mathbf{X}^\top \mathbf{X})^+ \mathbf{X}^\top$, we equivalently have

$\mathbf{XB} = \mathbf{HY}$, where \mathbf{Y} is some random matrix satisfying $\|\mathbf{Y}\|^2 \leq \sum_{i=1}^n \sup\{\|\mathbf{y}_i\|^2 : \mathbf{y}_i \in \text{supp}(\hat{\nu}_i)\} \leq n(\beta M)^2$. We obtain that the i th row of \mathbf{XB} has norm bounded by $\|\mathbf{h}_i\| \|\mathbf{Y}\| \leq \sqrt{n} \beta M \|\mathbf{h}_i\|$, where \mathbf{h}_i is the i th row of \mathbf{H} . Finally, since \mathbf{H} is an orthogonal projection, we have that

$$(106) \quad \|\mathbf{h}_i\|^2 = (\mathbf{H}\mathbf{H}^\top)_{ii} = \mathbf{H}_{ii} = \mathbf{x}_i^\top (\mathbf{X}^\top \mathbf{X})^+ \mathbf{x}_i \leq \frac{\mu p}{n}.$$

We obtain that the i th row of \mathbf{XB} has norm at most $\beta M \sqrt{\mu p}$.

Taking $R = M \max(1, \beta \sqrt{\mu p})$ completes the proof. \square

Lemma 7. *Let $\Omega = B_R \subseteq \mathbb{R}^d$ be the ball of radius R around the origin in \mathbb{R}^d . If $\nu \in \mathcal{P}(\Omega)$ and $\hat{\nu}$ is an empirical version of ν obtained from m i.i.d. samples, then*

$$(107) \quad \mathbb{E} \left[\sup_{\mu \in \mathcal{P}(\Omega)} |W_2^2(\mu, \nu) - W_2^2(\mu, \hat{\nu})| \right] \lesssim R^2 \begin{cases} m^{-2/d} & \text{if } d > 4, \\ m^{-1/2} \log(m) & \text{if } d = 4, \\ m^{-1/2} & \text{if } d < 4, \end{cases}$$

Proof. Following the proof of Lemma 3 in Chizat et al. (2020), we can bound the left side of (107) in terms of the semi-dual problem, yielding

$$\begin{aligned} & \mathbb{E} \left[\sup_{\mu \in \mathcal{P}_2(\Omega)} |W_2^2(\mu, \nu) - W_2^2(\mu, \hat{\nu})| \right] \\ & \leq \mathbb{E} \left[\sup_{\mu \in \mathcal{P}_2(\Omega)} \left(\left| \int \|y\|^2 d(\nu - \hat{\nu}) \right| + \sup_{\phi \in \mathcal{F}_R} \left| \int \phi d(\nu - \hat{\nu}) \right| \right) \right], \end{aligned}$$

where \mathcal{F}_R is the class of convex, R -Lipschitz functions defined in B_R . But the terms inside the supremum of the rhs do not depend on μ , hence

$$\begin{aligned} & \mathbb{E} \left[\sup_{\mu \in \mathcal{P}_2(\Omega)} |W_2^2(\mu, \nu) - W_2^2(\mu, \hat{\nu})| \right] \\ & \leq \mathbb{E} \left[\left| \int \|y\|^2 d(\nu - \hat{\nu}) \right| + \sup_{\phi \in \mathcal{F}_R} \left| \int \phi d(\nu - \hat{\nu}) \right| \right]. \end{aligned}$$

Lemma 4 in Chizat et al. (2020) yields the result. \square

APPENDIX F. FIRST ORDER GEOMETRY WASSERSTEIN LEAST SQUARES

In this section, we will describe the elements on $\mathcal{P}_2(\mathbb{R}^{p \times d})$ that make the Wasserstein gradient of G , the Wasserstein regression functional

$$G(Q) = \frac{1}{n} \sum_{i=1}^n W_2^2(Q_{\mathbf{x}_i}, \nu_i),$$

vanish. Our goal, as is usual in first-order optimization, is to gain knowledge of the set of minimizers for a Wasserstein least squares problem.

Proof of Lemma 1. As a simplifying assumption, we will consider $(Q, \nu_i) \in \mathcal{P}_{2, \text{ac}}(\mathbb{R}^{p \times d}) \times \mathcal{P}_{2, \text{ac}}(\mathbb{R}^d)$. Then we can compute the L_2 -first variation of G in Q by looking at the dual formulation of each $W_2^2(\nu_i, Q_{\mathbf{x}_i})$ and noting that $\phi_i = \|\cdot\| - \varphi_i$, i.e.

$$\begin{aligned}\delta G(Q) &= -\delta \frac{1}{n} \sum_{i=1}^n \left(\int_{\mathbb{R}^d} (\varphi_i - \frac{\|\cdot\|^2}{2}) dQ_{\mathbf{x}_i} - \int_{\mathbb{R}^d} \phi^* d\nu_i \right) \\ &= -\delta \frac{1}{n} \sum_{i=1}^n \int_{\mathbb{R}^d} (\varphi_i - \frac{\|\cdot\|^2}{2}) dQ_{\mathbf{x}_i},\end{aligned}$$

where we used the envelope theorem to eliminate the ν_i integrands. Using the gluing lemma to produce a coupling $Q_X \in \mathcal{P}_{2,ac}((\mathbb{R}^d)^n)$ where every $Q_{\mathbf{x}_i}$ is involved, we get

$$\begin{aligned}\delta G(Q) &= -\delta \int_{(\mathbb{R}^d)^n} \left(\frac{1}{n} \sum_{i=1}^n (\varphi_i - \frac{\|\cdot\|^2}{2}) \right) dQ_X \\ &= -\delta \int_{\mathbb{R}^{p \times d}} \left(\left(\frac{1}{n} \sum_{i=1}^n (\varphi_i - \frac{\|\cdot\|^2}{2}) \right) \circ L_X \right) dQ\end{aligned}$$

where $L_X : \mathbb{R}^{p \times d} \rightarrow (\mathbb{R}^d)^n$ is given by $L_X(B) = (\mathbf{B}^\top \mathbf{x}_1, \dots, \mathbf{B}^\top \mathbf{x}_n)$.

Hence

$$(108) \quad \delta G(Q) = -\left(\frac{1}{n} \sum_{i=1}^n (\varphi_i - \frac{\|\cdot\|^2}{2}) \right) \circ L_X.$$

The W_2 -gradient of G with respect to Q is the $\mathbb{R}^{p \times d}$ -gradient of δG , meaning

$$\begin{aligned}(109) \quad \nabla_Q G(Q) &= \nabla_{\mathbf{B}} \delta G(Q) \\ &= -\nabla_{\mathbf{B}} \left(\frac{1}{n} \sum_{i=1}^n (\varphi_i(\mathbf{B}^\top \mathbf{x}_i) - \frac{\|\mathbf{B}^\top \mathbf{x}_i\|^2}{2}) \right) \\ &= -\frac{1}{n} \sum_{i=1}^n (\mathbf{x}_i (\nabla \varphi_i(\mathbf{B}^\top \mathbf{x}_i))^\top - \mathbf{x}_i \mathbf{x}_i^\top \mathbf{B}).\end{aligned}$$

□

The following observation appears in Theorem 7 of [Chewi et al. \(2020\)](#).

Lemma 8. *The function $F_{\nu_i} : \mathcal{P}_2(\mathbb{R}^d) \rightarrow \mathbb{R}$ with assignment rule*

$$\mu \mapsto W_2^2(\mu, \nu_i)$$

is smooth along Wasserstein geodesics in $\mathcal{P}_{2,ac}(\mathbb{R}^d)$.

Proof. Consider μ_s the constant speed geodesic joining μ_0 and μ_1 . Letting $s \in (0, 1]$, the NNC inequality reads as

$$\frac{W_2^2(\mu_s, \nu_i) - W_2^2(\mu_0, \nu_i)}{s} \geq [W_2^2(\mu_1, \nu_i) - W_2^2(\mu_0, \nu_i)] - (1-s)W_2^2(\mu_0, \mu_1).$$

Taking $s \rightarrow 0_+$ and recalling Proposition 7.3.6 in [Ambrosio et al. \(2008\)](#) yields the convergence of the left-hand side to

$$W_2^2(\mu_0, \nu_i)|_{s=0_+} = -2 \langle \nabla \varphi_{\mu_0 \rightarrow \nu_i} - \text{Id}, \log_{\mu_0}(\mu_1) \rangle_{\mu_0} = \langle \nabla_{\mu_0} F_{\nu_i}, \log_{\mu_0}(\mu_1) \rangle_{\mu_0}.$$

Upon reordering, we achieved the desired inequality, meaning

$$(110) \quad F_{\nu_i}(\mu_1) \leq F_{\nu_i}(\mu_0) + \langle \nabla_{\mu_0} F_{\nu_i}, \log_{\mu_0}(\mu_1) \rangle_{\mu_0} + W_2^2(\mu_0, \mu_1).$$

□

The following theorem relates (27) and (28) in a practical way. It is a generalization of Theorem 7 in Chewi et al. (2020).

Theorem 8. *Let $\eta = \frac{2}{n} \sum_{i=1}^n \|\mathbf{x}_i\|_2^2$ and $\tau > 0$. The Wasserstein least-squares functional G is η -smooth along Wasserstein geodesics. As a consequence, if we define $Q^+ := \exp_Q(-\nabla_Q G(Q))$ for every $Q \in \mathcal{P}_2(\mathbb{R}^{p \times d})$, then*

$$(111) \quad G(Q^+) - G(Q) \leq \left(\frac{\eta}{2} - \tau\right) \|\nabla_Q G\|_Q^2 \quad \forall Q \in \mathcal{P}_2(\mathbb{R}^{p \times d}).$$

Proof of Theorem 8. It is enough to verify that the function $G_i : \mathcal{P}_2(\mathbb{R}^{p \times d}) \rightarrow \mathbb{R}$ with assignment rule $Q \mapsto W_2^2(Q_{\mathbf{x}_i}, \nu_i)$ is smooth for $1 \leq i \leq n$. Let Q^s be the constant speed geodesic joining Q^0 and Q^1 in $\mathcal{P}_{2,\text{ac}}(\mathbb{R}^{p \times d})$. Due to Lemma 8

$$(112) \quad F_{\nu_i}(Q_{\mathbf{x}_i}^1) \leq F_{\nu_i}(Q_{\mathbf{x}_i}^0) + \langle \nabla_{Q_{\mathbf{x}_i}^0} F_{\nu_i}, \frac{d}{ds}(Q^s)_i|_{s=0_+} \rangle_{Q_{\mathbf{x}_i}^0} + W_2^2(Q_{\mathbf{x}_i}^0, Q_{\mathbf{x}_i}^1).$$

But, note that $G_i = F_{\nu_i} \circ \pi_i$ where $\pi_i : \mathcal{P}_{2,\text{ac}}(\mathbb{R}^{p \times d}) \rightarrow \mathcal{P}_{2,\text{ac}}(\mathbb{R}^d)$ is the i -th projection of Q , or $\pi_i(Q) = Q_{\mathbf{x}_i}$. So, by the chain rule,

$$\begin{aligned} \langle \nabla_{Q_{\mathbf{x}_i}^0} F_{\nu_i}, \frac{d}{ds}(Q^s)_{\mathbf{x}_i}|_{s=0_+} \rangle_{Q_{\mathbf{x}_i}^0} &= \langle \nabla_{\pi_i \circ Q} F_{\nu_i}, \frac{d}{ds}(\pi_i \circ Q^s)|_{s=0_+} \rangle_{\pi_i \circ Q^0} \\ &= \langle \nabla_{Q^0} F_{\nu_i} \circ \pi_i, \log_{Q^0}(Q^1) \rangle_{Q^0}. \end{aligned}$$

Then we can rewrite equation (112) as

$$G_i(Q^1) \leq G_i(Q^0) + \langle \nabla_{Q^0} G_i, \log_{Q^0}(Q^1) \rangle_{Q^0} + W_2^2(Q_{\mathbf{x}_i}^0, Q_{\mathbf{x}_i}^1).$$

Furthermore, using the Cauchy-Schwarz inequality, we get that

$$G_i(Q^1) \leq G_i(Q^0) + \langle \nabla_{Q^0} G_i, \log_{Q^0}(Q^1) \rangle_{Q^0} + \|\mathbf{x}_i\|_2^2 W_2^2(Q^0, Q^1).$$

as long as \mathbf{x}_i is not a null vector. Multiplying each of the n previous equations by $\frac{1}{n}$ and summing them up yields the smoothness:

$$(113) \quad G(Q^1) \leq G(Q^0) + \langle \nabla_{Q^0} G(Q^0), \log_{Q^0}(Q^1) \rangle_{Q^0} + \frac{\eta}{2} W_2^2(Q^0, Q^1).$$

with $\eta = \frac{2}{n} \sum_{i=1}^n \|\mathbf{x}_i\|_2^2$.

Letting $Q^0 = Q$ and $Q^1 = Q^+ := \exp_Q(\tau \nabla_Q G(Q))$ for any $Q \in \mathcal{P}_2(\mathbb{R}^{p \times d})$, and noting that

$$\langle \nabla_Q G(Q), \log_Q(Q^+) \rangle_{Q^0} = \tau \langle \nabla_Q G(Q), \nabla_Q G(Q) \rangle_{Q^0} = \tau W_2^2(Q, Q^+)$$

concludes the proof upon rearrangement. \square

Theorem 8 plays an important part in the convergence of (28) to a critical point of the Wasserstein least squares functional. For example, combining Theorem 8 with Proposition 4.7 in Boumal (2023) yields the following.

Proposition 4. *Choose $\tau > \eta/2$. Then, for every $K \in \mathbb{N}$ there exists a k in $0, \dots, K-1$ such that*

$$\|\nabla G(Q^k)\|_{Q^k} \leq \sqrt{\frac{G(Q^0)}{K(\tau - \eta/2)}}$$

where the sequence $(Q^k)_{k>0}$ was produced according to (28).

APPENDIX G. WASSERSTEIN LEAST SQUARES: THE GAUSSIAN CASE

In this section, we study the Wasserstein least squares problem under Gaussian responses. In conjunction with the benign properties derived in Section 2.3, the geometry of Gaussian measures equipped the Bures-Wasserstein metric will help us derive further connections with the Wasserstein barycenter problem via first-order conditions of the Wasserstein least squares functional.

Our analysis requires a careful treatment of $G : \mathcal{P}_2(\mathbb{R}^{p \times d}) \rightarrow \mathbb{R}$, the Wasserstein least squares functional for the data $(\mathbf{x}_i, \nu_i)_{i=1}^n$, given by

$$(114) \quad G(Q) := \sum_{i=1}^n W_2^2(\nu_i, Q_{\mathbf{x}_i}).$$

We begin by noting that, if each of the marginal measures is Gaussian, then Wasserstein least squares has a Gaussian solution.

Proposition 5. *Suppose ν_1, \dots, ν_n are Gaussian measures. Then there exists a Gaussian measure \tilde{Q} on $\mathbb{R}^{p \times d}$ such that*

$$(115) \quad \tilde{Q} \in \operatorname{argmin}_{Q \in \mathcal{P}_2(\mathbb{R}^{p \times d})} \frac{1}{n} \sum_{i=1}^n W_2^2(\nu_i, Q_{\mathbf{x}_i}).$$

Proof. We use the following fact [Gelbrich \(1990\)](#): for every $\xi, \xi' \in \mathcal{P}_2(\mathbb{R}^d)$

$$(116) \quad W_2^2(N_\xi, N_{\xi'}) \leq W_2^2(\xi, \xi'),$$

where N_ξ is the Gaussian distribution $\mathcal{N}(\mathbb{E}_\xi(X), \operatorname{Cov}_\xi(X))$ whose first two moments match those of ξ . Now, let Q be an arbitrary minimizer of (115), and let $\tilde{Q} = N_Q$ be the corresponding Gaussian. Note that the projected measure $\tilde{Q}_{\mathbf{x}_i}$ is a Gaussian with the same mean and variance as $Q_{\mathbf{x}_i}$, so (116) implies

$$W_2^2(\nu_i, \tilde{Q}_{\mathbf{x}_i}) \leq W_2^2(\nu_i, Q_{\mathbf{x}_i}),$$

so \tilde{Q} is also a minimizer in (115). \square

Proposition 5 implies that when solving the Wasserstein least squares problem with Gaussian responses we may restrict our attention to the subset of $\mathcal{P}_2(\mathbb{R}^{d \times p})$ consisting of Gaussian measures. This finite-dimensional space equipped with the 2-Wasserstein metric is known as the *Bures-Wasserstein* manifold [Bhatia et al. \(2019\)](#). The objects introduced in Section 2 have simplified analogues on this space, which we now introduce.

For notational convenience, we work with vectorized versions of random variables on $\mathbb{R}^{p \times d}$. If $Q \in \mathcal{P}(\mathbb{R}^{p \times d})$ is a Gaussian measure, then its representative in the Bures-Wasserstein manifold is given by $(m_Q, \Sigma_Q) \in \mathbb{R}^{dp} \times \mathbf{S}_{++}^{dp}$ where

$$(117) \quad \begin{cases} m_Q := \mathbb{E}[\operatorname{vec}(\mathbf{B}^\top)], \\ \Sigma_Q := \mathbb{E}_Q[\operatorname{vec}(\mathbf{B}^\top - m_Q)\operatorname{vec}(\mathbf{B}^\top - m_Q)^\top] \\ \mathbf{B} \sim Q, \end{cases}$$

where $\operatorname{vec}(\cdot)$ maps matrices to vectors by stacking the columns: if $\mathbf{B}^\top = [\mathbf{B}_1^\top | \dots | \mathbf{B}_p^\top] \in \mathbb{R}^{d \times p}$, then

$$\operatorname{vec}(\mathbf{B}^\top) = \begin{bmatrix} \mathbf{B}_1^\top \\ \vdots \\ \mathbf{B}_p^\top \end{bmatrix} \in \mathbb{R}^{pd}.$$

With abuse of notation, we will not distinguish between Q , the measure supported in $\mathbb{R}^{p \times d}$, and Q as a measure in $\mathcal{P}_2(\mathbb{R}^{dp})$ with vectorized mean m_Q and covariance Σ_Q . The following Lemma is a consequence of our parametrization.

Lemma 9. *Let $Q \in \mathcal{P}(\mathbb{R}^{p \times d})$ be a Gaussian measure.*

- (1) *If $\mathbf{B} \sim Q$ and $\mathbf{x}_i \in \mathbb{R}^p$, then $Q_{\mathbf{x}_i} := \text{Law}(\mathbf{B}^\top \mathbf{x}_i)$ is Gaussian measure with mean and variance*

$$(118) \quad \begin{aligned} m_{Q_{\mathbf{x}_i}} &= (\mathbf{x}_i^\top \otimes I_d) m_Q, \\ \Sigma_{Q_{\mathbf{x}_i}} &= (\mathbf{x}_i^\top \otimes I_d) \Sigma_Q (\mathbf{x}_i \otimes I_d). \end{aligned}$$

- (2) *A Brenier map, denoted by $\nabla \varphi_i$, between $Q_{\mathbf{x}_i}$ and ν_i has the expression*

$$(119) \quad \nabla \varphi(\cdot) = m_{\nu_i} + \Sigma_{Q_{\mathbf{x}_i}} \# \Sigma_{\nu_i}(\cdot) - m_{Q_{\mathbf{x}_i}},$$

where $\Sigma_1 \# \Sigma_2 := \Sigma_1^{\frac{1}{2}} (\Sigma_1^{-\frac{1}{2}} \Sigma_2 \Sigma_1^{-\frac{1}{2}})^{\frac{1}{2}} \Sigma_1^{\frac{1}{2}}$.

- (3) *The Bures-Wasserstein gradient of G with mean-zero Gaussian data $(\{\nu_i\}_{i=1}^n, Q)$ specializes to*

$$(120) \quad \nabla_Q G(Q) = -\frac{1}{n} \sum_{i=1}^n \mathbf{x}_i \mathbf{x}_i^\top \mathbf{B} (\Sigma_{Q_{\mathbf{x}_i}} \# \Sigma_{\nu_i} - I_d).$$

Proof. Let $\mathbf{x} \in \mathbb{R}^p$. On one hand, if $Z \sim \mu := \text{Law}(\mathbf{B}^\top \mathbf{x})$, then

$$(121) \quad \begin{aligned} m_\mu &= \mathbb{E}_\mu[Z] = \mathbb{E}_Q[\mathbf{B}^\top \mathbf{x}], \text{ and} \\ \Sigma_\mu &= \mathbb{E}_\mu[Z^\top Z] = \mathbb{E}_Q[(\mathbf{B}^\top \mathbf{x} - m_\mu)(\mathbf{x}^\top \mathbf{B} - m_\mu^\top)]. \end{aligned}$$

On the other hand, by properties of the vec operator

$$\mathbf{B}^\top \mathbf{x} = \text{vec}(\mathbf{B}^\top \mathbf{x}) = \text{vec}(I_d \mathbf{B}^\top \mathbf{x}) = \mathbf{x}^\top \otimes I_d \text{vec}(\mathbf{B}^\top).$$

Plugging the last equation back in (121) yields that

$$m_\mu = \mathbb{E}_Q[\mathbf{x}^\top \otimes I_d \text{vec}(\mathbf{B}^\top)] = (\mathbf{x}^\top \otimes I_d) m_Q.$$

Similarly, the covariance ends up being

$$\begin{aligned} \Sigma_\mu &= \mathbb{E}_Q[(\mathbf{x}^\top \otimes I_d) \text{vec}(\mathbf{B}^\top - m_Q) \text{vec}(\mathbf{B}^\top - m_Q)^\top (\mathbf{x} \otimes I_d)] \\ &= (\mathbf{x}^\top \otimes I_d) \mathbb{E}_Q[\text{vec}(\mathbf{B}^\top - m_Q) \text{vec}(\mathbf{B}^\top - m_Q)^\top] (\mathbf{x} \otimes I_d) \\ &= (\mathbf{x}^\top \otimes I_d) \Sigma_Q (\mathbf{x} \otimes I_d). \end{aligned}$$

Items 1 and 2 follow if:

- (1) We recall that the Brenier map between two Gaussian measures ξ, ξ' is given by

$$\nabla \varphi(\cdot) = m_{\xi'} + \Sigma_\xi \# \Sigma_{\xi'}(\cdot - m_\xi) = m_{\xi'} + \Sigma_\xi^{-\frac{1}{2}} (\Sigma_\xi^{\frac{1}{2}} \Sigma_{\xi'} \Sigma_\xi^{\frac{1}{2}})^{\frac{1}{2}} \Sigma_\xi^{-\frac{1}{2}}(\cdot - m_\xi).$$

- (2) We apply Lemma 1 to our data. □

Remark 8. *The interesting case of study is when ν_1, \dots, ν_n are centered. This reduction is reasonable since by Lemma 9, for general Gaussian data, the Wasserstein least squares functional decomposes to*

$$(122) \quad G(Q) = \sum_{i=1}^n \frac{1}{n} \|m_{\nu_i} - (\mathbf{x}_i^\top \otimes I_d) m_Q\|_2^2 + W_2^2(\tilde{\nu}_i, \tilde{Q}_{\mathbf{x}_i})$$

where $(\{\tilde{\nu}_i\}_{i=1}^n, \tilde{Q})$ are zero-mean Gaussian measures with the same covariance of $(\{\nu_i\}_{i=1}^n, Q)$.

The following statement is reminiscent of Theorem 6.1 in [Agueh and Carlier \(2011\)](#).

Proposition 6. *Let $S \in \mathbf{S}_+^{dp}$. Define by $S_i := (\mathbf{x}_i^\top \otimes I_d)S(\mathbf{x}_i \otimes I_d) \in \mathbf{S}_+^d$. Consider ν_1, \dots, ν_n d -dimensional Gaussian measures with null mean and covariances Σ_{ν_i} . Assume $\Sigma_{\tilde{Q}}$ is a solution of the normal matrix equation*

$$(123) \quad \frac{1}{n} \sum_{i=1}^n \mathbf{x}_i \mathbf{x}_i^\top \mathbf{B} S_i \# \Sigma_{\nu_i} = \frac{1}{n} \sum_{i=1}^n \mathbf{x}_i \mathbf{x}_i^\top \mathbf{B}$$

for every $\mathbf{B} \in \mathbb{R}^{p \times d}$. Then $\tilde{Q} = \mathcal{N}(0, \Sigma_{\tilde{Q}})$ is an optimal dual solution of [\(17\)](#).

Proof. By Theorem [5](#), it is enough to verify that the mappings $(\varphi_1, \dots, \varphi_n)$ given by

$$\varphi_i := \frac{1}{2} \langle \cdot, \Sigma_{\tilde{Q}_{\mathbf{x}_i}} \# \Sigma_{\nu_i}, \cdot \rangle.$$

are optimal dual solutions. The proposed maps are clearly the optimal Brenier potentials between $\tilde{Q}_{\mathbf{x}_i}$ and ν_i . So we now verify that

$$\frac{1}{n} \sum_{i=1}^n (\varphi_i(\mathbf{B}^\top \mathbf{x}_i) - \|\mathbf{B}^\top \mathbf{x}_i\|^2 / 2) = 0 \quad \mathbf{B}\text{-a.e.}$$

Consequently we check that if $\mathbf{B} \sim \tilde{Q}$, then

$$\begin{aligned} \frac{1}{n} \sum_{i=1}^n (\varphi_i(\mathbf{B}^\top \mathbf{x}_i) - \frac{\|\mathbf{B}^\top \mathbf{x}_i\|^2}{2}) &= \sum_{i=1}^n \frac{1}{2n} (\langle \mathbf{x}_i^\top \mathbf{B} \Sigma_{\tilde{Q}_{\mathbf{x}_i}} \# \Sigma_{\nu_i}, \mathbf{x}_i^\top \mathbf{B} \rangle - \|\mathbf{B}^\top \mathbf{x}_i\|^2) \\ &= \frac{1}{2} \langle \mathbf{B}, \frac{1}{n} \sum_{i=1}^n \mathbf{x}_i \mathbf{x}_i^\top \mathbf{B} \Sigma_{\tilde{Q}_{\mathbf{x}_i}} \# \Sigma_{\nu_i} \rangle_F + \sum_{i=1}^n \frac{1}{2n} \|\mathbf{B}^\top \mathbf{x}_i\|^2 \\ &= \frac{1}{2} \langle \mathbf{B}, \frac{1}{n} \sum_{i=1}^n \mathbf{x}_i \mathbf{x}_i^\top \mathbf{B} \rangle_F + \sum_{i=1}^n \frac{1}{2n} \|\mathbf{B}^\top \mathbf{x}_i\|^2 \\ &= 0. \end{aligned}$$

□

A further relationship between the Wasserstein barycenter problem and Wasserstein least squares is drawn in the following proposition.

Proposition 7. *Assume $\nu_i \sim \mathcal{N}_d(0, \Sigma_{\nu_i})$ and each $\mathbf{x}_i = a_i \mathbf{x}_1$ for a $a_i \neq 0$. If \tilde{Q} is an optimal dual solution for [\(17\)](#), then $\Sigma_{\tilde{Q}_{\mathbf{x}_i}}$ solves the Barycenter equation for $S \in \mathbf{S}_+^{dp}$*

$$(124) \quad \sum_{i=1}^n \tilde{\lambda}_i (S^{1/2} \Sigma_{\nu_i} S^{1/2})^{1/2} = S$$

Consequently, for this type of design matrix finding a solution of [\(17\)](#) is equivalent to solving the Wasserstein barycenter problem

$$(125) \quad \min_{b \in \mathcal{P}_{2,ac}(\mathbb{R}^d)} \sum_{i=1}^n \tilde{\lambda}_i W_2^2(b, \nu_i).$$

with $\tilde{\lambda}_i = \frac{a_i^2}{\sum_{j=1}^n a_j^2}$.

Proof. Note that by hypothesis

$$\Sigma_{\tilde{Q}_{\mathbf{x}_i}} = a_i^2 \mathbb{E}_{\mathbf{B} \sim \tilde{Q}}[\text{vec}(\mathbf{B}^\top \mathbf{x}_i) \text{vec}(\mathbf{B}^\top \mathbf{x}_i)^\top] = a_i^2 \Sigma_{\tilde{Q}_{\mathbf{x}_i}}.$$

As a consequence

$$\Sigma_{\tilde{Q}_{\mathbf{x}_i}} \# \Sigma_{\nu_i} = \Sigma_{\tilde{Q}_{\mathbf{x}_1}} \# \Sigma_{\nu_i} \quad \text{for } 1 \leq i \leq n.$$

Specializing equation (123) to our case and multiplying it on the left side by \mathbf{x}_1^\top yields

$$\sum_{i=1}^n a_i^2 Z \Sigma_{Q_{\mathbf{x}_1}} \# \Sigma_{\nu_i} = \sum_{i=1}^n a_i^2 Z$$

where $Z = \mathbf{x}_1^\top \mathbf{B} (\|\mathbf{x}_1\|_2^2)$. Since $Z \in \mathbb{R}^d$ is arbitrary, the previous equations are equivalent to

$$\sum_{i=1}^n a_i^2 \Sigma_{\tilde{Q}_{\mathbf{x}_1}} \# \Sigma_{\nu_i} = \sum_{i=1}^n a_i^2 I_d.$$

If we multiply this equation on both sides by $(\Sigma_{\tilde{Q}_{\mathbf{x}_1}})^{1/2}$ we get

$$\sum_{i=1}^n a_i^2 (\Sigma_{\tilde{Q}_{\mathbf{x}_1}}^{1/2} \Sigma_{\nu_i} \Sigma_{\tilde{Q}_{\mathbf{x}_1}}^{1/2})^{1/2} = \sum_{i=1}^n a_i^2 \Sigma_{\tilde{Q}_{\mathbf{x}_1}}$$

□

Proof of Proposition 3. We proceed to treat each item separately.

- (1) If we specialize this notion for a G depending on Gaussian responses $\nu_i \in \mathcal{P}_2(\mathbb{R}^d)$ with mean m_{ν_i} and variance Σ_{ν_i} , then the gradient flow equation reads as

$$\begin{cases} \dot{Q}^t = \frac{1}{n} \sum_{i=1}^n \mathbf{x}_i \mathbf{x}_i^\top (\cdot) (\Sigma_{Q_{\mathbf{x}_i}^t} \# \Sigma_{\nu_i} - I_d) + \frac{1}{n} \sum_{i=1}^n \mathbf{x}_i (m_{Q_{\mathbf{x}_i}^t}^\top \Sigma_{Q_{\mathbf{x}_i}^t} \# \Sigma_{\nu_i} - m_{\nu_i}^\top) \\ Q^0 = \mathcal{N}_{dp}(0, \Sigma_{Q^0}). \end{cases}$$

So, if we sample a random variable $\mathbf{B}_t^\top \sim Q^t$ at time $t > 0$, then previous equation reads as

(126)

$$\dot{\mathbf{B}}_t = v_t(\mathbf{B}_t) = \frac{1}{n} \sum_{i=1}^n \mathbf{x}_i \mathbf{x}_i^\top \mathbf{B}_t (\Sigma_{Q_{\mathbf{x}_i}^t} \# \Sigma_{\nu_i} - I_d) + \frac{1}{n} \sum_{i=1}^n \mathbf{x}_i (m_{Q_{\mathbf{x}_i}^t}^\top \Sigma_{Q_{\mathbf{x}_i}^t} \# \Sigma_{\nu_i} - m_{\nu_i}^\top)$$

under the particle interpretation of the continuity equation. Let's investigate the vectorized form of $\dot{\mathbf{B}}_t^\top$.

Note the vectorized form of the transpose of the first summand of equation (126) simplifies to

$$(127) \quad \left(\frac{1}{n} \sum_{i=1}^n \mathbf{x}_i \mathbf{x}_i^\top \otimes (\Sigma_{Q_{\mathbf{x}_i}^t} \# \Sigma_{\nu_i} - I_d) \right) \text{vec}(\mathbf{B}_t^\top)$$

by using the vector identities $\text{vec}(ABC) = (C^\top \otimes A) \text{vec}(B)$.

But, since $m_{Q_{\mathbf{x}_i}^t} = (\mathbf{x}_i \otimes I_d)m_Q$, the vectorized form of the transpose of the second summand of (126) is

$$\frac{1}{n} \left[\left(\sum_{i=1}^n \mathbf{x}_i \mathbf{x}_i^\top \otimes \Sigma_{Q_{\mathbf{x}_i}^t} \# \Sigma_{\nu_i} \right) m_{Q^t} - \sum_{i=1}^n \mathbf{x}_i \otimes m_{\nu_i} \right],$$

where we used the mixed-product property for Kronecker products $(A \otimes B)(C \otimes D) = (AC) \otimes (BD)$.

Putting these two expressions back together and taking expectation with respect to Q^t yields that

$$\dot{m}_{Q^t} = \sum_{i=1}^n \frac{1}{n} \left(\mathbf{x}_i \mathbf{x}_i^\top \otimes (2\Sigma_{Q_{\mathbf{x}_i}^t} \# \Sigma_{\nu_i} - I_d) \right) m_{Q^t} - \sum_{i=1}^n \frac{1}{n} \mathbf{x}_i \otimes m_{\nu_i}$$

for all $t > 0$.

In order to derive an expression for the variance of Q^t , recall that

$$\Sigma_{Q^t} = \mathbb{E}[\text{vec}(\mathbf{B}^\top - m_{Q^t})(\text{vec}(\mathbf{B}^\top) - m_{Q^t})^\top]$$

Taking the derivative of Σ_{Q^t} over time gives

$$\begin{aligned} \dot{\Sigma}_{Q^t} &= \partial_t \mathbb{E}[\text{vec}(\mathbf{B}^\top - m_{Q^t})(\text{vec}(\mathbf{B}^\top) - m_{Q^t})^\top] \\ &= \mathbb{E}[\text{vec}(\dot{\mathbf{B}}_t^\top - \dot{m}_{Q^t}) \text{vec}(\mathbf{B}_t^\top - m_{Q^t})^\top + \text{vec}(\mathbf{B}_t^\top - m_{Q^t}) \text{vec}(\dot{\mathbf{B}}_t^\top - \dot{m}_{Q^t})^\top]. \end{aligned}$$

But vectorizing $\dot{\mathbf{B}}_t^\top - \dot{m}_{Q^t}$ yields

$$\text{vec}(\dot{\mathbf{B}}_t^\top - \dot{m}_{Q^t}) = M_t \text{vec}(\mathbf{B}_t^\top - m_{Q^t})$$

where we define $M_t := (\frac{1}{n} \sum_{i=1}^n \mathbf{x}_i \mathbf{x}_i^\top \otimes (\Sigma_{Q_{\mathbf{x}_i}^t} \# \Sigma_{\nu_i} - I_d))$ for every $t > 0$.

Putting the two previous equations together yields the Lyapunov equation

$$\dot{\Sigma}_{Q^t} = M_t \Sigma_{Q^t} + \Sigma_{Q^t} M_t.$$

- (2) By Theorem 5.22 in [Chewi et al. \(2025\)](#), we just implicitly proved that for any $Q = \mathcal{N}(0, \Sigma_Q)$ in $\mathcal{P}(\mathbb{R}^{p \times d})$

$$M_k := -\mathbb{E}_Q[\nabla_{\mathbf{B}}^2 \delta G(Q)] = \left(\frac{1}{n} \sum_{i=1}^n \mathbf{x}_i \mathbf{x}_i^\top \otimes (\Sigma_{Q_{\mathbf{x}_i}} \# \Sigma_{\nu_i} - I_d) \right).$$

Then the update equation (28) reads

$$Q^{k+1} = \exp_{Q^k}(\tau \nabla_{Q^k} G) = \mathcal{N}(0, (\tau M_k + I_{dp}) \Sigma_{Q^k} (\tau M_k + I_{dp})).$$

□

COURANT INSTITUTE OF MATHEMATICS, COMPUTING, AND DATA SCIENCE, NEW YORK UNIVERSITY, NEW YORK, NY 10011, USA

Email address: uriel.leon@nyu.edu

COURANT INSTITUTE OF MATHEMATICS, COMPUTING, AND DATA SCIENCE, NEW YORK UNIVERSITY, NEW YORK, NY 10011, USA

Email address: jnw@cims.nyu.edu